PREPARATION AND CHARACTERIZATION OF Y - Ba - Cu - O HIGH Tc SUPERCONDUCTORS

A Thesis Submitted
In Partial Fulfilment of the Requirements
for the Degree of

MASTER OF TECHNOLOGY

by

SUVANKAR SENGUPTA

to the

INTERDISCIPLINARY PROGRAMME IN MATERIALS SCIENCE

INDIAN INSTITUTE OF TECHNOLOGY, KANPUR

MAY, 1989

8/5/89

CERTIFICATE

Certified that this work on "PREPARATION AND CHARACTERIZATION OF Y-Ba-Cu-O HIGH T_c SUPERCONDUCTORS" by Suvankar Sen Gupta has been carried out under my supervision and that this has not been submitted elsewhere for a degree.

K Shahi

May, 1989.

(K. Shahi)
Assistant Professor
Materials Science Technology
Indian Institute of Technology
KANPUR

ACKNOWLEDGEMENTS

I am deeply indebted to Dr. K. Shahi for his meticulous guidance, patient assistance and ever encouraging attitude. It was a great pleasure to work with complete freedom under his erstwhile guidance. Mere words cannot express the extent of cooperation I received from him and my regards for him will always remain.

I have no words to express my gratitude to my dear sister for her immense help and constant encouragement.

Special thanks to Mr. Dipankar Sanyal, VPN Padmanabhan, Shantanu Bhattacharya, L. Vijay Raghavan and Akhil Biswas for their contribution towards the completion of my thesis.

I thank all my friends, colleagues and all those who have made my stay in IIT Kanpur a memorable one.

I am also grateful to the Staff and Faculty of Materials Science Programme for their invaluable help, and timely assistance.

Last but not the least typing by U.S. Mishra, sketching by Mr. A.K. Ganguly and Xeroxing by Vishwanath Singh deserve special appreciation.

CONTENTS

Page

CHAPTER-3

Results and Discussions

LIST OF TABLES

LIST OF FIGURES

ABSTRACT

$YBa_2Cu_3O_x$ superconducting compounds have been prepared under different atmospheric conditions and cooling rates. The oxygen content (x) has been determined by weight measurements before and after heat treatment of the samples.

The XRD patterns were used to calculate the lattice constants of various samples. The major XRD peaks in orthorhombic and tetragonal phases have been used to determine the relative amounts of the two phases, the orthogonal and the tetragonal phase. The results of the weight loss measurements and intensity ratio are by and large consistent.

The various superconducting properties such as resistivity and critical temperature T_c have been investigated as a function of temperature, oxygen content and intensity ratio. It has been found that the resistivity increases with decreasing oxygen content and the quenched samples showing very less oxygen content show a distinct semiconducting behaviour, while those having higher oxygen content show metallic behaviour. A good coorelation between the oxygen content (or deficiency), intensity ratio, resistivity, lattice parameters and critical temperatures was evident.

The dielectric constant measurements done on tetragonal quenched phase strongly contradict the previously published data. Our results further demonstrate that dielectric constant measurements can be extremely difficult to reproduce if the samples are quite conducting as the quenched tetragonal phase.

CHAPTER - 1

INTRODUCTION

The superconductive state is an outstanding example of a quantum state of macroscopic size. This was originally deduced indirectly from the evidence available especially through the work of London (1,2) in the 1930's. It was confirmed directly in 1961 when the quantization of the flux in a ring carrying a persistent current was observed.

The history of superconductivity commenced in 1911 at Leyden, Netherlands. Kammerling Onnes first developed the cryogenic techniques to cool samples to a few degrees above the absolute zero. He was the first to have successfully liquified helium and thereby opened the door for study of low temperature physics.

After liquifying the He, Kammerling Onnes (3,4) started the investigation of the electrical conductivity of metals at the new low temperature below $4.2^{\circ}K$. To reduce the resistance caused by impurities, he studied mercury of high purity and was not surprised when he found no measurable resistance. However, it soon became clear that the experiment was not in accord with the expectation. The addition of impurities to the mercury did not increase its resistance. Furthermore, the resistance

did not decrease smoothly to zero but dropped almost discontinuously to zero within a temperature range of $0.01^{\circ}K$ at about $4^{\circ}K$. By 1913 he had concluded that "mercury has passed into a new state which, on account of its remarkable electrical properties, may be called the superconductive state". The temperature at which the transition takes place is the critical (or transition) temperature and is denoted by T_c (Fig. 1.1).

1.1 THE WAY TO THE HIGH TEMPERATURE SUPERCONDUCTIVITY:

Soon after the discovery of superconductivity in Hg by Onnes, considerable effort was made by both theorists and experimentalists, to understand this new phenomenon. In this process, a large number of metals and alloys were found to exhibit the superconductivity and also there was a rise in critical temperatures (T_c) with the passage of time; the progress was however slow but regular (Fig.1.2). In 1973, it was possible to reach a critical temperature of $23.3^{\circ}K$ (5) for an alloy of niobium and germanium (Nb_3Ge). Thirteen years later, physicists were still at the same point and many of them were convinced that the battle should have been given up long before. For all that, superconductivity found numerous applications, such as in the development of liquid helium cryogenics, particularly for making electromagnets used in particle physics and medical imagery.

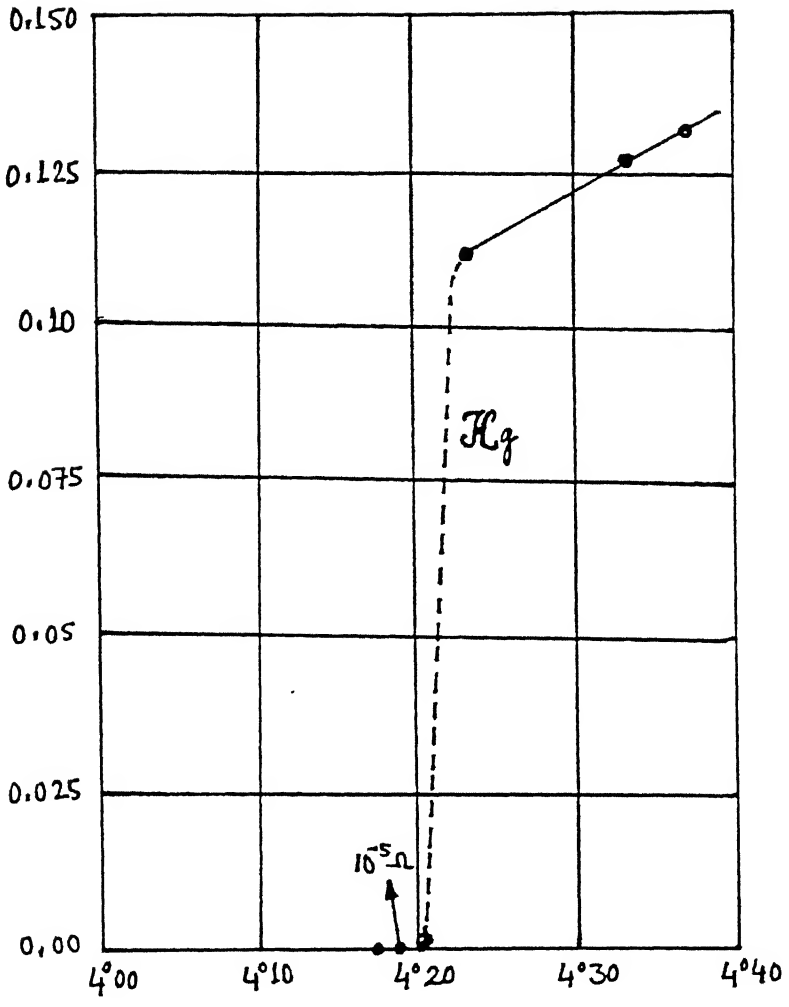

Figure 1.1 : Resistance in ohms of a specimen of mercury versus absolute temperature. This plot by Kamerlingh Onnes marked the discovery of superconductivity.

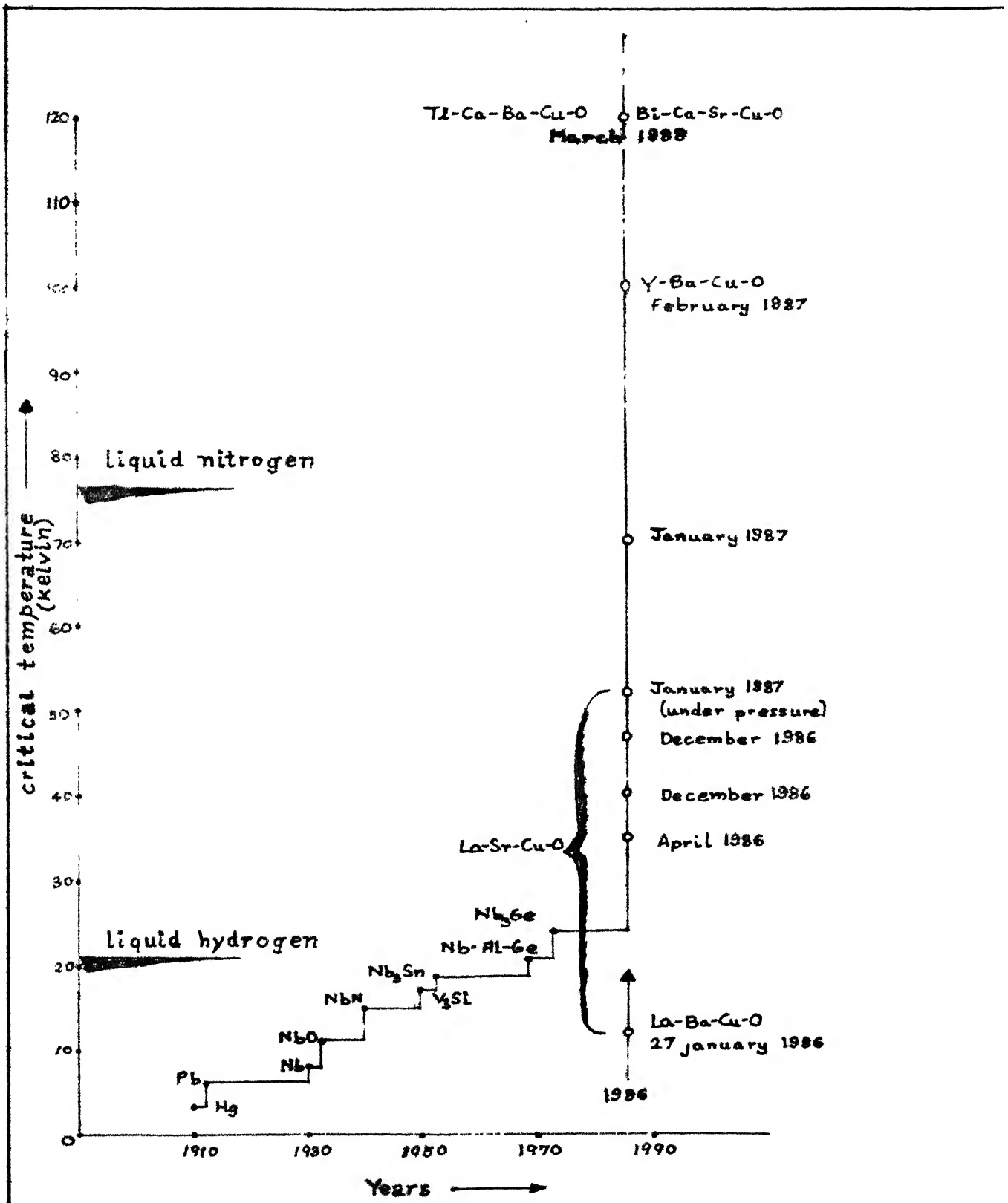

Fig 1-2 : The progress in bringing up critical temperature of the superconductors. The dramatic increase in T_c in recent years is evident.

The first tangible instance of possible high temperature superconductivity was discovered in January 1986, at an IBM research laboratory at Zurich. While cooling a sample of an oxide of copper, barium and lanthanum, Bendroz (6) noticed that electrical resistance of the sample began decreasing rapidly with temperatures, i.e. at a temperature of about twenty degrees Kelvin. On altering the concentration of barium he observed the commencement of the decrease in resistivity at temperatures of $30^{\circ}K$.

Till 1986, a very small number of superconducting oxides were known. For example in the 1960s, it was shown that reduced $SrTiO_3$ had a very low transition temperature of $0.3^{\circ}K$ (7). Subsequent research facilitated the task of raising the critical temperature to $0.8^{\circ}K$, after having doped it with a compound of niobium (8). This turned out to be something new, an "exotic" superconductivity of sorts. But interests were limited on account of the low transition temperature involved.

About ten years later, Johnston and his colleagues obtained a very significant result with an oxide of titanium and lithium (Li-Ti-O), at a critical temperature of $13.7^{\circ}K$ (9). Then in 1975, Sleight and his collaborators (10) observed a transition temperature of $13^{\circ}K$ in a compound of mixed valency, this was a compound of barium doped with bismuth $BaPb_{1-x}Bi_xO_3$.

In studying the properties of superconducting oxides in greater details, many groups arrived at the same result, conceiving the essential characteristics of these compounds, that is the low concentration of electrons carrying electric current. The figures were $2x10^{20}/cm^3$ in strontium titanate (11) and 2 to $4x10^{21}/cm^3$ in a compound like Ba-Pb-Bi-O (12); these figures were an order of magnitude lower than those for metals. That this was the key to the argument was deduced by a sufficiently intuitive argument on the "BCS" theory of superconductivity.

The BCS theory was formulated in 1957 by Barden, Cooper and Schrieffer (13). The theory describes how superconduct electrons assemble to form pairs and regroup in the same quantum states. In an ordinary conductor, the electric current is carried by "individual" electrons, each electrons having its proper path. Each electron is therefore subjecte to a large number of collisions and loses some of its energy in the process. Two bound electrons, on the other hand, constitute a quantum object of a different nature. Contrary to individual electrons, electron pairs can be found in the same quantum state, forming a macroscopic quantum wave. The circulation of electric current is effected by the movement of an ensemble of paired electrons, without the individual dissipation of energy or encountering electric resistance. The BCS theory for the first time provided a quantitative description of this phenomena.

In their theory, the formation of pairs is explained in terms of the existence of a certain type of indirect interaction between electrons. This interaction is attractive and opposes the Coulomb force of repulsion between electrons. This was due to the positive ions of the crystal reacting to the passage of electrons in their neighbourhood. During its passage, a conduction electron gives rise to a local deformation in the crystal lattice on account of its attraction for cations. This deformation takes the form of lattice vibrations that can interact with a second electron. The net result of this process is that it gives rise to an attraction between two electrons that find themselves paired via the lattice. In terms of field theory, we say that the interactic of a couple of electrons is mediated by the phonons. The pairs of electrons so formed are called "Cooper pairs".

The electron-phonon-electron interaction produces a modification in the spectrum of the energy of electrons. We know that in the case of a solid, the energy states available to electrons are grouped in successive bands. The level upto which the electrons are filled is called the Fermi level and the corresponding energy as the Fermi energy, E_F. The BCS theory predicts, that in superconductors, at the energy E_F, there is a gap separating the ground state of the system of paired electrons, from the excited states occupied by unpaired normal electrons. The width of

the band corresponds to the energy required to break a pair. This width is a function of temperature, being maximum at zero and zero at $T = T_c$. In case of ordinary superconductors the value of Δ is of the order of 10^{-3} to 10^{-4} E_F. In some cases, superconductivity is manifested in the absence of the gap.

Within the framework of the BCS model, the criteria for the appearance of superconductivity is that the transition temperature T_c is proportional to $\omega_D \exp[-1/N(E_F)V]$, where ω_D is the Debye frequency $N(E_F)$ is the density of electronic states per unit energy at the threshold Fermi energy, and V is the intensity of electron-phonon coupling. Now for the oxide superconductors discovered in 1960s and 1970s, to obtain a transition temperature of the order of $13^{\circ}K$, with a density of states that is one or two orders of magnitude lower than that of metals, it is necessary that the intensity of the electron-phonon coupling be much higher since the product of the two quantities $N(E_F)V$ appears in the formula. Since intermetallic compounds did not produce any spectacular results, the oxide superconductors naturally became one of the important areas for research in superconductors.

Bendroz and Muller (1983) started their first investigations on Ni-compounds at the IBM research laboratory at Zurich. Inspired by some good results, they soon turned their attention to Cu-compounds. They came to know from a publication of Michel et al. (14) that an oxide of

copper viz. exhibits the required mixed valency with the general formula $Ba_xLa_{5-x}Cu_5O_{5(3-y)}$. Since barium is divalent (Ba^{2+}), lanthanum trivalent (La^{3+}) and all the charges are in equilibrium with those of oxygen (O^{2+}), copper is found in mixed valency state Cu^{2+}/Cu^{3+}. In addition the degree of the mixed valency is controlled by the value of x that indicates the concentration of barium in the compound. Bendroz and Muller (6) used the method of coprecipitation to synthesize this compound.

Towards the beginning of January 1986, they had measured the resistivity of these samples as a function of temperature. They observed that the resistivity first decreases linearly like that of a metal, then stabilizes to decrease again, before falling rapidly by orders of magnitude as the temperature approaches zero in certain case. This was the first manifestation of superconductivity.

X-ray diffraction analysis revealed that the resultant material is a multiphase compound. The first one was copper oxide CuO, which is an insulator. The second one was $Ba_xLa_{5-x}Cu_5O_{5(3-y)}$, which is metallic and the third phase was $Ba_xLa_{2-x}CuO_{4-y}$. This contained a small proportion of barium and its structure K_2NiF_4 consisted of layers of octahedral perovskites of CuO_6 and oxygen defects alternating with layer of LaO. It was this phase that was superconducting, as was confirmed by subsequent measurement of superconductivity. The observed transition temperature was close to $40^{o}K$.

Chu and his collaborators (15) at the University of Housten, were interested in the effect of pressure on barium compounds. By applying hydrostatic pressure they succeeded in raising the transition temperature to $52^{o}K$. This oriented the efforts of researchers towards the reproduction of the results by using internal pressure, that is, by changing the nature of the ions. In collaboration with Wu's group at the University of Alabama Huntsville, Chu found that on replacing lanthanum by yttrium they successfully achieved a T_c of $92^{o}K$ in a multiphase Y-Ba-Cu-O system (16). In a short time, many groups obtained comparable results and were able to isolate the superconducting phase, $Y_1Ba_2Cu_3O_{7-\delta}$.

Michel et al (17) first reported occurrence of superconductivity in a new system namely, Bi-Sr-Cu-O with $T_c \simeq 20^{o}K$. However, Maeda and his colleagues (18) at National Research Institute for Metals (NIRM) recently reported a new superconducting material with T_c possibly as high as $120^{o}K$ in the Bi-Ca-Sr-Cu-O system, although the material prepared seemed to be multi phasic. Another new member was added to the copper oxide-based superconductors when Shen and Hemen (19) reported a new superconducting compound Tl-Ca-Ba-Cu-O with $T_c \simeq 120^{o}K$.

At present a large number of scientists and technologists around the world are engaged in the development of new high T_c superconducting materials, as there is a great deal of expectation that superconductors with T_c at

or near room temperature will be found out many of existing technologies will be revolutionized.

1.2 SOME FUNDAMENTAL PROPERTIES OF SUPERCONDUCTORS:

1.2.1 Meissner Effect

Although the infinite conductivity or zero resistivity is most obviously the true nature of superconducting state, this state appears more clearly in its magnetic effect. Consider a normal metal in a uniform magnetic field. When the sample is cooled and becomes superconducting, Meissner and Ochsenfeld first demonstrated that all magnetic flux is expelled from the interior (Fig. 1.3a).

The magnetization curve expected for a superconductor under the conditions of Meissner-Ochsenfeld experiment is sketched in Fig. 1.3(b). This applies quantitatively to a specimen in the form of a long solid cylinder placed in a longitudinal magnetic field. Pure specimen of many materials exhibiting. This behaviour, are called "Type I" superconductors or formally soft superconductors. The values of critical magnetic field (H_c) that destroys superconductivity are always too low for type I superconductors to have any useful technical application in coil for superconducting magnets.

A second type of superconducing materials exhibits magnetization curve as form in Fig. 1.3(b) is known as type II or hard superconductors. They are either alloy or transition metals with high values of electrical resistivity

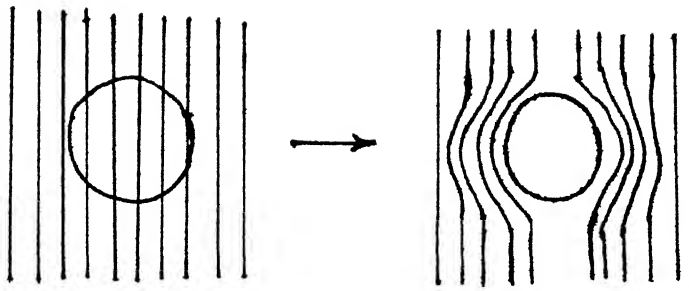

Figure 1·3 (a): Meissner effect in a superconducting sphere cooled in a magnetic field.

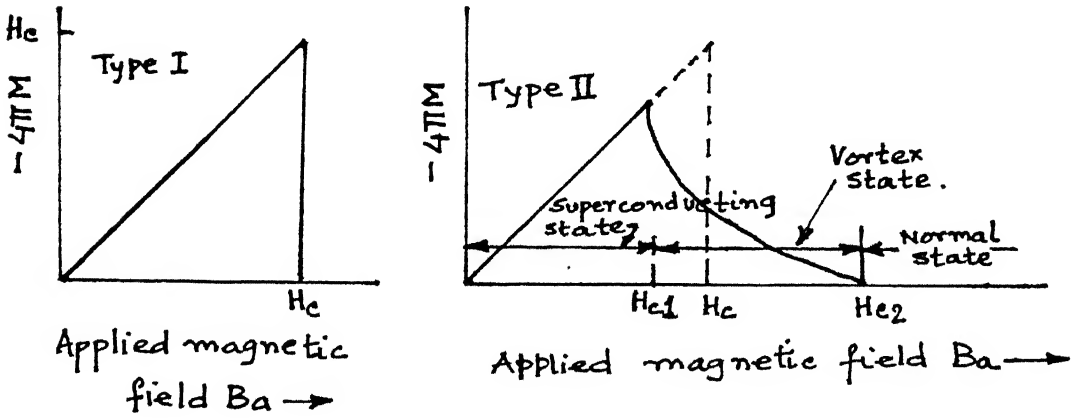

Figure 1·3 (b): Magnetization versus applied magnetic field for a type I and type II superconductor.

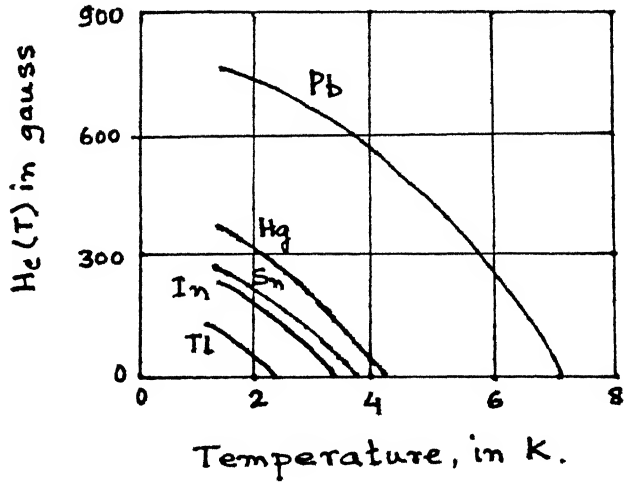

Figure 1·4: Variation of critical field Hc(T) versus temperature, for several superconductors.

in normal state i.e.mean free path λ is short. Newly discovered high T_c oxide superconductors also fall in this class. Type II superconductors have superconducting electrical properties upto a field denoted by H_{c_2}. Between the lower critical field H_{c_1} and upper critical field H_{c_2} the flux density $\vec{B} \neq 0$ and the Meissner effect is said to be incomplete. The region between H_{c_1} and H_{c_2} the superconductor is threaded by flux lines and is said to be vortex. Owing to their high H_{c_2}, type II superconductors are used in the commercial solenoids.

1.2.2 Critical Field

The Meissner effect occurs only for sufficiently low magnetic fields. For simplicity we consider a long cylinder of pure superconductor in a parallel applied magnetic field H, where there are no demagnetizing effect. If the sample is superconducting at temperature T in new field, there is a unique critical field $H_c(T)$ above which the sample becomes normal. This transition is reversible for superconductivity reappears as soon as H is reduced below $H_c(T)$ (Fig. 1.4). Experiments on pure superconductors shows that

$$H_c(T) = H_c(0)\left[1 - \left(\frac{T}{T_c}\right)^2\right]$$

1.2.3 Persistent Currents and Flux Quanization

Consider a normal metallic ring placed in a magnetic field perpendicular to its planes (Fig. 1.5). When the temperature is lowered, the metal becomes superconducting

and expels the flux. Suppose the external field is then removed no flux can pass through the superconducting metal and the total trapped-flux must remain constant being maintained by the circulating supercurrent itself. Such persistent current have been observed over long periods. Furthermore the flux trapped in sufficiently thick rings is quantized units of

$$\phi_o = \frac{hc}{2e} = 2.07 \times 10^{-7} \text{ gauss,cm}^2$$

known as fluxoid.

1.2.4 Specific Heat and Energy Gap

In addition to its magnetic behavior, a typical superconductor also has distinctive thermal properties. For zero applied field the transition is second order, which implies a discontinuous specific heat but no latent heat. The electronic specific heat C_n in normal state varies linearly with temperature. In superconducting state however, the specific heat C_s initially exceeds C_n for $T < T_c$, but then drops below C_n and vanishes exponentially as $T \to 0$ (Fig. 1.6)

$$C_s \propto \exp\left(\frac{-\Delta}{kT}\right)$$

This dependence indicates the existence of a gap in the energy spectrum separating the excited states from the ground state of an energy Δ . For most superconducting elements Δ_o is somewhat less than $2 k T_c$.

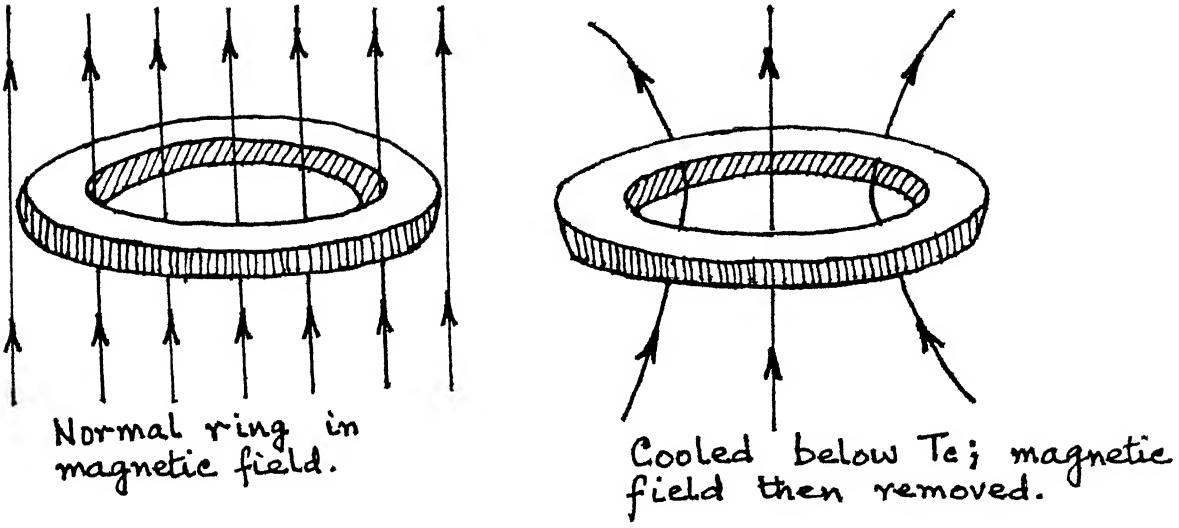

Figure 1.5 Flux trapping in a superconducting ring.

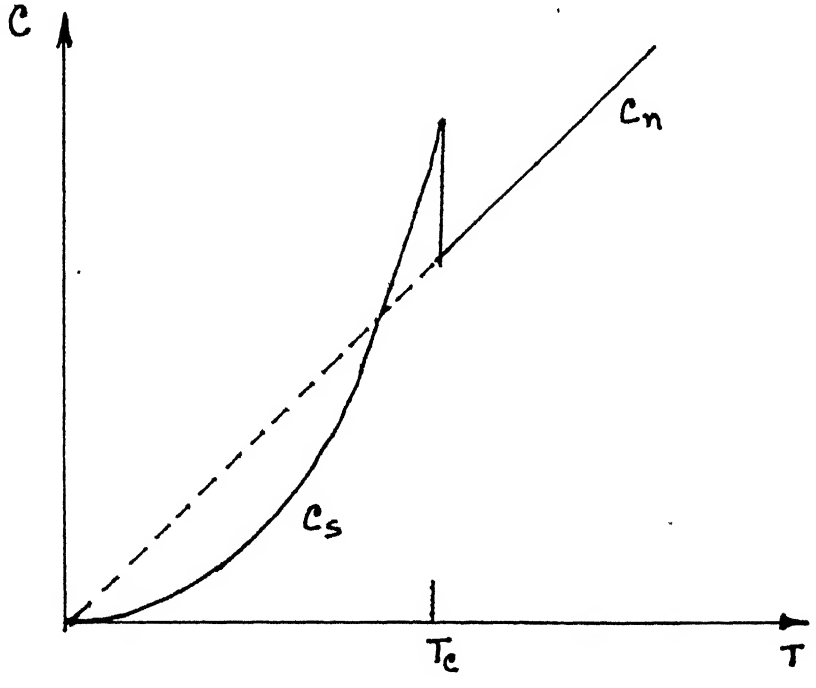

Figure 1.6 Schematic diagram of specific heat in a superconductor.

1.2.5 Isotope Effect

A distinctive property of superconductors is of the isotope effect. Careful studies of isotopically pure samples showed that the ionic lattice plays an important role in superconductivity, and the transition temperature varies typically with ionic mass

$$T_c \propto m^{-1/2}$$

These results indicate the importance of the attractive electron-phonon interaction.

1.2.6 The Josephson Junction

The junction is formed when two superconducting bodies are placed in electrical contact. In practice most commercial Josephson junctions have an extremely thin layer (a few atomic thickness) of an insulator (eg. Al_2O_3) between the two pieces of conductors. A current can be made to flow from one part of junction to the other, but if the current suddenly exceeds the critical value of the superconducting transition, a high resistance state is produced. These junctions switch very fast (within one picosecond) and could soon replace the transistors in computer.

— 3 APPLICATIONS

3 - 1 Applications Using the Property of Zero Resistance

— 1 - A Low Loss Power Transmission

One of the major losses in low voltage power

transmission is the Joules loss i.e. loss due to resistive heating. Superconductors have zero resistance and so an electric current will flow through a superconducting wires without generating any heat. Thus there will be no resistive heating and hence no energy is lost in ideal condition, thus a lot of energy can be saved.

1.3.1.B Powerful Magnets

Huge powerful magnets can be made from large coils of superconducting wires. The advantage of using superconducting wires is that a large amount of current can be sent through it without any loss due to heating, thus generating large magnetic fields. With the discovery of high T_c superconductors the manufacturing cost of superconducting magnets has reduced considerable as LN2 is about 1000 times cheaper than liquid He.

1.3.1.c Radio Antennae for very Low Frequency Signal

Electrical resistance in normal radio aerials makes it difficult to receive very low frequency signals. The only way, we can receive this signal is by using very large radio dishes and miles and miles of wires of aerials. Aerials and antennae made from superconducting materials will be much smaller.

It will be much easier for submarines to communicate with their shore bases. Radio astronomers will be able to

use smaller and cheaper radio telescopes.

1.3.1.D Energy Storage

Because there is no electrical resistance in a superconducting wire or ring, an electrical current can be made to travel around a closed electrical circuit or ring indefinitely. So atleast theoretically one can store energy in form of electrical energy in superconducting rings.

1.3.2 Applications Using Josephson Junctions

1.3.2.A SQUIDS

Josephson junctions are used in "SQUIDS" (superconducting quantum interference devices) in high speed logic switches, analog digital convertors, and voltage standards. SQUIDS can be used to detect minute changes in magnetic fields and so potential applications are in security, prospecting for minerals and oils, imaging atomic structures, monitoring corrosion and the measurement of magnetic pulses generated by the human brain or heart.

Josephson junctions are likely to replace transistor in new computers. It is predicted that by using new superconducting components the speed of the future supercomputer will be in excess of 1000 millions instruction per second (MIPS) compared with 50 MIPs of today's supercomputers.

1.3.3 Applications using Meissner Effect

The Meissner effect or the property of perfect diamagnetism also has various application The most interesting one is that it will find extensive use in daily life. For example leviating trains can be made which owing to their low friction will move faster with lower fuel consumption. Actually most of the fuel in trains or in any other vehicles are consumed in overcoming friction. So once leviating vehicles become feasible there will be little friction and hence enormous amount of fuel can be saved. Frictionless bearing etc. can also be made using superconductors.

1.4 HIGH T_c SUPERCONDUCTORS : A BRIEF REVIEW

Superconductivity in metal oxides has been known for some time. $SrTiO_3$ when reduced or doped with Nb shows superconductivity at $0.2^{\circ}K$ (8). $BaPb_{1-x}Bi_xO_3$ with a perovskite structure becomes a superconducting (20) for $0.05 \leq x \leq 0.$ with T_c in the range $9^{\circ}K$-$13^{\circ}K$. The phenomenon of high temperature superconductivity was first reported by Bednorz and Muller (6) in a CuO-based system, viz., $La_{5-x}Ba_xCu_5O_{5(3-y)}$ On cooling, the resistivity (ρ) of the samples with $x \leq 1.0$ initially decreases and then rises prior to sharp drop starting at temperatures as high as $35^{\circ}K$. For some samples, a zero resistance state was achieved below $12^{\circ}K$, although all were multiphasic system.

Chu et al (15) reported that under pressure T_c increases from 32°K to 40.2°K at 13 K bar at a rate of 0.9×10^{-3} K bar^{-1}. It was then found (21) that pressure could enhance the T_c of La-Ba-Cu-O system at a rate greater than 10^{-3}K bar^{-1} to a value of 57°K. Wu et al (16) subsequently reported superconductivity at temperatures above the boiling point of LN , namely at 93°K, in a new mixed phase Y-Ba-Cu-O compound system at ambient pressure. One noteworthy feature of this system was that pressure had only a slight effect on T_c in strong contrast to La-Ba-Cu-O and La-Sr-Cu-O system (7). This may be due to chemical pressure associatedwith the smaller Y atoms already present in Y-Ba-Cu-O system. Cava et al (22) prepared and identified, a single phase responsible for high temperature superconductivity in the chemical system Y-Ba-Cu-O-δ It has an orthorhombic distorted, oxygen deficient perovskite structure of stoichiometry $Y_1Ba_2Cu_3O_{9-\delta}$ ($\delta \leq 2.1$). Samples exhibit zero resistance at 91°K. All the observed x-ray diffraction peaks can be accounted for by a crystallographic unit cell of a = 3.822 Å, b = 3.891 Å, c = 11.677 Å. Immediately, after the discovery of superconductivity at temperatures above the boiling point of LN2, a massive effort all over the world is being made to develop materials with higher T_c. One of the favourite means to achieve this end appears to substitute Y, Ba and even Cu by other elements. Table 1.1 gives a summary of various such systems and their transition

temperatures.

While the work on Y-Ba-Cu-O was in full swing, Michel et al (17) reported occurrence of superconductivity in a new system, i.e. Bi-Si-Cu-O, with $T_c \sim 20^oK$. However, Maeda and coworkers (18) recently reported a new superconductor with T_c possibly as high as 120^oK in the Bi-Ca-Sr-Cu-O system, although the material prepared seemed to be multicomponent. Resistivity measurements show two step transition at 110^oK and 75^oK in the Bi-Ca-Sr-Cu-O systems. The lower transition was found to be rather insensitive to the composition, while the higher T_c was not observed after prolonged annealing below 800^oC.

Shen et al (19) recently added a new member to the new class of high T_c superconductors, namely Tl-Ca-Ba-Cu-O with T_c as high as 120^oK, and it is expected that many more will be discovered in near future.

1.5 STATEMENT OF THE PROBLEM

The discovery of a new class of oxide-based superconductors with T_c above the boiling point of LN2 temperature was no doubt a great mile-stone in the history of superconductivity which indeed made this field accessible to even nonspecialists. The $YBa_2Cu_3O_{7-\delta}$ compound appears to be a very promising system. In general it contains two phases: (i) superconducting orthorhombic phase and (ii) semiconducting tetragonal phase. The critical temperature and other superconducting properties depend on the

ratio of orthorhombic and tetragonal phases present in a particular sample.

The aim of this project was to synthesize the $YBa_2Cu_3O_{7-\delta}$ or popularly called "123" compound under different preparational conditions, and examine the resulting materials for their structural and electrical properties. In particular various samples of $YBa_2Cu_3O_{7-\delta}$ have been prepared at a fixed sintering temperature of $\sim 940^{o}C$ under different atmosphere (air/oxygen) and at different cooling rate. All samples have been examined by x-ray diffraction analysis. Weight loss measurement has been used to calculate the "average" oxygen content of the samples. The analysis of the major XRD peaks at $2\theta \simeq 32.4^{o}$ and 32.7^{o} has been used to estimate the relative concentration of ortho and tetragonal phases and attempt has been made to correlate this with the superconducting properties (resistivity and T_c) of the samples on one hand and the weight loss (oxygen content) on the other.

The tetragonal phase present in $YBa_2Cu_2O_{7-\delta}$ system exhibits semiconducting properties and its electric and dielectric properties may be of considerable interest. The resistivity of the tetragonal phase increases slowly as the temperature is decreases. It has been reported (30) to have unusually large value of static dielectric constant.

Considerable effort was therefore made to measure the dielectric constant reliably and reproducibly. However owing to relatively high conductivity of the semiconducting tetragonal phase ($\simeq$ 1 Ohm cm) the dielectric constant measurement was not very successful and we suspect the earlier data may not be reliable and meaningful.

Table 1.1 : Various High T_c Superconducting Oxide Systems

System	T_c	Remarks	References
1. $Y_{1-x}Zr_xBa_2Cu_3O_{9-y}$		$0.1 \leq x \leq 0.7$ showed the presence of $YBa_4Cu_5O_8$ and barium zirconate	23
$x = 0.6$	85^oK		
0.5	91^oK	T_c decreases and amount	
0.25	93^oK	of barium zirconate increases with increasing x.	
2. $Y_{1-x}Pr_xBa_2Cu_3O_{7-\delta}$		T_c decreases with increasing x	24
$x = 0$	92^oK		
$= 0.1$	88^oK		
0.2	80^oK		
0.3	70^oK		
0.4	55^oK		
0.5	35^oK		
3. $Y_{1-x}Na_xBa_2Cu_3O_{7-\delta}$		T_c decreases with increasing x	24
$x = 0$	90^oK		
0.1	89^oK		
0.2	88^oK		
0.3	80^oK		
0.4	50^oK		
0.5	40^oK		
4. $ABa_2Cu_3O_{6+x}$		T_c does not changes much on replacing Y by any other rare-earth elements	25
A = Y	98^oK		
La	91^oK		
Nd	91^oK		
Sm	94^oK		
Eu	94^oK		
Gd	95^oK		
Ho	93^oK		
Er	94^oK		

Table 1.1(Continued):

System	T_c	Remarks	References
A = Lu	91°K		
5. $YBa_2Cu_{3-x}Sn_xO_{7-y}$ with $0.1 \leq x \leq 3.00$		Electrical resistivity shows that the value of x=1 is the critical value above which superconductivity disappears. The T_c is almost independent of x for $x \leq 1$. The decrease in T_c with increasing Sn concentration is quite abrupt; T_c decreases only ~ 5°K as x varies from 0 to 0.9. For $x < 1.0$ the samples are metallic above T_c. For all samples with $x > 1$ the $T_c < 4$°K and exhibits semiconducting properties	26
6. $YBa_2(Cu_{1-x}M_x)_3O_{7-y}$		T_c decreases, with increasing concentration of Al, Mo and Zn	27
M = Al			
x = 0.01	84°K		
0.02	70°K		
0.035	55°K		
0.05	50°K		
M = Mo			
x = 0.01	82°K		
0.02	68°K		
0.035	55°K		
0.05	55°K		
M = Zn			
x = 0.01	79°K		
0.02	61°K		
0.035	50°K		
0.05	35°K		
0.075	Semiconducting		
0.01			

Table 1.1 (Continued):

System		T_c	Remarks	References
7. Y $Ba_2Cu_{3(1-x)}M_{3x}O$			Structure	28
M	x			
-	0	92°K	Orthorhombic	
-	0	-	Tetragonal	
Li	0.051	73°K	Orthorhombic	
Li	0.096	46°K	Orthorhombic	
Cr	0.097	86°K	Orthorhombic	
Mn	0.101	92°K	Orthorhombic	
Fe	0.052	90°K	Tetragonal	
Fe	0.101	50°K	Tetragonal	
Co	0.053	78°K	Tetragonal	
Co	0.1	50°K	Tetragonal	
Co	0.150	-	Tetragonal	
Ni	0.147	76°K	Orthorhombic	
Ni	0.095	73°K	Orthorhombic	
Zn	0.041	40°K	Orthorhombic	
Ag	0.051	92°K	Orthorhombic	
Pt	0.049	92°K	Orthorhombi	

CHAPTER - 2

EXPERIMENTAL DETAILS

The present investigation was aimed to study the effect of oxygen content on various properties of $Y_1Ba_2Cu_3O_{7-\delta}$. The experimental efforts involved are:

(i) Preparation of samples.

(ii) Development of furnace for preparation of samples in desired atmospheres (air and oxygen).

(iii) Estimation of oxygen content.

(iv) Determination of lattice constants and to study the effect of oxygen content on them, using X-ray diffraction.

(v) Design and fabrication of sample holders for
   (a) electrical resistivity measurement at room temperature,
   (b) electrical resistance measurement between liquid nitrogen and room temperature,
   (c) dielectric constant measurement at any desired temperature.

(vi) Measurement of electrical resistivity as a function of oxygen content and temperature.

(vii) Determination of dielectric constant.

2.1 SAMPLE PREPARATION:

2.1.1 Description of Apparatus

For sample preparation a furnace was locally designed and developed in which the atmosphere could be controlled. The system (Fig. 2.1) consists of a furnace, a temperature controller, thermocouples, quartz tube, rubber and steel tubes for passing oxygen, rubber corks and flowmeter.

Kanthal wire of 2 mm diameter was wound uniformly at the rate of about 10 turns per inch on a mullite tube (45 cm length, 4.8 cm internal diameter). The total resistance of the heating element was ~ 42 Ohms. A high temperature cement was applied directly over the windings to a thickness of about 1/4 inch and then allowed to dry at room temperatures for a few days. Later a small current was passed to further dry up the cement.

The mullite tube wound with Kanthal wire was housed in a cylindrical aluminium construction which was open at both ends. The space between outer aluminium shell and central mullite tube was filled with MgO powder to minimize the heat loss.

A quartz tube about 1 m in length was inserted in the furnace and the two open ends were sealed with rubber corks. Two Al_2O_3 bricks cut in the form of cylinders were kept inside near the ends of the quartz tube to protect the rubber corks from the heat of the furnace.

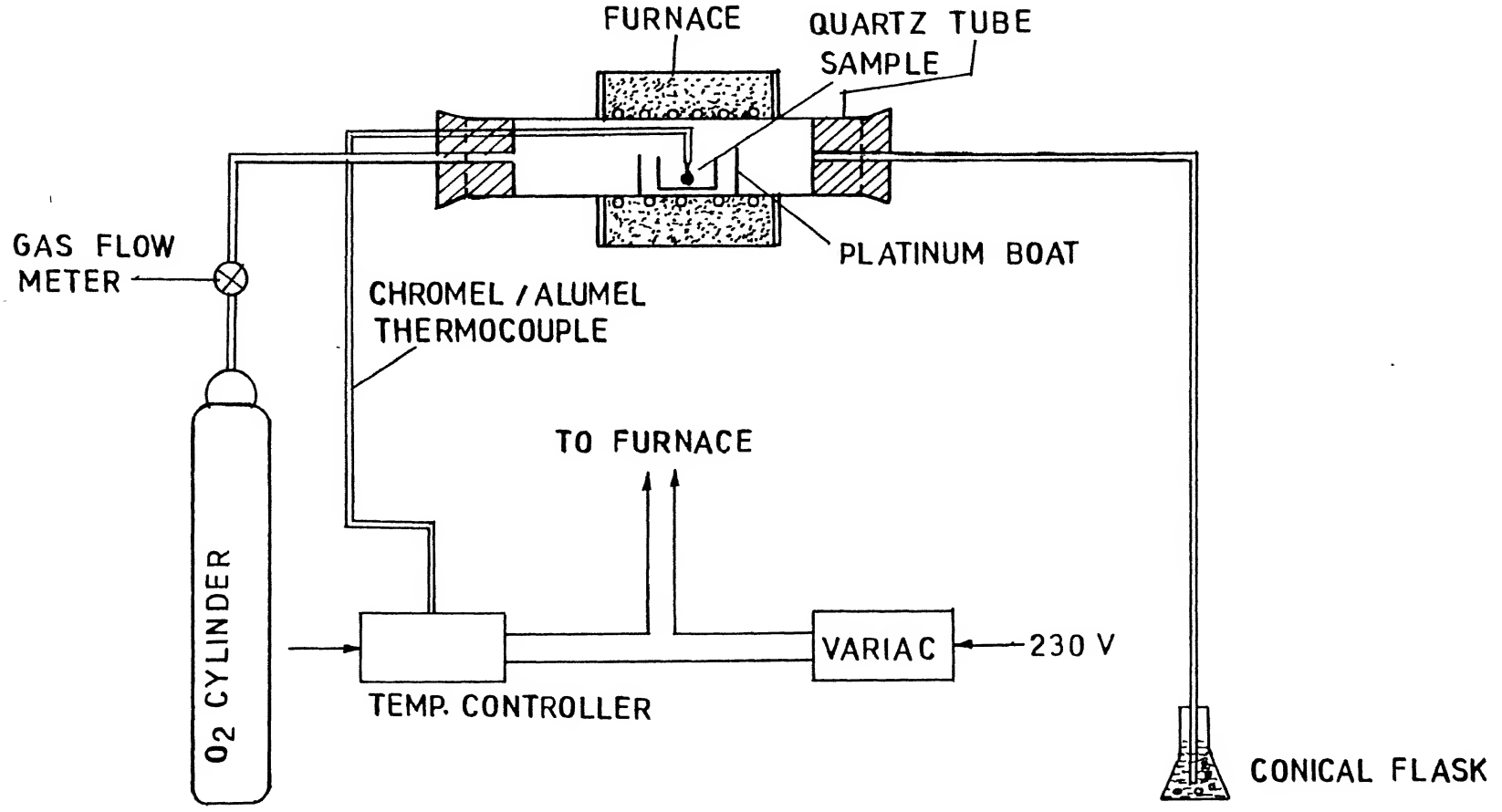

FIG. 2.1 ARRANGEMENT FOR PREPARATION OF HTSC MATERIALS UNDER FLOW OF OXYGEN

Either Platinum-rhodium/Platinum or chromel-alumel thermocouple (depending upon the availability of controller) and a steel tube for the gas to flow-in were inserted through a pair of holes in the first cork. Another hole in the other cork was made and a stainless steel tube was inserted to let the gas flow-out through a conical flask containing water. The flow rate of oxygen was monitored by observing the number of bubbles formed in the flask. The number of bubbles was kept 6-10 bubbles per minute. For heating the current was monitored so that heating rate never exceeds $5^{o}C$/minute.

2.1.2 Preparation of Pellets

High purity Y_2O_3, $BaCO_3$ and CuO were used as starting materials.

Y_2O_3 of 99.99% purity was obtained from Aldrich Chemicals (U.S.A.). Its physical properties are given in Table 2.1.

Table 2.1 : Physical Properties of Y_2O_3

Properties	Values
1. Molecular weight	225.81
2. Crystalline properties	White powder
3. Specific gravity	5.01
4. Melting Point	$2410^{o}C$

$BaCO_3$ of 99.00% purity was obtained from Qualigens Fine Chemicals (India). Physical properties of $BaCO_3$ are given in Table 2.2.

Table 2.2 : Physical Properties of $BaCO_3$

Properties	Values
1. Molecular weight	197.35
2. Crystalline form	White, hexagonal
3. Specific gravity	4.43
4. Melting point	1740°C

Ultrapure (99.99%) CuO was obtained from Alpha Chemicals (U.S.A.). Some of the physical properties of CuO are given in Table 2.3 below:

Table 2.3 : Physical Properties of CuO

Properties	Values
1. Molecular weight	79.54
2. Crystalline properties	Black powder, monoclinic
3. Specific gravity	6.30 - 6.49
4. Melting point	1326°C

Y_2O_3, $BaCO_3$ and CuO are taken in proper proportion and were intimately mixed in an agate mortar. The fine powdered mixture was then transferred to a die made from die steel as shown in Fig. 2.2. After levelling the powder by means of the die piston, the whole assembly was placed in a hand - operated hydraulic press. The pressure used in all cases was 4 ton/cm^2. The piston diameter fixed the diameter of the pellets to about 1 cm while the thickness of the pellets usually varied between 0.25 cm and 0.35 cm. Thorough cleaning of the die with acetone before and after use was done as a standard practice.

The pellet was then kept in a small platinum boat which in turn was kept in a bigger platinum boat. Weight of the smaller platinum boat with and without pellet was measured using a Mettler AE-160 digital single-pan balance. The balance was usually given the desired warm up time of about 1 hour for better stability. The bigger platinum boat carrying the small boat with the pellet was then inserted into the furnace. The temperature was raised to 900°C in about 4-5 hours. The set point was found accurately by noting the thermo-emf of the thermocouple using a Keithley DMM 197. For completion of the solid state reaction the temperature was kept constant at $\simeq$ 900°C for 12 hrs. Depending upon preparation condition oxygen was passed.

After that various types of cooling procedures were used. Details of cooling process will be described in Chapter 3. After cooling, the weight of the small boat with and without the pellet was registered once more. The oxygen content after solid state reaction was calculated from the weight loss.

The pellet was pulverised and pelletilised once more in a manner described earlier. The weight of the smaller platinum boat with and without sample was also taken again. The sample was then inserted into the furnace and the temperature was raised to 940^{o}C at the previous rate of 5^{o}C/min. and kept there for 12 hours. Depending on the requirements oxygen gas was passed through out the sintering followed by cooling. The small platinum boat with and without pellet was again weighed. The oxygen content was calculated from it. Details of the calculations are given in Chapter 3.

2.2 ESTIMATION OF OXYGEN CONTENT

The basic principle used for estimation of oxygen content was to measure the weight loss accurately and then to calculate weight loss due to oxygen thus finding the oxygen content. Since the weight loss is very small (0.15 to 0.17 gm approximately for solid state reaction and 0.002 gm to 0.03 gm for sintering) depending upon the cooling condition, the accurate measurement can only be done if the difference of two small weights is taken. For this one

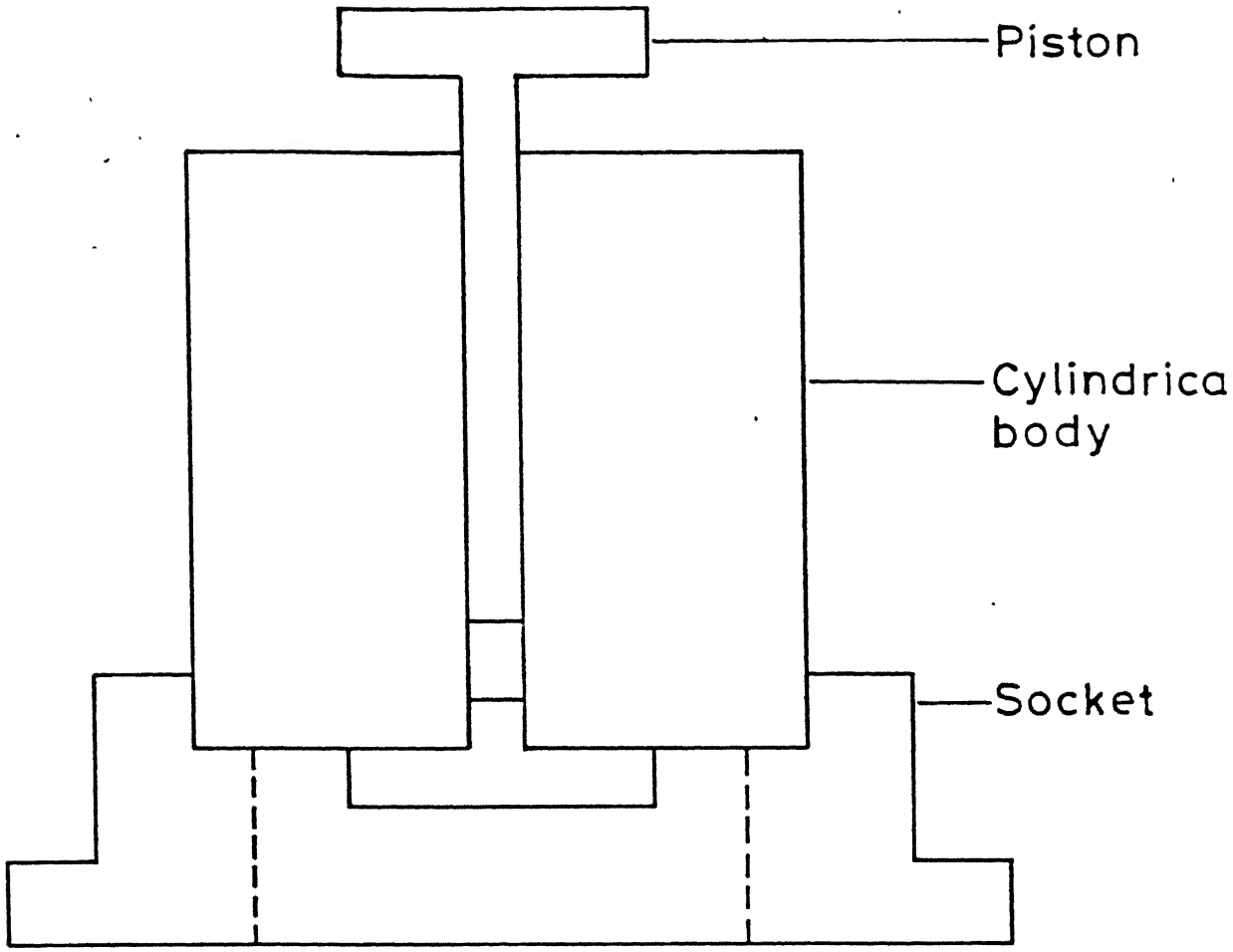

Figure 2.2: Schematic diagram of steel die.

small platinum boat has been constructed using a thin foil of weight about 0.8 gm. The weight of the pellet was about 1.4 gm so that the overall weight was of the order of 2.2 gm. Weight of the small boat with and without pellet was taken before and after each heat treatment.

2.3 DETERMINATION OF STRUCTURE USING X-RAY DIFFRACTION (XRD):

X-ray diffraction (XRD) patterns of various samples were recorded using "Reich Seifert Iso-Debyefley 2002 Diffractometer". The radiation employed as CuK_{α} (λ_o = 1.5418 Å).

Specimens were made by fixing the pellets into a rectangular perspex sample holder using plasticine. The surface was levelled by pressing it with a glass slide over it.

The XRD patterns were recorded in the 2θ range of 20° to 70°. The operating conditions are given in Table 2.4.

Table 2.4 : Operating Conditions of the Diffractometer

1. Current	20 mA
2. Voltage	30 kV
3. Time constant	10 sec
4. Beam slit width	2 mm
5. Detector slit width	0.3 mm
6. Scan speed	1.2°/mm in 2θ
7. Chart speed	30 mm/min
8. Full scale intensity	200 counts/sec.

Both superconducting orthorhombic and semiconducting tetragonal forms of $YBa_2Cu_3O_{7-\delta}$ have prominent peaks near $2\theta = 32^{\circ}-33^{\circ}$ which were recorded separately at a slower chart speed. The operational details for these recordings are listed in Table 2.5.

Table 2.5 : Operating Conditions of the Diffractometer for Slow Recording of Major Peaks in $YBa_2Cu_3O_{7-\delta}$ near $2\theta = 32^{\circ}-33^{\circ}$

1. Current	20 mA
2. Voltage	30 kV
3. Time constant	10 sec.
4. Beam slit width	2 mm
5. Detector slit width	0.3 mm
6. Scan speed	0.3°/min
7. Chart speed	30 mm/min.
8. Full scale intensity	500 counts/min.

From the XRD patterns, the crystal structure and the lattice constants were found out which are reported in Chapter 3.

2.4 MEASUREMENT OF RESISTIVITY AT ROOM TEMPERATURE:

2.4.1 Sample Holder

A standard four probe sample holder was made in which the probes are arranged in a square array. Fig. (2.3)

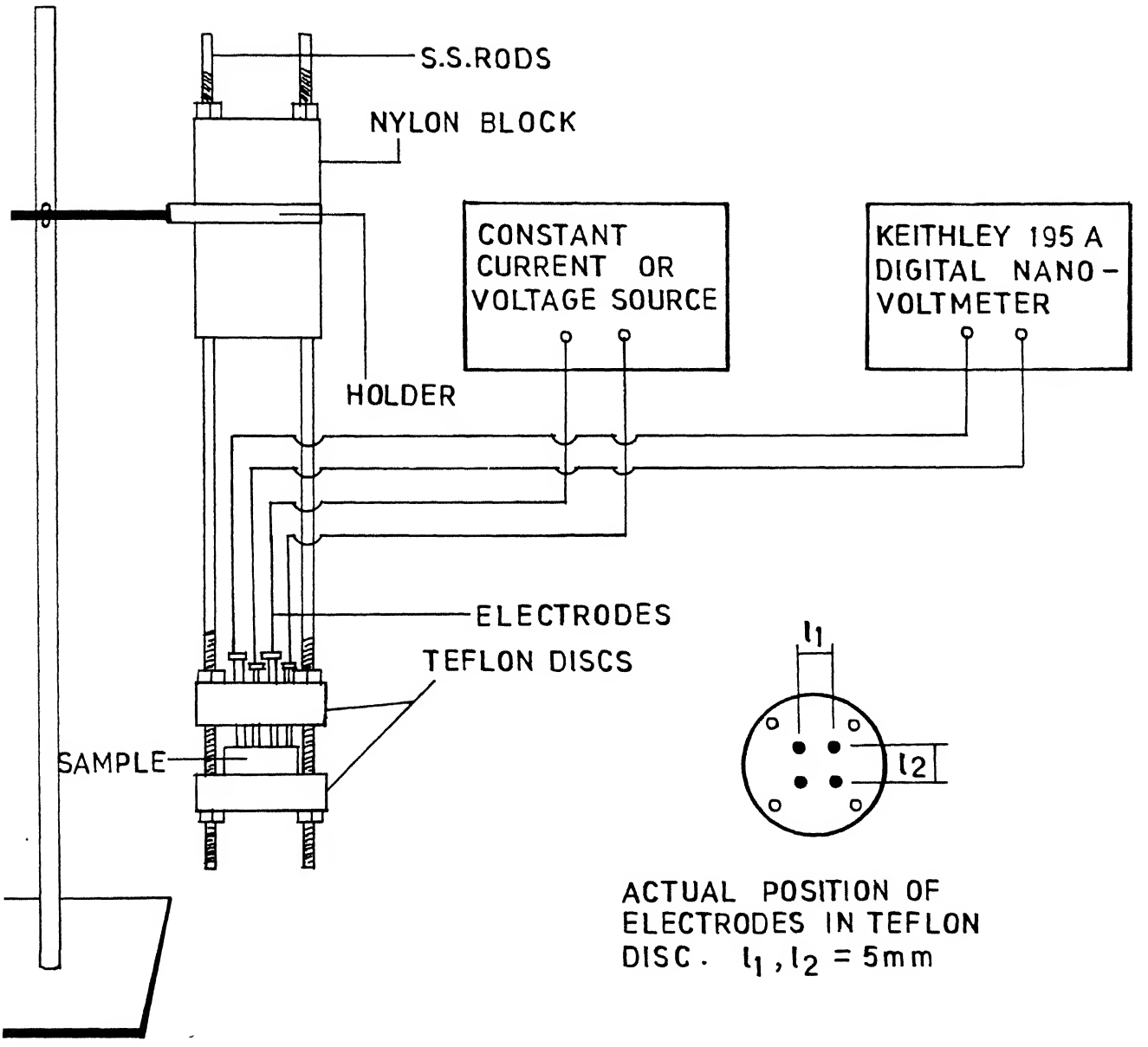

FIG. 2.3 SCHEMATIC DIAGRAM FOR FOUR PROBE RESISTIVITY MEASURMENTS AT ROOM TEMPERATURE

shows the schematic diagram of the sample holder. It essentially consists of two teflon discs, each of dia 2.43 cm and thickness 1.60 cm, and a nylon cylinder, length = 4.746 cm, dia = 2.43 cm. All these discs were coaxially arranged as shown in Fig. 2.3 with the help of a pair of stainless steel rods which provides the necessary support. One of the discs has a flat surface on which rests the sample pellet, while the other teflon disc holds the four electrodes/probes as described below. Four through holes were drilled at the corners of a square on the lower face of the disc. A small cylinderical bush with threads on the inner surface was pushed through each of these four holes. Electrodes were made in the form of screws with pointed tips and were tightened in each of the four cylindrical bushes. The sample was kept over the upper flat face of the lower teflon disc and good electrical contacts were ensured by tightening the individual screw-type electrodes. The nylon cylinder was for fixing the samples holder with a laboratory stand.

2.4.2 Resistivity Measurements

Figure 2.3 shows the block diagram of the set up used for resistivity measurement. The voltage across a pair of probes was measured with a Keithley-181 nanovoltmeter while a known current was passed through the other pair of probes by means of a precision current/voltage source (Knick model - West Germany).

Before loading the samples for resistivity measurement, the flat surfaces of the cylindrical pellets were polished on different grades of fine polishing papers to remove any surface contamination and also to obtain parallel and smooth surfaces. The sample was then fixed between the electrodes and lower teflon disc. Any of the two electrodes on the same side were selected as current terminals and the other two as voltage terminals. Depending upon the resistance of the sample, current often in the range of 1 μA to 1 mA was passed. The voltage developed was measured by the nanovoltmeter. The thickness of the sample was measured with the help of a slide callipers. From the thickness, current passed and the measured voltage, the resistivity of the sample was calculated.

2.5 MEASUREMENT OF ELECTRICAL RESISTANCE BELOW ROOM TEMPERATURE:

2.5.1 Sample Holder

A relatively simple sample holder was made for this purpose (See Fig. 2.4). It consists of a teflon disc (dia. 2.43 cm, thickness = 1.6 cm), a nylon cylinder (length = 4.746 cm, dia = 2.43 cm), and two stainless steel rods. Threads were cut in the stainless steel rods and nuts were used to hold the teflon discs and the nylon cylinder in their respective positions. This entire assembly can be enclosed in a quartz tube which can be evacuated. The electrical levels for thermocouple, voltage and current probes were taken out through holes in the

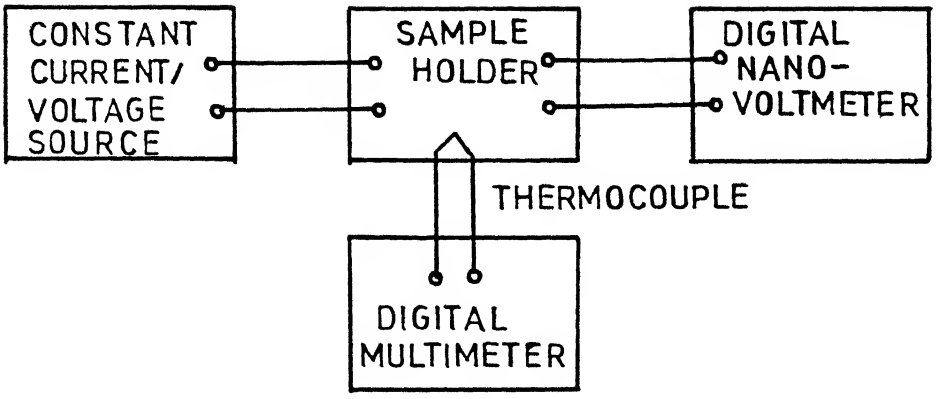

(a)

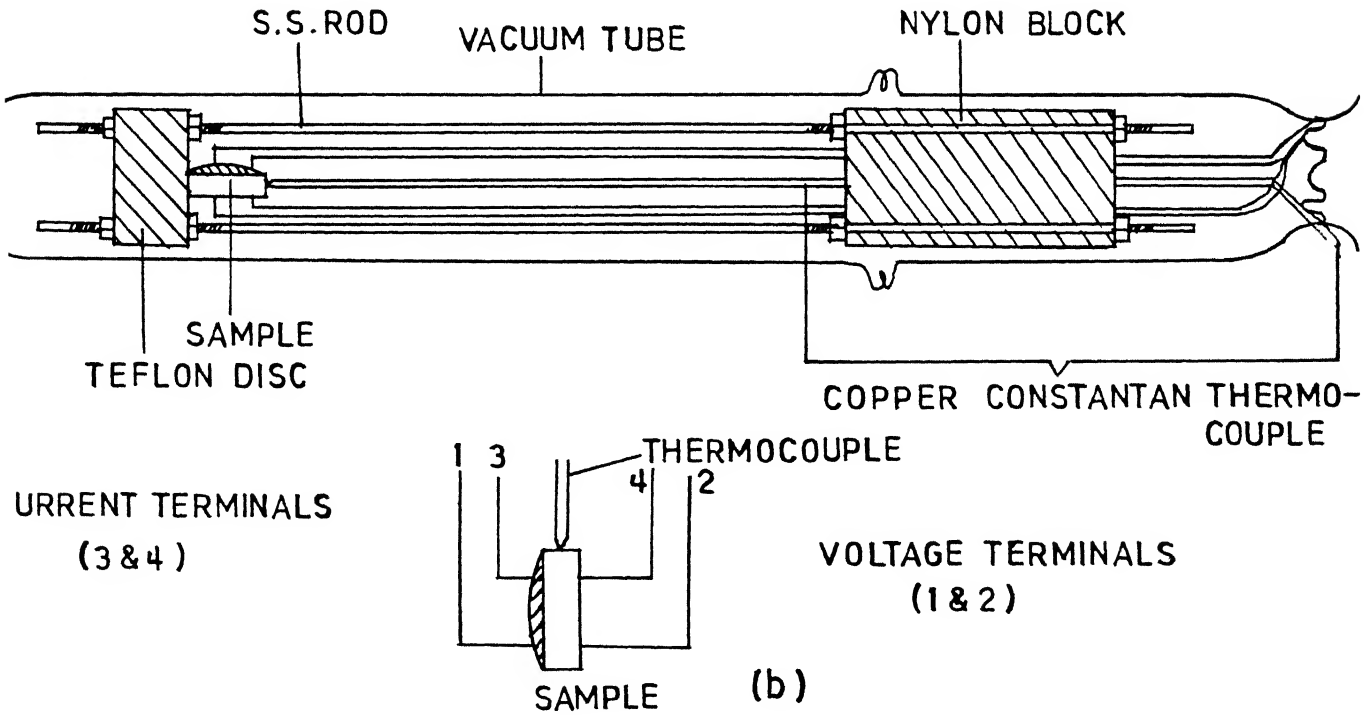

(b)

2.4 (a) BLOCK DIAGRAM (b) SAMPLE HOLDER FOR FOUR TERMINAL RESISTANCE MEASUREMENT AT LIQUID NITROGEN TEMPERATURE

quartz tube and sealed subsequently by araldite.

2.5.2 Experimental Setup and Measurements

The experimental setup is shown schematically in Fig. (2.4). The pellet was first polished with different grades of fine polishing papers and then cleaned properly with acetone. The four-terminal method was used for measurement of electrical resistance. Four thin copper wires were connected with the sample, two on each side, with the help of silver paint. One from each side was taken as current terminals, and the remaining two as voltage terminals as shown in Fig. (2.4).

Copper-constantan thermocouple was used for measuring the temperature. The reference junction was kept in an oil bath whose temperature was measured precisely ($\pm$ 0.1^{o}C) using a thermometer. Two copper wires were taken from the reference junction to measure the thermo emf. of the thermocouple.

The quartz tube was then evacuated to 10^{-2} - 10^{-3} atmospheric pressure and was lowered in a deewar flask filled with liquid nitrogen. The flask was then properly sealed with cotton to minimize the rate of evaporation of LN_2. Due to natural evaporation of LN_2, the temperature increased very slowly with time. Resistance at any temperature was calculated from the measured voltage corresponding to a certain value of the current passed through the sample.

2.6 MEASUREMENT OF DIELECTRIC CONSTANT:

2.6.1 Sample Holder

The sample holder for measuring dielectric constant was specially equipped for recording measurements under vacuum. Vacuum is needed for working at low temperatures. Figure (2.5) shows the schematic diagram of the sample holder. It consists of an inner body which is enclosed by a quartz tube and can be evacuated. The inner body comprises of three identical Lava discs. Lava material can be machined easily, it can withstand both high and low temperatures and is a good electrical insulator. Each Lava disc has nine through holes. Eight holes are located symmetrically along the circumference and one is at the centre of the disc. At the centre of each Lava disc indentions were made so that the spring and the quartz tube can be fixed as shown in Fig. (2.5). Two stainless steel rods which provide mechanical support to the sample holder were inserted through two of the diametrically opposite holes. A third hole was used for inserting the thermocouple (Chromel-alumel for high temperatures and copper-constantan for low temperatures). The fourth hole was used for taking one of the silver leads brazed onto the lower stainless steel electrode. The other silver wire lead brazed to the upper stainless steel electrode, was passed through the quartz tube and spring, eventually carrying out of the central hole of the bakelite block.

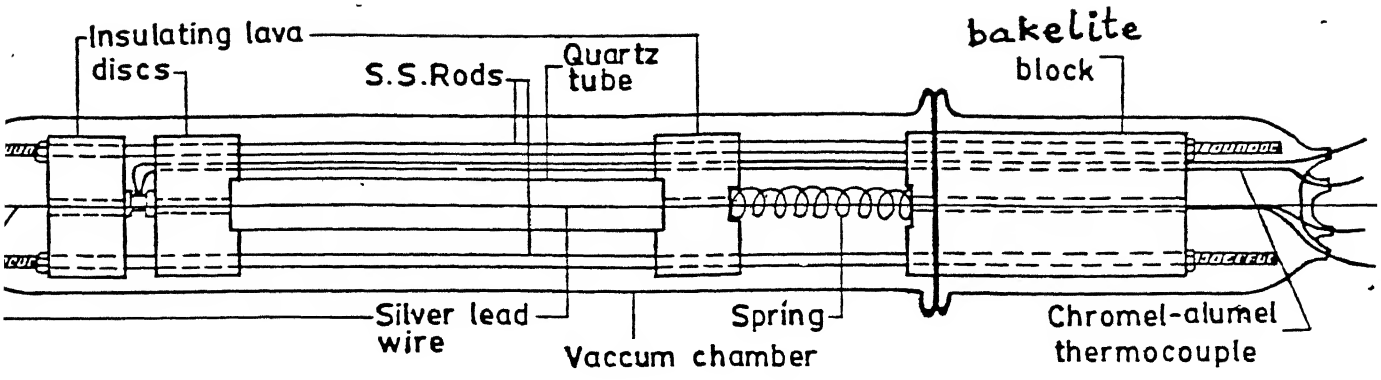

Figure 2.5(a): SAMPLE HOLDER FOR DIELECTRIC CONSTANT MEASUREMENTS.

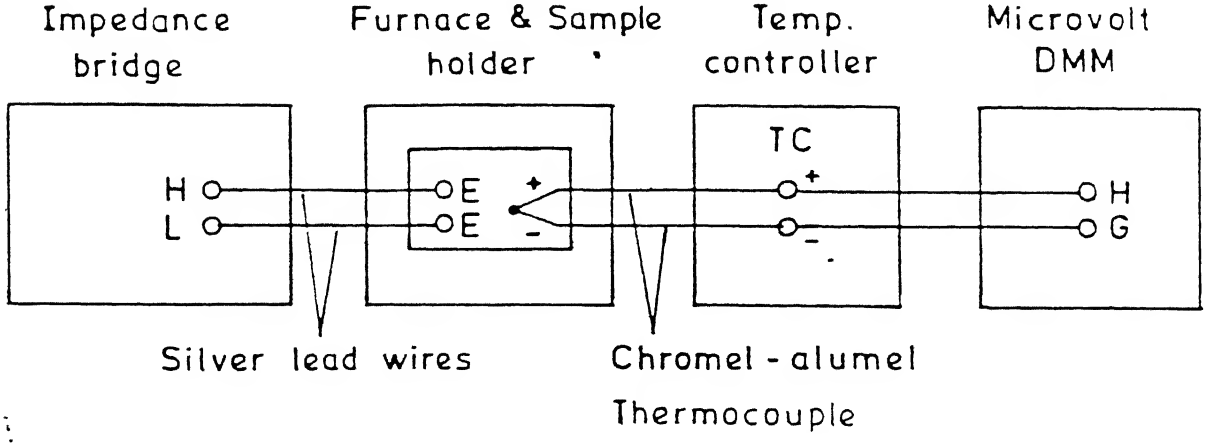

Figure 2.5(b): BLOCK DIAGRAM FOR DIELECTRIC CONSTANT MEASUREMENTS.

The spring located outside the furnace exerts sufficient uniform pressure required for point to point contact between the electrodes and the sample. Various types of electrodes, other than stainless steel discs were also used for better results. For example, gold was deposited on the sample, it was then covered with two platinum foils. The sample was finally placed between two stainless steel electrodes. In some cases silver paint was also been used.

After machining, the Lava disc were heated to 1000^{o}C slowly and kept at that temperature for 2 hours inside a furnace before it was furnace cooled. This kind of heat treatment is necessary to harden the Lava disc and also to remove any moisture which might be present. The effect of the latter is to increase the resistivity of the Lava disc significantly.

2.6.2 Measurements

This work involved measurements of electrical resistance, capacitance, reactance, impedance and the phase angle θ in the frequency range 5 Hz to 13 MHz. For high temperature measurements, the sample was kept inside a furnace whose temperature was controlled using a temperature controller (Indotherm Model 401). A Keithley microvolt DMM-197 was used to measure the thermocouple voltage and hence the temperature. HP-4192A LF impedance analyser was used for measuring various electrical parameters

at different temperatures. This instrument has a wide frequency range of 5 Hz to 13 MHz.

For low temperature measurements the same set up was dipped into a Dewar flask containing liquid nitrogen instead of the furnace. The thermocouple was changed from chromel-alumel to copper-constantan. An oil bath was used as reference junction of the thermocouple.

To measure the various electrical parameters of the sample, the flat surface was first polished with sand paper of various grades. Then various electrodes (as described earlier) were used. Various electrodes were tried for improving electrical contacts which play an important role in these types of measurements. The frequency was monitored and the corresponding electrical parameters were recorded.

CHAPTER - 3

RESULTS AND DISCUSSIONS

3.1 OXYGEN CONTENT DETERMINATION:

Oxygen content of high T_c superconducting $YBa_2Cu_3O_{7-\delta}$ was calculated from the weight loss after each heat treatment. For this purpose, the following assumptions are made:

(i) Mixing in the agate mortar is uniform, so that the loss of material due to transferring and handling does not affect the proportions of Y_2O_3, $BaCO_3$ and CuO.

(ii) None of the ingradients had absorbed water. This has been tested particularly for $BaCO_3$ which was suspected to contain absorbed water, by heating it at 150°C for 2 hrs. and then recording the weight loss. No measurable weight loss was observed.

(iii) The material obtained after the heat treatment is a single phase, i.e. the oxygen content is same or even if phases are different, atleast the oxygen content is same. Since this assumption in general is not true, the measured oxygen content may be taken as the average oxygen content of the sample, and not the true oxygen content of a particular phase present in the sample.

(iv) All the ingredients are stoichiometric, i.e. the cation to anion ratio is in accordance with their chemical formulae

(v) All the carbon present in $BaCO_3$ was decomposed and released out in the form of a mixture of carbon monoxide and carbondioxide at the time of solid state reaction.

Two types of heat treatment given to the samples are:

(1) Solid state reaction, and

(2) Sintering.

3.1.1 Oxygen Content Determination after Solid State Reaction

The synthesis of "123" compound, viz., $YBa_2Cu_3O_x$, is assumed to proceed via the following solid state reaction:

$$YO_{3/2} + 2BaCO_3 + 3CuO \xrightarrow{900^oC} YBa_2Cu_3O_x + 2(CO/CO_2)$$

where $BaCO_3$ is supposed to decompose into BaO and release carbon in the form of CO/CO_2 mixture. Thus some oxygen and the entire carbon of $BaCO_3$ is released out, and whatever remains in the platinum boat is $YBa_2Cu_3O_x$ where x is to be determined. To do this a known amount of material containing $YO_{3/2}$, $BaCO_3$ and CuO in the ratio of 1:2:3 moles respectively was thoroughly mixed and pelletized. This pellet was then kept in a small platinum boat whose empty mass was predetermined and the combined weight of boat and pellet was taken. This boat and pellet assembly was then heated at 900^oC for 12 hours, followed by cooling and weighing. Let

m_i = initial mass of the pellet

m_f = final mass of the pellet (i.e. after heat treatment)

W_r = molecular weight of the reactants (746 gms)

W = sum of the atomic weights of 1Y, 2Ba and 3Cu

= $1\ W_Y + 2\ W_{Ba} + 3\ W_{Cu}$

= 554 gms.

Then the oxygen content x in $YBa_2Cu_3O_x$ is given by

$$x = \frac{1}{16}\left[\frac{W_r\, m_f}{m_i} - W\right]$$

The maximum possible error in the values of x listed in the Table 3.2 can be calculated as below:

$$\frac{\delta x}{x} = \frac{W_r \delta m_f + W \delta m_i}{W_r m_f - m_i W} + \frac{\delta m_i}{m_i}$$

Using a typical value of $x = 6.\dot{4}$, $m_f = 1.2$ gm, $m_i = 1.4$ gm, $\delta m_i = \delta m_f = 0.005$ gm (even though the actual accuracy of weight measurement was 0.0001 gm).

We get,

$$\frac{\delta x}{x} = 0.00546 + 0.000357$$

$$= 0.0058$$

$$\Rightarrow \delta x = (0.0058)6.\dot{4}$$

$$= 0.0\dot{4}$$

Details of the heat treatment during solid state reaction along with the corresponding oxygen contents are given in Table 3.1. Table 3.2 gives the break-up in terms of initial and final weight of pellets and oxygen content.

3.1.2 Oxygen Content Determination after Sintering

During sintering $YBa_2Cu_3O_{x'}$ is expected to release some of its oxygen according to the following solid state reaction:

$$YBa_2Cu_3O_{x'} \xrightarrow[940^{o}C]{\text{Sintering}} Y\,Ba_2Cu_3O_x + nO_2\uparrow$$

where the unknown quantities, n and x can be determined. Let m_i and m_f be the initial and final masses of the pellet, W the sum of atomic weights of 1Y, 2Ba and 3Cu, i.e.

$W = 88.9 + 2 \times 137.3 + 3 \times 63.5 = 554$ gm, and

$W_o = 16$, the atomic weight of oxygen, then the value of oxygen content x in the final product is given by

$$x = \frac{x' m_f - 34.6 \Delta m}{m_i}$$

where $\Delta m = m_i - m_f$ is the weight loss of the pellet during sintering. The calculated values of x from the above equation are listed in Table 3.4. The maximum possible error in the values of x listed in this table can be calculated as

below:

$$\frac{\delta x}{x} = \left[\frac{x' \delta m_f + 34.6\, \delta(\Delta m)}{(x' m_f - 34.6\, \Delta m)} + \left(\frac{\delta m_i}{m_i}\right) \right.$$

Using typical values of $x' = 6.4$, $m_f \simeq m_i \simeq 1.2$ gm, $\delta m_f = \delta m_i = 0.0005$ gm (even though the actual accuracy of weight measurement was 0.0001 gm), $\Delta m \simeq 0.02$ and $\delta(\Delta m) = \delta[m_i + m_f] = \delta m_i + \delta m_f = 0.001$ gm, we get,

$$\frac{\delta x}{x} = \frac{0.00325 + .0346}{(7.8 - 34.6(0.02))} + \frac{0.0005}{1.2}$$

$$= 0.0053 + 0.0004$$

$$= 0.0057$$

$$\delta x = (0.0057)x$$

$$= 0.0365$$

or $\delta x \simeq 0.04$.

Details of sintering along with the corresponding final oxygen contents are given in Table 3.3.

3.2 X-RAY DIFFRACTION ANALYSIS:

The d_{hkl} values of various peaks in the observed XRD pattern were calculated using the corresponding θ values and the Bragg's law:

Table 3.1 : Details of Heat Treatment and Oxygen Content (x) during Solid State Reaction in $YBa_2Cu_3O_x$

Sample No.	Heat Treatment						Oxyg cont (x
	Reaction Temperature (^oC)	Reaction time (hrs)	Atmosphere	Time required to raise the furnace temperature (hrs)	Special Treatments (if any)	Sample cooling mode	
1.	900	12	Oxygen	$5\frac{1}{2}$	Oxygen flow rate: 8-10 bubbles/min started at 600^oC and stopped after the sample is again cooled to 600^oC	Furnace cooled	6.4
2.	900	12	Air	3	After 12 hrs. Sample was kept near furnace window for 2-3 mins. and again inserted into 900^oC zone inside	Furnace cooled	6.8
3.	900	12	Air	$3\frac{1}{4}$	--	Furnace cooled	6.6
4.	900	12	Air	$4\frac{1}{2}$	After 12 hours sample was kept near furnace window for 3-5 mins and again inserted into 900^oC zone	Furnace cooled	7.3
5.	900	12	Air	5	--	Furnace cooled	6.6

Continued....

	Heat Treatment						
Sample No.	Reaction Temperature (^{o}C)	Reaction time (hrs)	Atmosphere	Time required to raise the furnace temperature (hrs)	Special Treatments (if any)	Sample Cooling mode	Oxyge conte (x)
6.	900	12	Air	$4\frac{1}{2}$	--	Furnace cooled	6.93
7.	900	12	Air	$5\frac{1}{2}$	--	Furnace cooled	6.82
8.	900	12	Air	4	--	Furnace cooled	6.66
9.	900	12	Air	5	--	Furnace cooled	6.72

Table 3.2 : Details of Oxygen Content (x) Calculations after Solid State Reaction

Sample No.	Weight of the boat (gm)	Initial weight of the boat and pellet (gm)	Weight of boat and pellet after heat treatment (gm)	Initial weight of the pellet m_i (gm)	Weight of the pellet after heat treatment m_f (gm)	Oxygen content x
1.	0.8178	2.2494	2.0786	1.4316	1.2608	6.44
2.	0.8179	2.2424	2.0847	1.4245	1.2668	6.84
3.	17.1647	18.5945	18.4298	1.4298	1.2651	6.63
4.	0.8126	2.2702	2.1259	1.4576	1.3133	7.39
5.	0.7915	2.2431	2.0756	1.4516	1.2841	6.62
6.	0.8187	2.2661	2.1082	1.4474	1.2895	6.93
7.	0.8190	2.2612	2.1015	1.4422	1.2825	6.82
8.	0.7942	2.2072	2.0455	1.413	1.2507	6.66
9.	0.8128	2.2469	2.0847	1.4341	1.2719	6.72

Table 3.3 : Details of Sintering with Corresponding Oxygen Content (x) in $YBa_2Cu_3O_x$

Sample No.	Heat Treatment						Oxygen content (x)
	Sintering temperature (^oC)	Sintering time (hr)	Atmosphere	Time required for raising the temperature (from room temperature) (hr)	Special treatment (if any)	Cooling mode	
1.	940	12	Oxygen	6	Oxygen flow rate: 6-8 bubbles per min. Started at 600°C and stopped when temperature dropped to 600°C	Furnace cooled	6.37
2.	940	12	Air	6	After 12 hrs sample was kept near an open window of the furnace	Furnace cooled	6.36
3.	940	12	Air	$5\frac{1}{2}$	--	Furnace cooled	6.34
4.	940	12	Air	4	--	Furnace cooled	6.31
5.	940	12	Air	6	--	Furnace cooled	6.05
6.	940	12	Air	5	After 12 hrs sample was pulled near one of the furnace windows which was open, for 1 hr	Taken out of furnace and quenched to room temperature	6.03

Table 3.3 (Continued):

Sample No.	Heat Treatment						Oxygen content (x)
	Sintering temperature (^{o}C)	Sintering time (hr)	Atmosphere	Time required for raising the temperature (from room temperature) (hr)	Special treatment (if any)	Cooling mode	
7.	940	12	Air	6	After 12 hrs. sample was pulled near an open furnace window and kept for ~30 mins.	taken out of furnace and quenched to room temperature	5.82
8.	940	12	Air	8	--	Taken out of furnace and quenched to room temperature	5.68
9.	940	12	Air	$5\frac{1}{2}$	--	Taken out of furnace and quenched to room temperature	5.67

Table 3.4 : Details of the Calculation of Oxygen Content (x) in $YBa_2Cu_3O_x$ after Sintering

Sam-Ple No.	Oxygen content before sinter-ing (x')	Weight of boat (gm)	Initial weight of boat and pellet (gm)	Weight of boat and pellet after sin-tering (gm)	Initial mass of pellet m_i (gm)	Final mass of pellet m_f (gm)	Mass loss m (gm)	Oxygen content (x)
1.	6.44	0.8177	2.0283	2.0263	1.2106	1.2086	0.0020	6.37
2.	6.84	0.8180	2.0470	2.0324	1.2290	1.2144	0.0146	6.36
3.	6.63	0.7917	2.0082	1.9997	1.2165	1.2080	0.0085	6.34
4.	7.39	0.8113	2.0809	2.0483	1.2696	1.2370	0.0326	6.31
5.	6.62	0.7950	2.0536	2.0363	1.2586	1.2413	0.0173	6.05
6.	6.93	0.8190	2.0789	2.0515	1.2599	1.2325	0.0274	6.03
7.	6.82	0.8230	2.0794	2.0491	1.2564	1.2261	0.0303	5.82
8.	6.66	0.7948	2.0208	1.9910	1.2260	1.1962	0.0298	5.68
9.	6.72	0.8129	2.0590	2.0275	1.2461	1.2146	0.0315	5.67

$$d_{hkl} = \frac{\lambda}{2 \sin \theta} \qquad (1)$$

where

d_{hkl} = interplanar distance

θ = Bragg's angle

λ = wavelength used (For Cu K_α = 1.5418 Å)

Each of the peaks was indexed for orthorhombic or tetragonal structure by comparing it with the reported values (29). The lattice constants were calculated precisely by using Cohen's method. It was found that for any crystal, the most accurate value of the lattice parameter is found by plotting the value of the parameter for each reflection, against a particular function, which depends on the kind of camera used, and extrapolating to a value at $\theta = 90^{\circ}$. This procedure has two advantages: (i) systematic errors are eliminated by selection of the proper extrapolation function and (ii) random errors are reduced in proportion to the skill of the investigator in drawing the best straight line through the experimental points. Cohen proposed in effect, that the least-squares method be used to find the best straight line so that the random errors would be minimised in a reproducible and objective manner. We define:

$$\frac{\Delta d}{d_{hkl}} = K \cos^2 \theta \qquad (2)$$

as the extrapolation function.

(The factor 10 is introduced into the definitions of the quantities A and solely to make the coefficients of various terms in the normal equations of the same order of magnitude). A is the Drift constant which is a measure of total systematic error involved in the determination.

The experimental values of $\mathrm{Sin}^2\theta$, α, β, γ, and δ are now substituted into Eq. (4) for each higher ($2\theta > 40^\circ$) order line used in the determination. This gives n (= number of lines considered) equations in the unknown constants A, B, C and D and these equations can be solved for the most probable values of A, B, C and D by the method of least squares:

$$\begin{aligned}
\Sigma\delta \sin^2\theta &= A\,\Sigma\delta^2 + B\,\Sigma\alpha\delta + C\,\Sigma\beta\delta + D\,\Sigma\gamma\delta \\
\Sigma\alpha \sin^2\theta &= A\,\Sigma\alpha\delta + B\,\Sigma\alpha^2 + C\,\Sigma\alpha\beta + D\,\Sigma\alpha\gamma \\
\Sigma\beta \sin^2\theta &= A\,\Sigma\beta\delta + B\,\Sigma\alpha\beta + C\,\Sigma\beta^2 + D\,\Sigma\beta\gamma \\
\Sigma\gamma \sin^2\theta &= A\,\Sigma\delta\gamma + B\,\Sigma\alpha\gamma + C\,\Sigma\beta\gamma + D\,\Sigma\gamma^2
\end{aligned} \tag{5}$$

Similarly for tetragonal lattice, Eq. (4) can be written as:

$$\mathrm{Sin}^2\theta = A\,\delta + B\,\alpha + C\,\beta \tag{6}$$

where,

$$A = D/10,\ \delta = 10\ \mathrm{Sin}^2 2\theta,\ B = \frac{\lambda^2}{4a^2},\ C = \frac{\lambda^2}{4c^2}$$

$$\alpha = h^2 + k^2, \beta = l^2 \quad .$$

The normalized equations are:

$$\begin{aligned} \Sigma\delta \sin^2 \theta &= A\,\Sigma\delta^2 + B\,\Sigma\alpha\delta + C\,\Sigma\beta\alpha \\ \Sigma\alpha \sin^2 \theta &= A\,\Sigma\alpha\delta + B\,\Sigma\alpha^2 + C\,\Sigma\alpha\beta \\ \Sigma\beta \sin^2 \theta &= A\,\Sigma\beta\delta + B\,\Sigma\beta\alpha + C\,\Sigma\beta^2 \end{aligned} \qquad (7)$$

Details of 2θ, $\sin\theta$, h, k, l, d_{obs}, d_{cal}, a, b, c for sample numbers 1 to 9 are given in Tables 3.5 to 3.13. The system of oxides studied are mostly multiphasic. They are generally a mixture of orthorhombic and tetragonal phases. Separation of these two phases is very difficult, because the peaks corresponding to these in the XRD pattern are located very close to each other. For example, the peaks corresponding to orthorhombic sample #1, due to planes (0 1 3) and {(1 1 0), (1 0 3)} are at 32.47° and 32.67° respectively, and that of tetragonal sample #9 due to planes (0 1 3) and (1 1 0) are at 32.47° and 32.68° respectively. Thus it is very difficult to separate out the contribution due to orthogonal and tetragonal phases in the intermediate samples. Figure 3.4 shows how the peaks near 32.47° and 32.67° change with oxygen deficiency $\delta = 7-x$ where x is the oxygen content in $YBa_2Cu_3O_x$. It has been found for the orthorhombic phase, that the peak near 32.67° has higher intensity, while, for the tetragonal phase the peak near

32.47^{o} has higher intensity. Therefore, the intensity ratio between the two peaks was calculated to estimate the relative amount of orthorhombic and tetragonal phases present in a sample. Intensities corresponding to each of the peaks were calculated by tracing the intensity peaks on a graph paper and thereby finding the area under the curve. The details are given in Table 3.14.

Figure 3.5 shows the variation of the intensity ratio I_1/I_2 with oxygen deficiency δ, of the sample.

Table 3.5 : Details of Lattice Parametter Calculation for $Y_1Ba_2Cu_3O_x$ with X = 6.37

Sample # 1

λ_o (Cu K_α) = 1.5418 Å (Radiation used - CuK_α)

Line No.	2θ	Sinθ	d^*_{obs} Å	h k l	Lattice Parameters a Å	b Å	c Å	Drift constant A	d^+_{cal} Å
1.	22.76	0.197	3.907	0 1 0					3.884
				0 0 3					3.883
2.	27.48	0.237	3.246	0 1 2					3.231
3.	27.72	0.240	3.218	1 0 2					3.196
4.	30.76	0.265	2.907	0 0 4					2.912
5.	32.47	0.280	2.757	0 1 3					2.746
6.	32.67	0.281	2.741	1 1 0					2.725
				1 0 3					2.724
7.	36.32	0.312	2.473	1 1 2					2.468
8.	38.12	0.327	2.361	0 1 4					2.330
				0 0 5					2.330
9.	40.28	0.343	2.239	1 1 3					
10.	46.56	0.395	1.951	0 0 6	3.823(3)	3.883(7)	11.649(7)	-0.000167	1.942
				0 2 0					1.941
11.	47.52	0.403	1.913	2 0 0					1.911
12.	51.40	0.434	1.778	1 1 5					1.771
13.	52.68	0.444	1.737	0 1 6					1.738
				1 0 6					1.731
14.	53.28	0.448	1.719	1 2 1					1.713
				2 1 0					1.715
15.	58.20	0.486	1.585	1 2 3					1.581
				1 1 6					1.582
16.	58.64	0.490	1.574	2 1 3					1.569
17.	62.44	0.518	1.487	1 2 4					1.488
18.	62.80	0.521	1.480	2 1 4					1.478
				2 0 5					1.478
19.	68.16	0.560	1.376	0 2 6					1.373
20.	68.68	0.564	1.367	2 2 0					1.362
				2 0 6					1.362

* $d_{obs} = \frac{\lambda}{2 \sin\theta}$

\+ $d_{cal} = (h^2/a^2 + k^2/b^2 + l^2/c^2)^{-1/2}$

Table 3.6 : Details of Lattice Parameter Calculation for $Y_1Ba_2Cu_3O_x$ with x = 6.36

Sample # 2

λ_o (Cu K_α) = 1.5418 Å (Radiation used - CuK_α)

Line No.	2θ	Sinθ	d_{obs} Å	h k l	Lattice Parameters a Å	b Å	c Å	Drift constant Å	d_{cal} Å
1.	22.80	0.198	3.899	0 0 3					3.89
				0 1 0					3.88
2.	32.49	0.280	2.756	0 1 3					2.75
3.	32.73	0.282	2.736	1 1 0					2.72
				1 0 3					2.72
4.	36.28	0.312	2.470	1 1 2					2.47
5.	38.60	0.331	2.332	0 1 4					2.33
				0 0 5					2.33
6.	40.36	0.344	2.240	1 1 3					2.23
7.	46.60	0.396	1.949	0 0 6					1.94
				0 2 0	3.824(5)	3.889(2)	11.673(3)	-0.00007817	1.94
8.	47.48	0.405	1.904	2 0 0					1.91
9.	51.48	0.434	1.775	1 1 5					1.77
10.	52.60	0.443	1.740	0 1 6					1.74
				1 0 6					1.73
11.	53.36	0.449	1.717	1 2 1					1.71
				2 1 0					1.71
12.	58.24	0.487	1.584	1 2 3					1.58
				1 1 6					1.58
13.	58.72	0.490	1.572	2 1 3					1.57
14.	68.12	0.560	1.377	0 2 6					1.37
15.	68.76	0.565	1.365	2 2 0					1.36
				2 0 6					1.36

Table 3.7 : Details of Lattice Parameter Calculation for $Y_1Ba_2Cu_3O_x$ with X = 6.34

Sample # 3

λ_o (Cu K_α) = 1.5418 Å (Radiation used - CuK_α)

ıe	2θ	Sinθ	d_{obs} Å	h k l	Lattice parameters a Å	b Å	c Å	Drift constant Å	d_{cal} Å
	22.84	0.198	3.893	0 0 3					3.902
				0 1 0					3.901
	27.88	0.241	3.200	0 1 2					3.246
				1 0 2					3.207
	29.20	0.252	3.058						
	32.50	0.280	2.755	0 1 3					2.759
	32.72	0.282	2.737	1 1 0					2.734
				1 0 3					2.735
	36.36	0.312	2.471	1 1 2					2.477
	38.56	0.330	2.335	0 1 4					2.341
				0 0 5					2.341
	40.44	0.346	2.230	1 1 3	3.834(0)	3.900(7)	11.704(8)	-0.000125	2.239
	46.48	0.396	1.946	0 0 6					1.951
				0 2 0					1.950
	47.56	0.403	1.912	2 0 0					1.917
	51.28	0.433	1.782	1 1 5					1.778
	52.72	0.444	1.736	0 1 6					1.745
				1 0 6					1.738
	58.28	0.487	1.573	1 2 3					1.588
				1 1 6					1.588
	58.68	0.490	1.573	2 1 3					1.574
	62.84	0.521	1.479	2 1 4					1.483
				2 0 5					1.483
	68.16	0.560	1.376	0 2 6					1.379
	68.76	0.565	1.365	2 2 0					1.367
				2 0 6					1.367

ble 3.8 : Details of Lattice Parameter Calculation for $Y_1Ba_2Cu_3O_x$ with X = 6.31

Sample # 4

λ_o (Cu K_α) = 1.5418 Å (Radiation used - CuK_α)

ne	2θ	Sinθ	d_{obs} Å	h k l	Lattice Parameter a Å	b Å	c Å	Drift constant Å	d_{cal} Å
									3.883
	28.80	0.198	3.900	0 1 0					3.887
				0 0 3					3.232
	27.48	0.236	3.245	0 1 2					3.197
	27.80	0.240	3.209	1 0 2					2.747
	32.48	0.289	2.756	0 1 3					2.725
	32.68	0.281	2.740	1 1 0					2.728
				1 0 3					2.468
	36.36	0.312	2.470	1 1 2					2.331
	38.32	0.328	2.349	0 1 4					2.332
				0 0 5					2.231
	40.28	0.344	2.238	1 1 3					1.990
	45.80	0.389	1.981	1 1 4					1.941
10.	46.64	0.396	1.947	0 2 0	3.824(0)	3.882(9)	11.659(7)	-0.000126	1.943
				0 0 6					1.912
11.	47.28	0.401	1.922	2 0 0					1.772
12.	51.40	0.434	1.778	1 1 5					1.738
13.	52.60	0.443	1.730	0 1 6					1.732
				1 0 6					1.581
14.	58.16	0.486	1.586	1 2 3					1.582
				1 1 6					1.569
15.	58.68	0.490	1.573	2 1 3					1.492
16.	62.16	0.516	1.493	0 2 5					1.478
17.	62.72	0.520	1.4813	2 1 4					1.478
				2 0 5					1.421
18.	65.52	0.541	1.424	1 1 7					1.374
19.	68.16	0.560	1.375	0 2 6					1.362
20.	68.76	0.564	1.365	2 2 0					1.363
				2 0 6					

Table 3.9 : Details of Lattice Parameter Calculation for $Y_1Ba_2Cu_3O_x$ with x = 6.05

Sample # 5

λ_o (Cu K_α) = 1.5418 Å (Radiation used - CuK_α)

Line No.	2θ	Sinθ	d_{obs} Å	h k l	Lattice Parameters a Å	b Å	c Å	Drift constant Å	d_{cal} Å
1.	32.50	0.280	2.755	0 1 3					2.75
2.	32.73	0.282	2.737	1 1 0					2.73
				1 0 3					2.73
3.	35.64	0.306	2.519						
4.	38.36	0.329	2.347	0 1 4					2.33
				0 0 5					2.33
5.	40.32	0.345	2.237	1 1 3					2.23
6.	46.72	0.397	1.942	0 0 6					1.94
				0 2 0	3.846(2)	3.891(5)	11.686(7)	-0.000736	1.94
7.	47.44	0.402	1.916	2 0 0					1.92
8.	51.40	0.434	1.778	1 1 5					1.77
9.	58.28	0.487	1.584	1 2 3					1.58
				1 1 6					1.58
10.	58.64	0.490	1.574	2 1 3					1.57
11.	62.40	0.518	1.488	1 2 4					1.49
12.	62.64	0.520	1.483	2 1 4					1.48
				2 0 5					1.48
13.	68.68	0.564	1.367	2 2 0					1.36
				2 0 6					1.36

Table 3.10 : Details of Lattice Parameter Calculation for $Y_1Ba_2Cu_3O_x$ with x = 6.03

Sample #6

λ_o (Cu K_α) = 1.5418 Å (Radiation used - CuK_α)

Line No.	2θ	Sinθ	d_{obs} Å	h k l	Lattice Parameters a Å	b Å	c Å	Drift constant A	d_{cal} Å
1.	22.80	0.198	3.900	0 0 3					3.886
				0 1 0					3.887
2.	27.80	0.240	3.209	1 0 2					3.201
				0 1 2					3.234
3.	29.28	0.252	3.058						
4.	32.53	0.280	2.752	0 1 3					2.748
5.	32.73	0.282	2.736	1 1 0					2.728
				1 0 3					2.728
6.	38.56	0.331	2.339	0 1 4					2.332
				0 0 5					2.332
7.	40.32	0.345	2.237	1 1 3					2.333
8.	45.56	0.388	1.991						
9.	46.68	0.396		0 0 6					1.943
				0 2 0					1.944
10.	47.56	0.403	1.913	2 0 0	3.830(3)	3.887(0)	11.659(3)	-0.000107	1.915
11.	51.44	0.434	1.776	1 1 5					1.773
12.	52.60	0.443	1.740	0 1 6					1.733
				1 0 6					1.738
13.	53.24	0.441	1.730	1 2 1					1.714
				2 1 0					1.718
14.	58.24	0.487	1.584	1 2 3					1.583
				1 1 6					1.583
15.	58.64	0.490	1.574	2 1 3					1.571
16.	62.60	0.520	1.484	2 1 4					1.480
				2 0 5					1.480
17.	68.16	0.560	1.376	0 2 6					1.374
18.	68.76	0.565	1.365	2 2 0					1.364
				2 0 6					1.364

Table 3.11 : Details of Lattice Parameter Calculation for $Y_1Ba_2Cu_3O_x$ with x = 5.82
Sample # 7
λ_o (Cu K_α) = 1.5418 Å (Radiation used - CuK_α)

Line No.	2θ	Sinθ	d_{obs} o A	h k l	Lattice Parameters a Å	c Å	Drift constant A	d^*_{cal} o A
1.	22.72	0.197	3.913	0 0 3				3.899
				0 1 0				3.855
2.	26.48	0.229	3.365					
3.	27.72	0.240	3.218	0 1 2				3.220
4.	29.36	0.253	3.042					
5.	30.60	0.264	2.921	0 0 4				2.924
6.	32.56	0.280	2.750	0 1 3				2.742
7.	32.68	0.281	2.740	1 1 0				2.728
8.	35.72	0.307	2.513					
9.	36.28	0.311	2.476	1 1 2				2.472
10.	38.48	0.330	2.339	0 0 5				2.339
11.	40.28	0.344	2.238	1 1 3	3.857(8)	11.696(7)	-0.000046	2.235
12.	51.40	0.433	1.777	1 1 5				1.776
13.	58.24	0.487	1.584					
14.	58.56	0.489	1.576	1 2 3				1.578
15.	62.40	0.518	1.488	0 2 5				1.488
				1 2 4				1.485
16.	68.40	0.562	1.371	0 2 6				1.374
17.	68.76	0.565	1.365	2 2 0				1.365

$^*d_{cal} = (h^2+k^2/a^2 + l^2/c^2)^{-1/2}$

Table 3.12: Details of Lattice Parameter Calculation for $Y_1Ba_2Cu_3O_x$ with x = 5.68

Sample # 8

λ_o (Cu K_α) = 1.5418 Å (Radiation used - CuK_α)

Line No.	2θ	Sinθ	d_{obs} Å	h k l	Lattice Parameters a Å	c Å	Drift constant A	d_{cal} Å
1.	22.44	0.196	3.962	0 0 3				3.926
				0 1 0				3.884
2.	27.36	0.237	3.260	0 1 2				3.242
3.	29.76	0.257	3.000					
4.	30.28	0.261	2.952					
5.	30.48	0.263	2.933	0 0 4				2.944
6.	32.48	0.260	2.757	1 1 3				2.761
7.	32.72	0.281	2.737	1 1 0				2.746
8.	38.32	0.328	2.349	0 0 5				2.355
9.	38.44	0.329	2.342	0 1 4				2.346
10.	40.20	0.341	2.243	1 1 3				2.251
11.	45.52	0.346	2.276					
12.	45.56	0.387	1.991	1 1 4				2.008
13.	46.28	0.393	1.962	0 0 6				1.963
14.	46.96	0.398	1.935	0 2 0	3.884 (0)	11.779 (2)	0.000318	1.942
15.	51.24	0.432	1.783	1 1 5				1.788
16.	57.96	0.485	1.594	1 1 6				1.597
17.	58.98	0.487	1.583	1 2 3				1.588
18.	62.16	0.516	1.493	0 2 5				1.498
				1 2 4				1.496
19.	68.20	0.561	1.375	0 2 6				1.380
20.	68.64	0.564	1.367	2 2 0				1.373

Table 3.13 : Details of Lattice Parameter Calculation for $Y_1Ba_2Cu_3O_x$ with x = 5.67

Sample # 9

λ_o (Cu K_α) = 1.5418 Å (Radiation used - CuK_α)

Line No.	2θ	Sinθ	d_{obs} Å	h k l	Lattice Parameters a Å	c Å	Drift constant Å	d_{cal} Å
1.	22.64	0.196	3.927	0 0 3				3.939
2.	23.00	0.199	3.887	0 1 0				3.877
3.	27.68	0.239	3.223	0 1 2				3.241
4.	32.47	0.280	2.757	0 1 3				2.768
5.	32.68	0.281	2.740	1 1 0				2.741
6.	38.28	0.328	2.351	0 0 5				2.364
7.	38.36	0.329	2.347	0 1 4				2.345
8.	40.28	0.344	2.239	1 1 3				2.
9.	45.32	0.385	2.000	1 1 4				2.009
10.	46.32	0.393	1.960	0 0 6				1.970
11.	47.24	0.401	1.924	0 2 0				1.938
12.	51.28	0.433	1.782	1 1 5				1.790
13.	54.60	0.457	1.68		3.876(5)	11.817(6)	0.000244	
14.	57.88	0.484	1.593	1 1 6				1.600
15.	58.44	0.488	1.579	1 2 3				1.590
16.	60.00	0.500	1.542	0 1 7				1.548
17.	62.40	0.518	1.488	0 2 5				1.491
				1 2 4				1.495
18.	65.20	0.539	1.431	1 1 7				1.438
19.	68.24	0.561	1.375	0 2 6				1.382
20	68.68	0.564	1.367	2 2 0				1.371

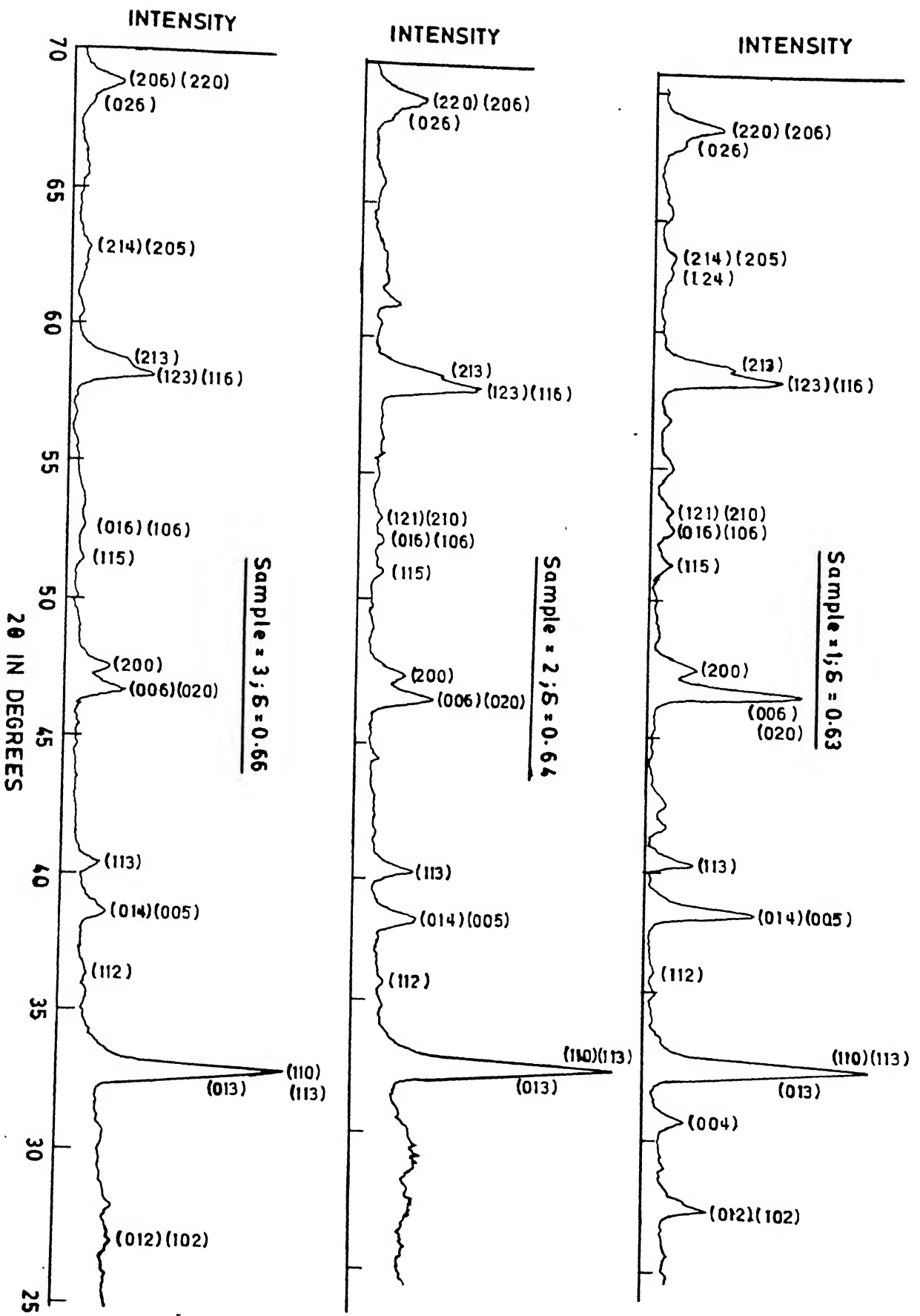
INTENSITY
INTENSITY
INTENSITY
70
65
60
55
50
45
40
35
30
25
2θ IN DEGREES
(206) (220)
(026)
(214) (205)
(213)
(123) (116)
(016) (106)
(115)
(200)
(006) (020)
(113)
(014) (005)
(112)
(110)
(113)
(013)
(012) (102)
Sample = 3; S = 0.66
(220) (206)
(026)
(213)
(123) (116)
(121) (210)
(016) (106)
(115)
(200)
(006) (020)
(113)
(014) (005)
(112)
(110) (113)
(013)
Sample = 2; S = 0.64
(220) (206)
(026)
(214) (205)
(124)
(213)
(123) (116)
(121) (210)
(016) (106)
(115)
(200)
(006)
(020)
(113)
(014) (005)
(112)
(110) (113)
(013)
(004)
(012) (102)
Sample = 1; S = 0.63

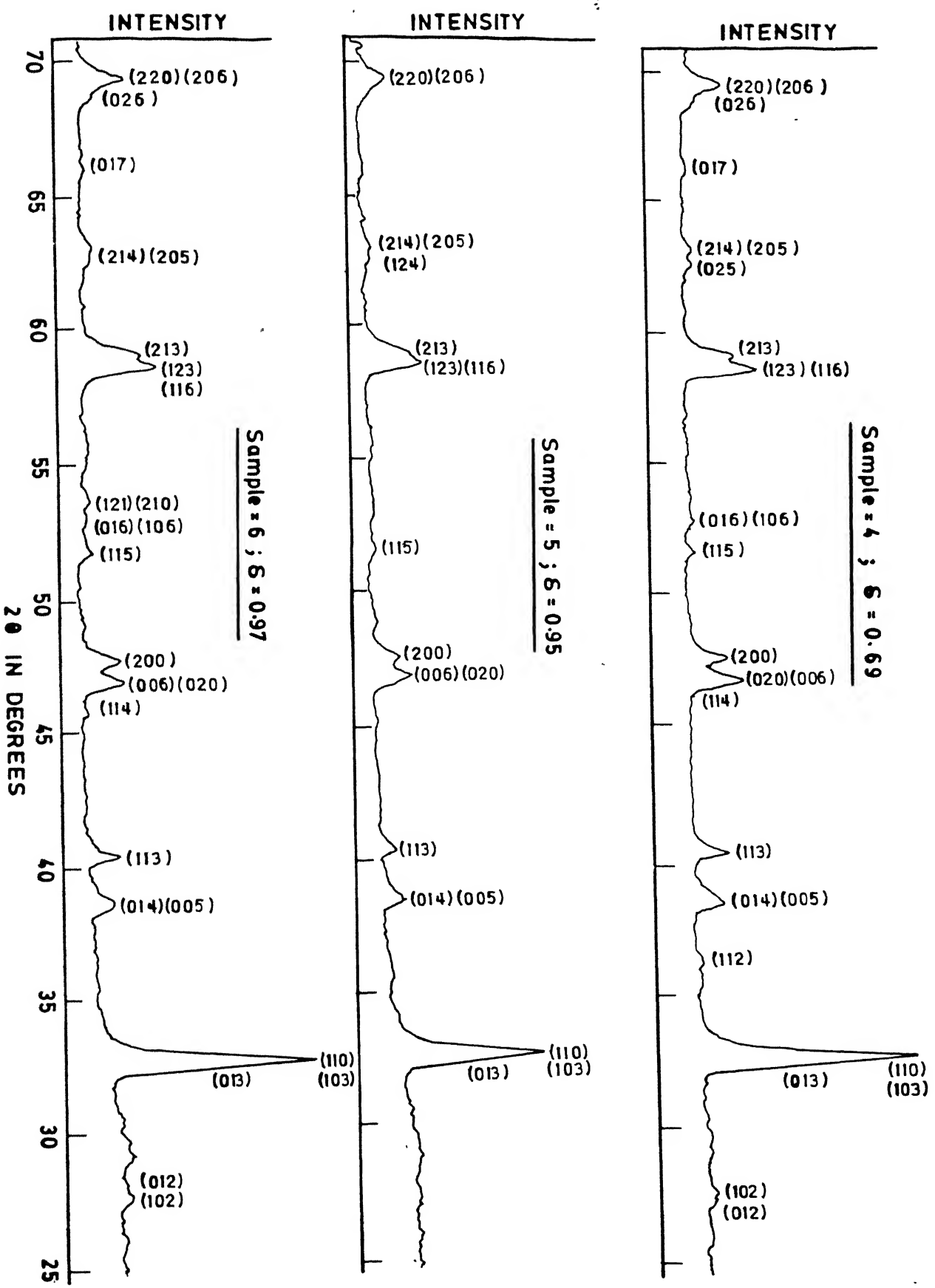
INTENSITY
INTENSITY
INTENSITY
70
65
60
55
50
45
40
35
30
25
2θ IN DEGREES
(220)(206)
(026)
(017)
(214)(205)
(213)
(123)
(116)
(121)(210)
(016)(106)
(115)
(200)
(006)(020)
(114)
(113)
(014)(005)
(110)
(103)
(013)
(012)
(102)
Sample = 6 ; S = 0.97
(220)(206)
(214)(205)
(124)
(213)
(123)(116)
(115)
(200)
(006)(020)
(113)
(014)(005)
(110)
(103)
(013)
Sample = 5 ; S = 0.95
(220)(206)
(026)
(017)
(214)(205)
(025)
(213)
(123)(116)
(016)(106)
(115)
(200)
(020)(006)
(114)
(113)
(014)(005)
(112)
(110)
(103)
(013)
(102)
(012)
Sample = 4 ; S = 0.69

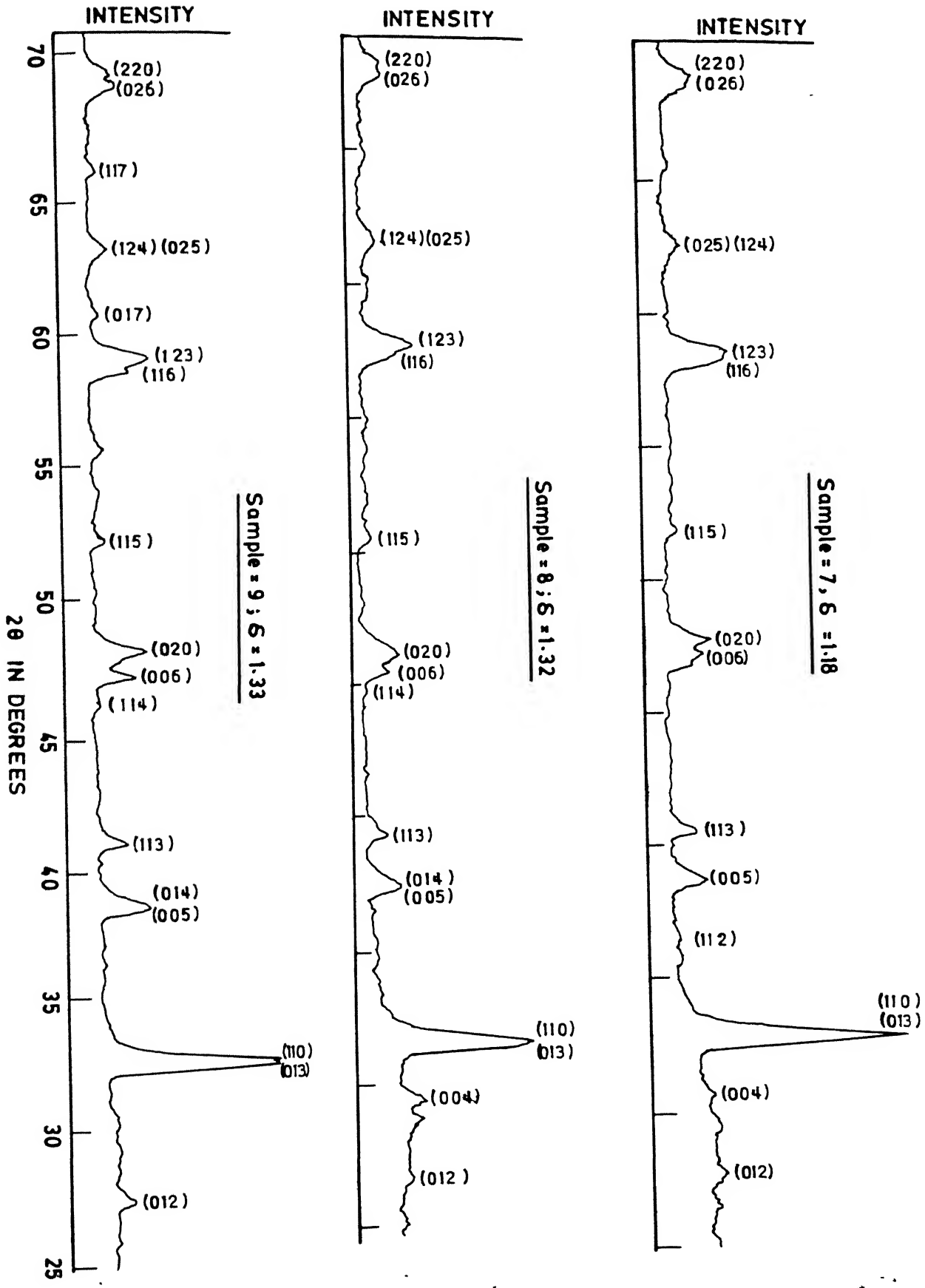
INTENSITY
INTENSITY
INTENSITY
2θ IN DEGREES
70
65
60
55
50
45
40
35
30
25
(220)
(026)
(117)
(124) (025)
(017)
(123)
(116)
(115)
(020)
(006)
(114)
(113)
(014)
(005)
(110)
(013)
(012)
Sample = 9 ; G = 1.33
(220)
(026)
(124)(025)
(123)
(116)
(115)
(020)
(006)
(114)
(113)
(014)
(005)
(110)
(013)
(004)
(012)
Sample = 8 ; G = 1.32
(220)
(026)
(025) (124)
(123)
(116)
(115)
(020)
(006)
(113)
(005)
(112)
(110)
(013)
(004)
(012)
Sample = 7, G = 1.18

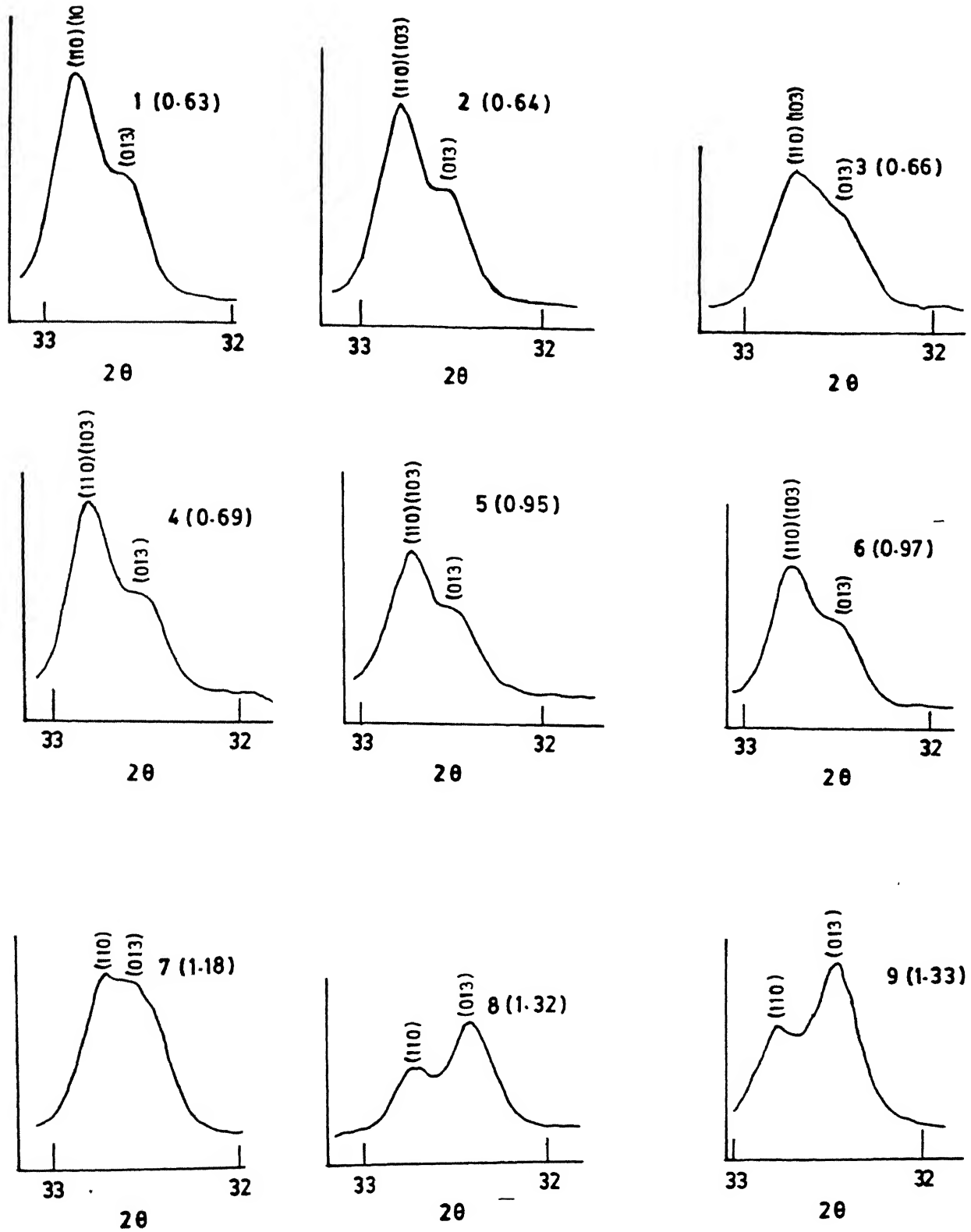

FIG. 3.4 VARIATION OF MAJOR XRD PEAKS AT $2\theta \simeq 32.4^{\circ}$ AND 32.7° WITH δ IN $Y_1 Ba_2 Cu_3 O_{7-\delta}$ AT ROOM TEMPERATURE

Table 3.14 : Details of Intensity Calculation

Sample No.	Oxygen content (x)	Intensity* near $2\theta = 32.67^{o}$ I_1 in terms of area (cm^2)	Intensity+ near $2\theta = 32.47^{o}$ I_2 in terms of area (cm^2)	Intensity ratio (I_1/I_2)
1.	6.37	33.50	17.52	1.9121
2.	6.36	31.04	18.75	1.6550
3.	6.34	24.64	15.40	1.6000
4.	6.31	28.25	15.16	1.8630
5.	6.05	24.52	15.40	1.5900
6.	6.03	21.50	15.32	1.4033
7.	5.82	28.70	32.60	0.8804
8.	5.68	9.26	19.42	0.5889
9.	5.67	16.00	25.80	0.4770

* Corresponds to (110),(103) for orthorhombic or (110) for tetragonal phase.

+ Corresponds to (013) for both orthorhombic and tetragonal phase.

3.3 DETERMINATION OF RESISTIVITY

The resistivity was measured by the standard four probe technique wherein probes were arranged in a square array(31). The voltage-current relations for a rectangular piece of isotropic material of dimensions l_1, l_2 and l_3, and resistivity ρ_j with small electrodes at four corners of the l_1 l_2 face, have been calculated by Logan et. al. (32) and can be expressed as:

$$\rho = HER_1$$

where H is a function of l_2/l_1 as shown in Figs.3(.5) and Table 3.1b, E is an effective thickness which is equal to the actual thickness l_3 when $l_3 << (l_1\ l_2)^{1/2}$, but never gets much greater than $(l_1\ l_2)^{1/2}$. In normalized form $E/(l_1\ l_2)^{1/2}$ depends mainly on $l_3/(l_1\ l_2)^{1/2}$ and is nearly independent of l_2/l_1 over much of its useful range as shown in Fig. 3.6 , R_1 is the ratio (V_1/I_1) of the voltage across the two contacts on an l_1 edge to the current between the other two opposite contacts, as depicted in Fig. 3.5 .

For our case the pellets are assumed to be squares, where the electrode spacing fixes the dimension of the square. The thickness of the pellets lies between 0.24 cm and 0.30 cm. The probe spacing is 0.5 cm, so we can take the thickness of the sample as the effective thickness E of the sample.

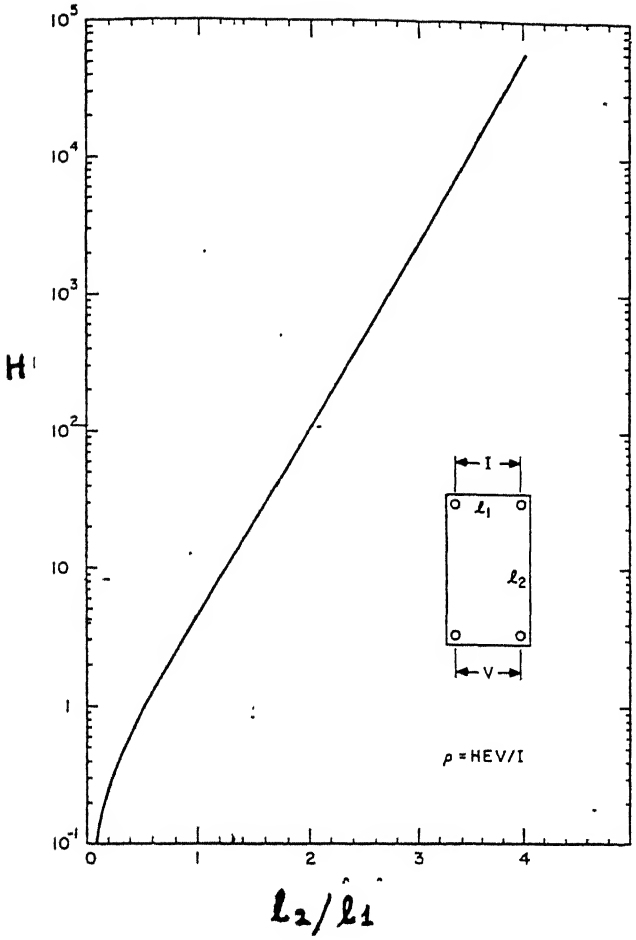

TABLE 3.15: Selected values of the function H of figure.

ℓ_2/ℓ_1	0.25	0.5	0.6667	1.0	1.5	2.0	4.0
H	0.3207	0.8911	1.562	4.531	21.86	105.1	56 300.0

Figure 3.5 FUNCTION H RELATING ρ TO SAMPLE DIMENSIONS & $\frac{V}{I}$

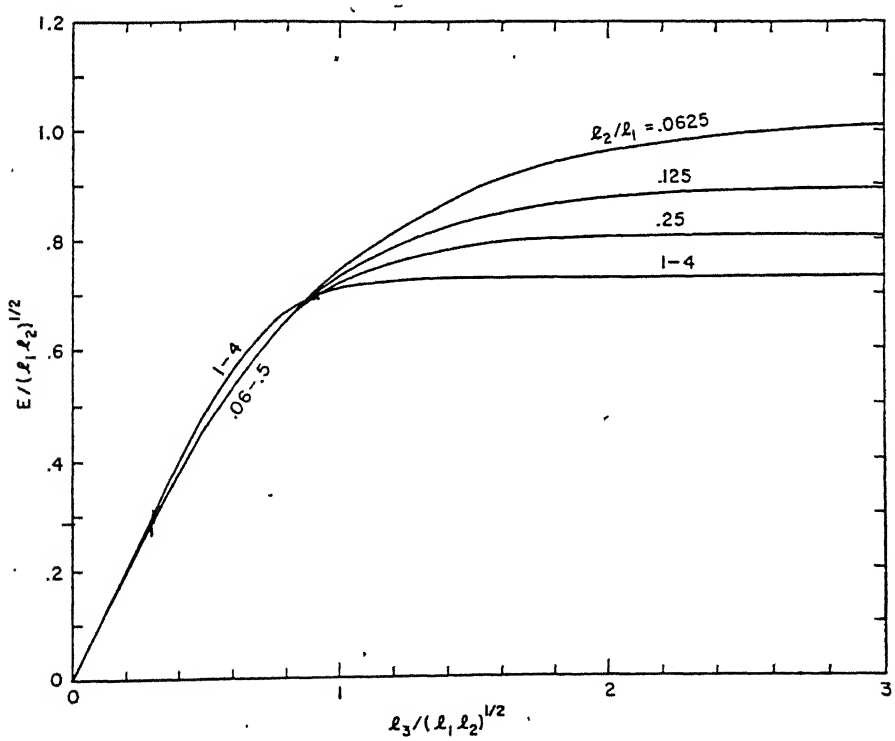

Figure 3.6 NORMALIZED EFFECTIVE THICKNESS Vs. NORMALIZED SAMPLE THICKNESS FOR VARIOUS RATIOS OF SAMPLE DIMENSIONS.

Since the array in our experiments was in the form of a square, $l_1/l_2 = 1$ and H = 4.531. The values of thickness E, resistance R_1, the oxygen content (x) and the resistivity ρ of various samples of $YBa_2Cu_3O_x$ are given in Table 3.16.

Figure (3.7) shows the variation of ln ρ vs. oxygen content. Table 3.17(a) gives details of resistivity and the intensity ratio. Fig.3.8 shows the variation of ln ρ as a function of the intensity ratio I_1/I_2 for $YBa_2Cu_3O_x$ samples.

3.4 MEASUREMENT OF RESISTANCE FROM LIQUID NITROGEN TEMPERATURE TO ROOM TEMPERATURE

The resistance for each sample was measured with the help of standard four-terminal technique, as described earlier in Chapter 2. The values of resistance at different temperatures were calculated from the measured value of voltage and current. The calculated resistance was then normalized with respect to the room temperature resistance (R_{RT}). The relation between the resistivity ρ and the resistance R of a certain material is given by:

$$\rho = GR$$

where, G is the geometrical factor. Therefore, the room temperature resistivity ρ_{RT} and that at any temperature $\rho(T)$ could be written as:

$$\rho_{(RT)} = G \quad (R_{(RT)}$$

Sample No.	Oxygen content (x)	Thickness (cm)	Resistance $R_1 = V/I$ (Ohm)	Resistivity $= HER_1$ (Ohm cm)	ln ρ
1.	6.37	0.260	8.46×10^{-4}	9.97×10^{-4}	-6.91
2.	6.36	0.286	2.23×10^{-3}	2.88×10^{-3}	-5.85
3.	6.34	0.240	4.28×10^{-3}	4.65×10^{-3}	-5.37
4.	6.31	0.286	1.51×10^{-3}	1.96×10^{-3}	-6.23
5.	6.05	0.270	4.43×10^{-3}	5.41×10^{-3}	-5.22
6.	6.03	0.209	2.24×10^{-2}	2.12×10^{-2}	-3.85
7.	5.82	0.278	4.41×10^{-2}	5.55×10^{-2}	-2.89
8.	5.68	0.264	2.66	3.18	1.16
9.	5.67	0.276	2.78	3.47	1.24

Table 3.17(a) : Details of Resistivity and Intensity Ratio

Sample No.	Resistivity (Ohm-cm)	ln ρ	Intensity Ratio I_1/I_2
1.	9.97 $x10^{-4}$	-6.91	1.91
2.	2.88 $x10^{-3}$	-5.8	1.66
3.	4.65 $x10^{-3}$	-5.37	1.60
4.	1.96 $x10^{-3}$	-6.23	1.86
5.	5.41 $x10^{-3}$	-5.22	1.59
6.	2.12 $x10^{-2}$	-3.85	1.40
7.	5.55 $x10^{-2}$	-2.89	0.88
8.	3.18	1.16	0.59
9.	3.47	1.24	0.48

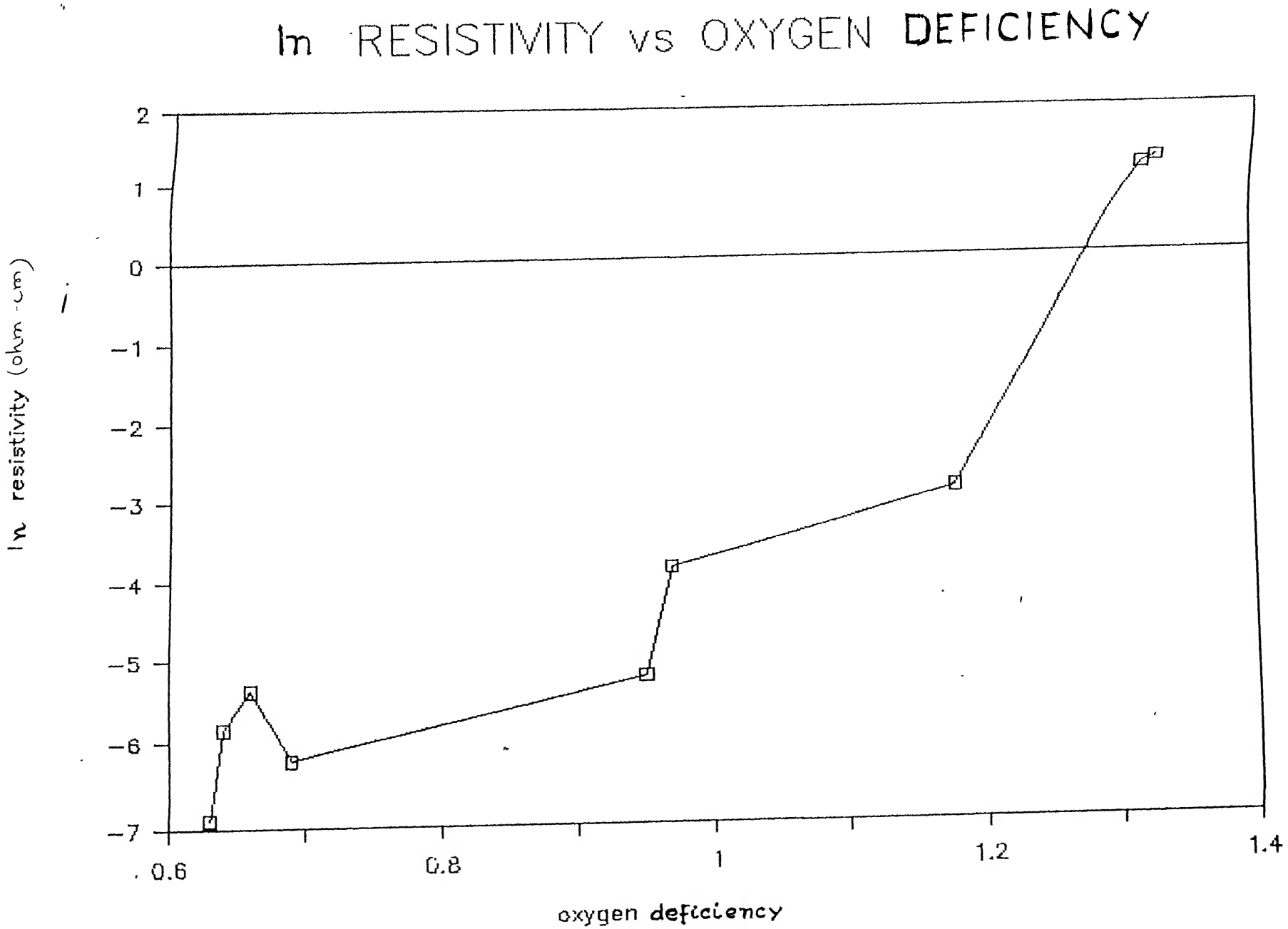
ln RESISTIVITY vs OXYGEN DEFICIENCY
ln resistivity (ohm-cm)
2
1
0
−1
−2
−3
−4
−5
−6
−7
0.6
0.8
1
1.2
1.4
oxygen deficiency

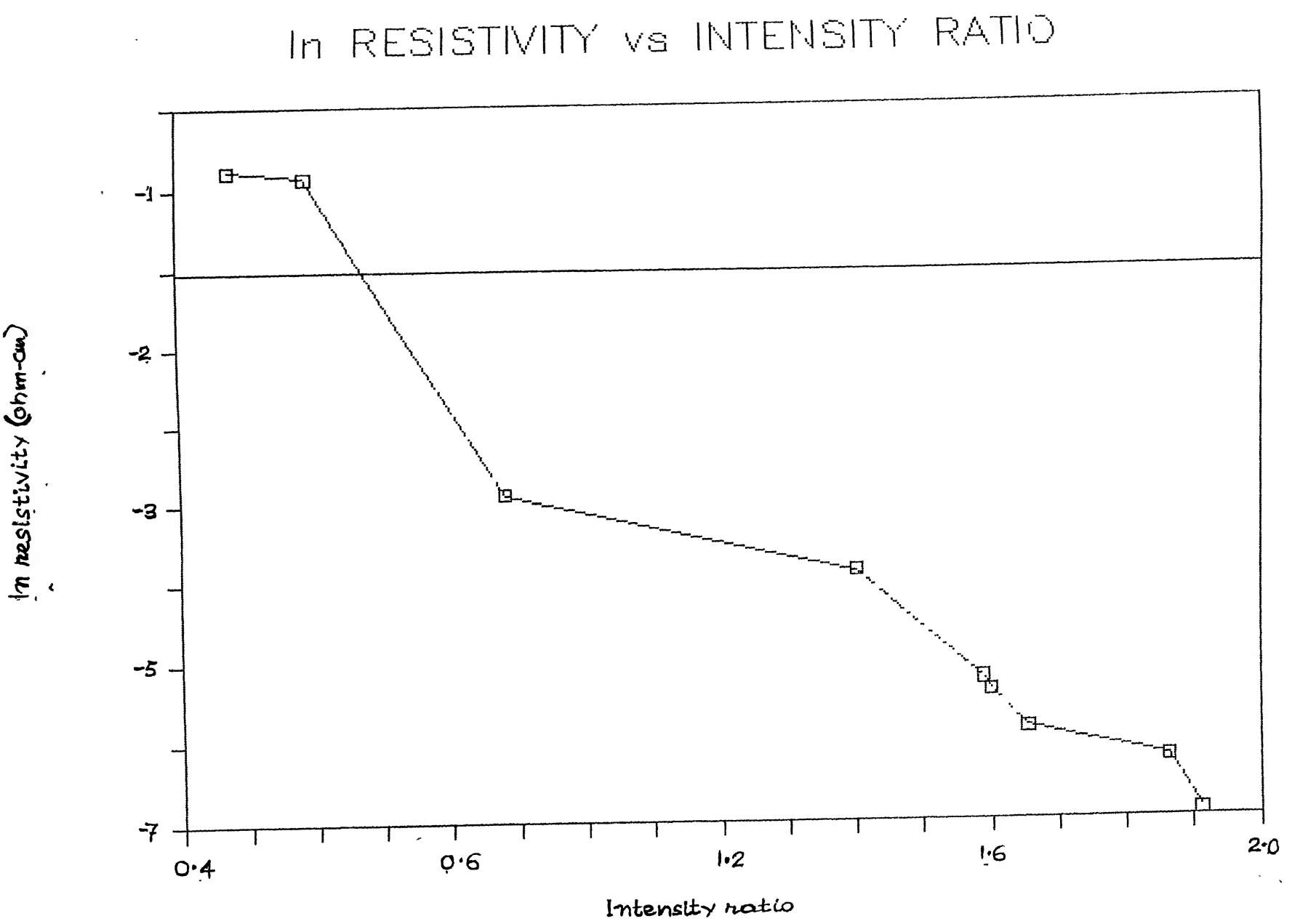
ln RESISTIVITY vs INTENSITY RATIO
ln resistivity (ohm-cm)
-1
-2
-3
-5
-7
0·4
0·6
1·2
1·6
2·0
Intensity ratio

FIGURE 3.8

and

$$\rho_{(T)} = GR_{(T)}$$

or

$$\frac{\rho_{(T)}}{\rho_{(RT)}} = \frac{R_{(T)}}{R_{(RT)}}$$

Thus the normalized resistivity is same as the normalized resistance. and hence if we know ρ_{RT} and the normalized resistance at a certain temperature, we can find out resistivity ρ at that temperature.

Figures 3.9 to 3.17 give the variations of normalized resistance as a function of temperature. Table 3.17(b) gives the details of oxygen content and the critical temperature (T_c) of various superconducting samples $YBa_2Cu_3O_x$. It may be pointed out that the T_c of sample numbers 6 to 8 with lower O_2-content could not be measured because of experimental limitations, only T_c's above 87K were accessible.

3.5 DIELECTRIC CONSTANT MEASUREMENT:

Testardi et al. (30) reported that the quenched (tetragonal) phase of $Y_1Ba_2Cu_3O_x$ exhibits a static dielectric constant of ~30 at 4.3K and as high as ~700 at room temperature (290K), which is comparable only with those of ferroelectrics. They have measured the dielectric constant by measuring the capacitance from two terminal

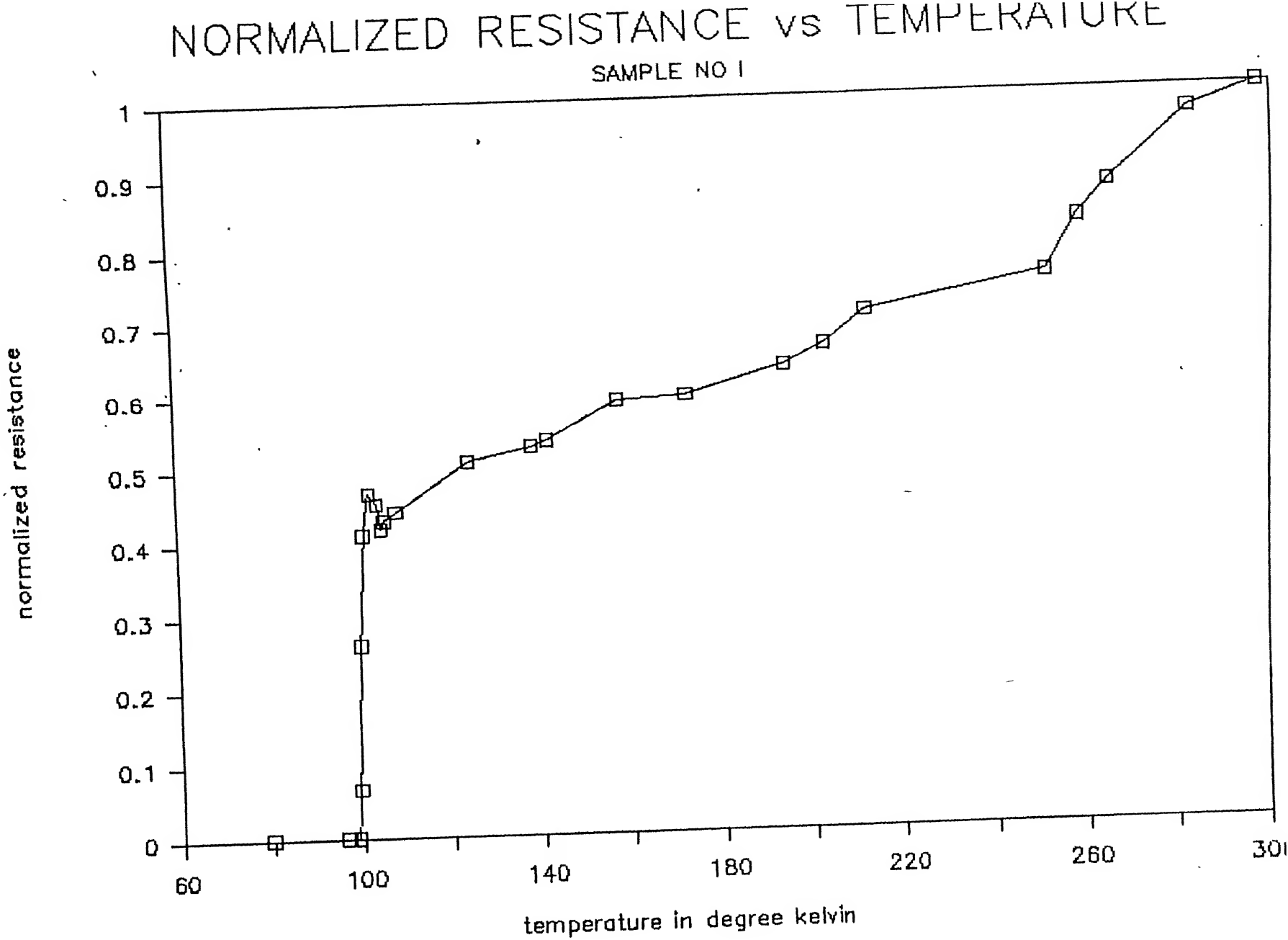
NORMALIZED RESISTANCE vs TEMPERATURE
SAMPLE NO I
normalized resistance
1
0.9
0.8
0.7
0.6
0.5
0.4
0.3
0.2
0.1
0
60
100
140
180
220
260
temperature in degree kelvin

NORMALIZED RESISTANCE vs TEMPERATURE

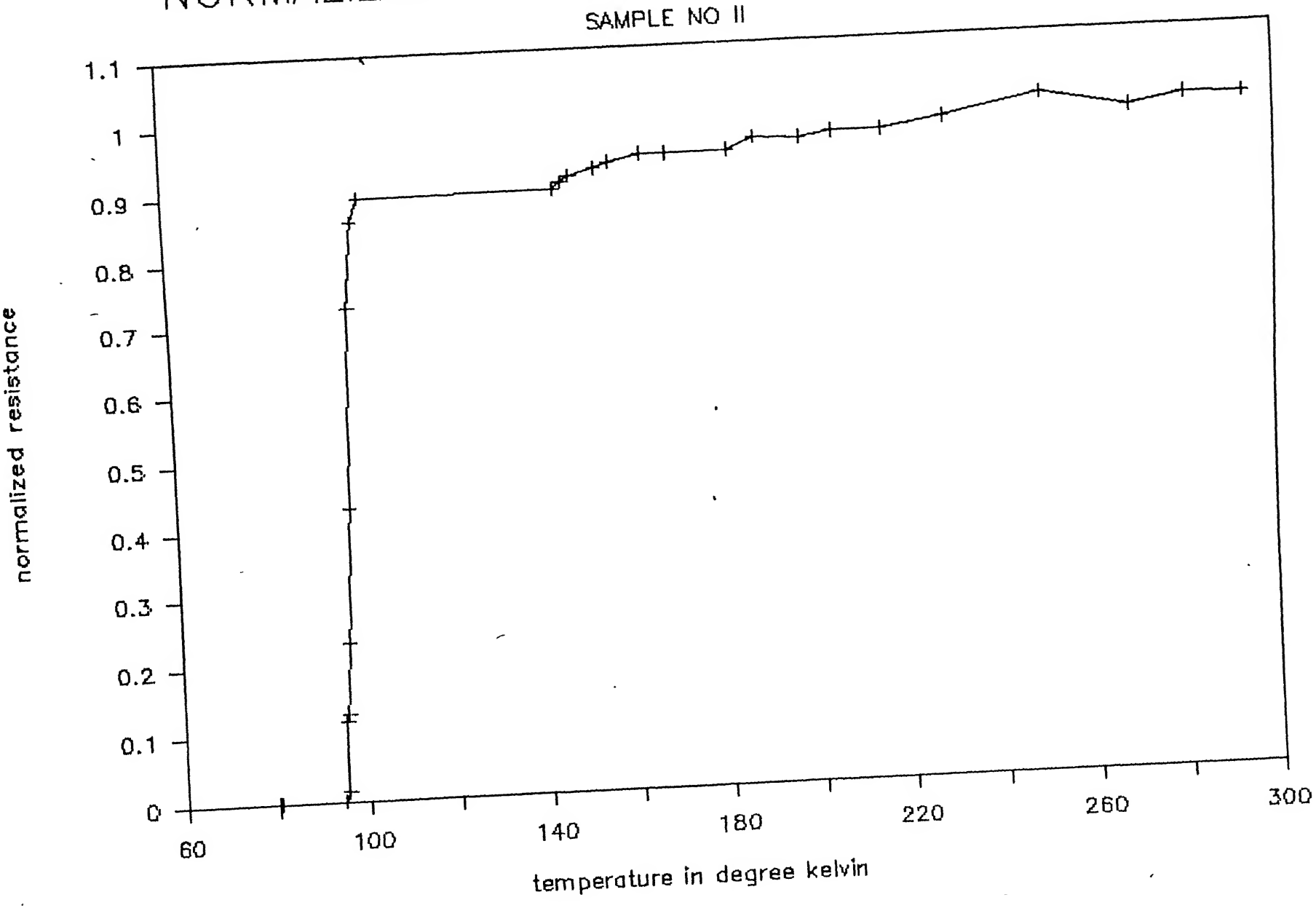

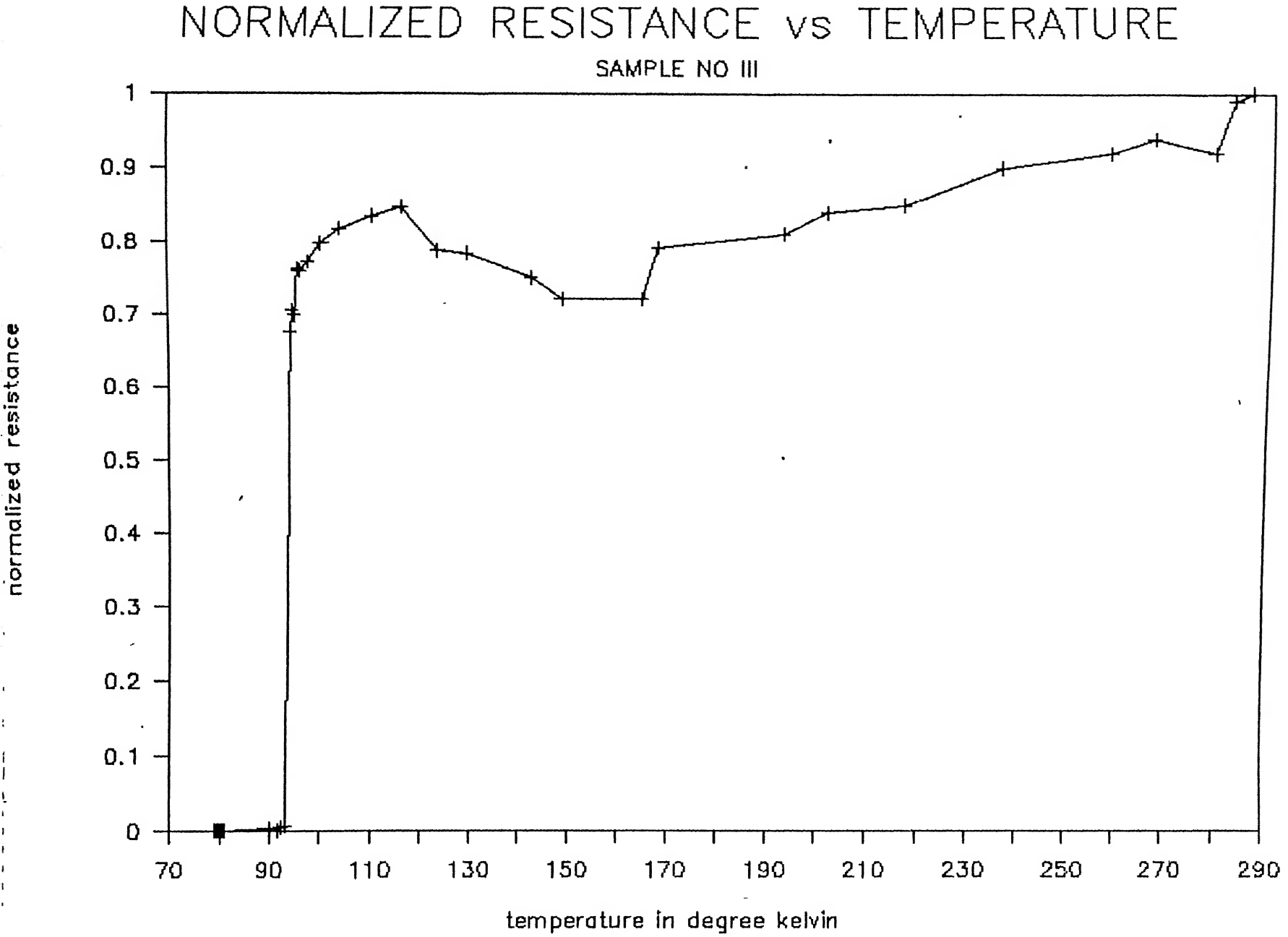
NORMALIZED RESISTANCE vs TEMPERATURE
SAMPLE NO III
normalized resistance
1
0.9
0.8
0.7
0.6
0.5
0.4
0.3
0.2
0.1
0
70
90
110
130
150
170
190
210
230
250
270
290
temperature in degree kelvin

FIGURE 3·11

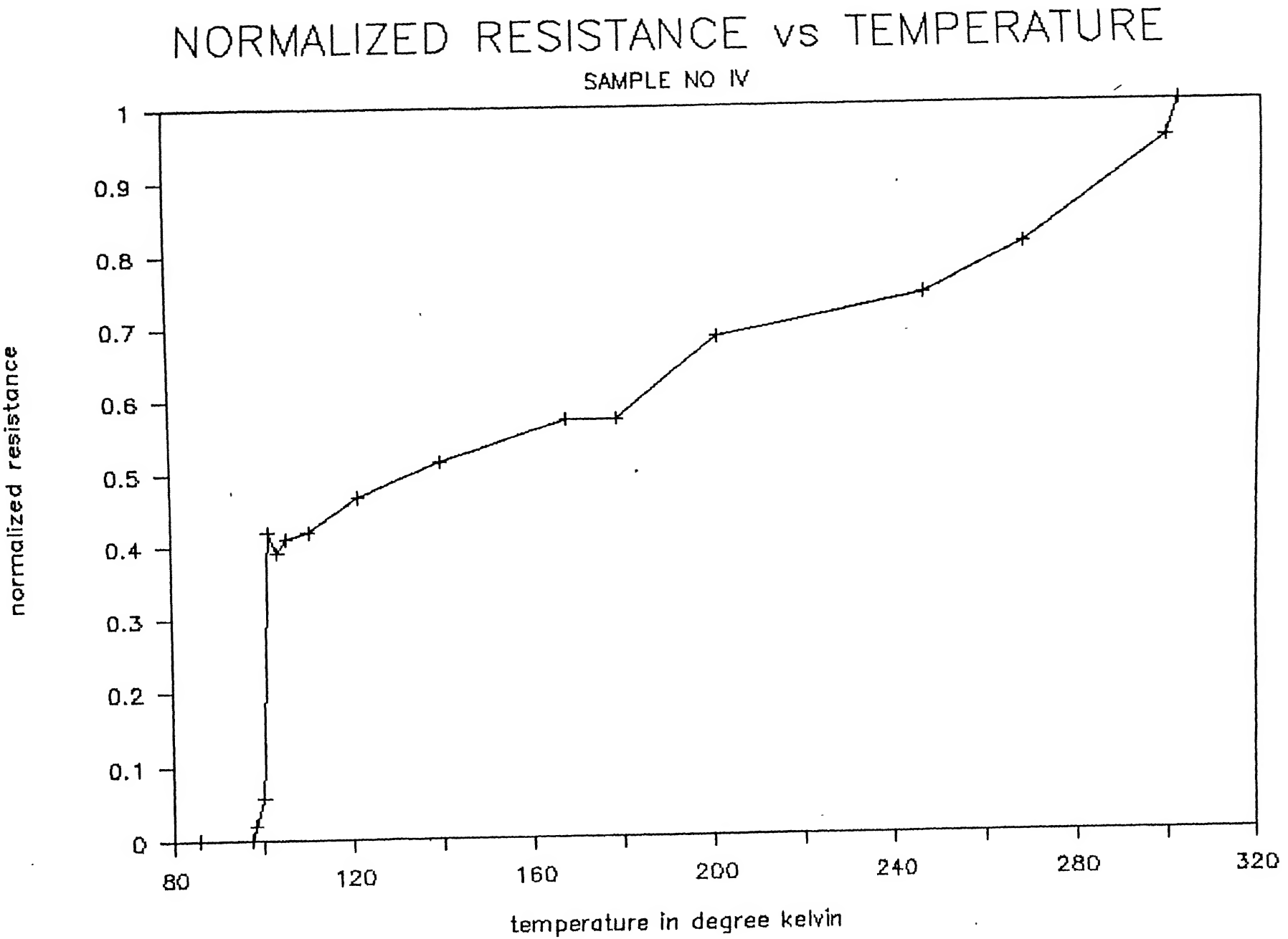
NORMALIZED RESISTANCE vs TEMPERATURE
SAMPLE NO IV
normalized resistance
1
0.9
0.8
0.7
0.6
0.5
0.4
0.3
0.2
0.1
0
80
120
160
200
240
280
320
temperature in degree kelvin

FIGURE 3.12

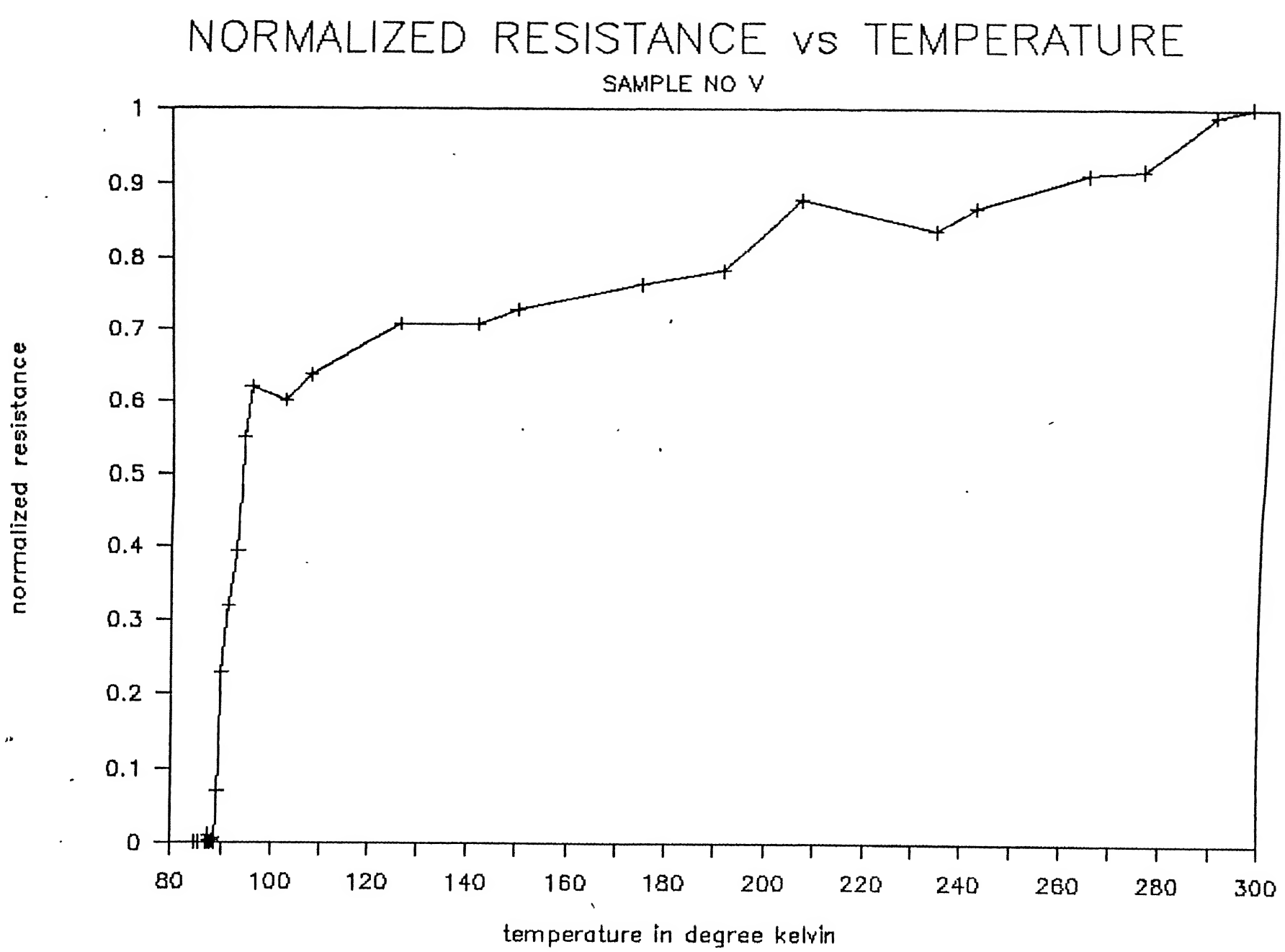
NORMALIZED RESISTANCE vs TEMPERATURE
SAMPLE NO V
normalized resistance
1
0.9
0.8
0.7
0.6
0.5
0.4
0.3
0.2
0.1
0
80
100
120
140
160
180
200
220
240
260
280
300
temperature in degree kelvin

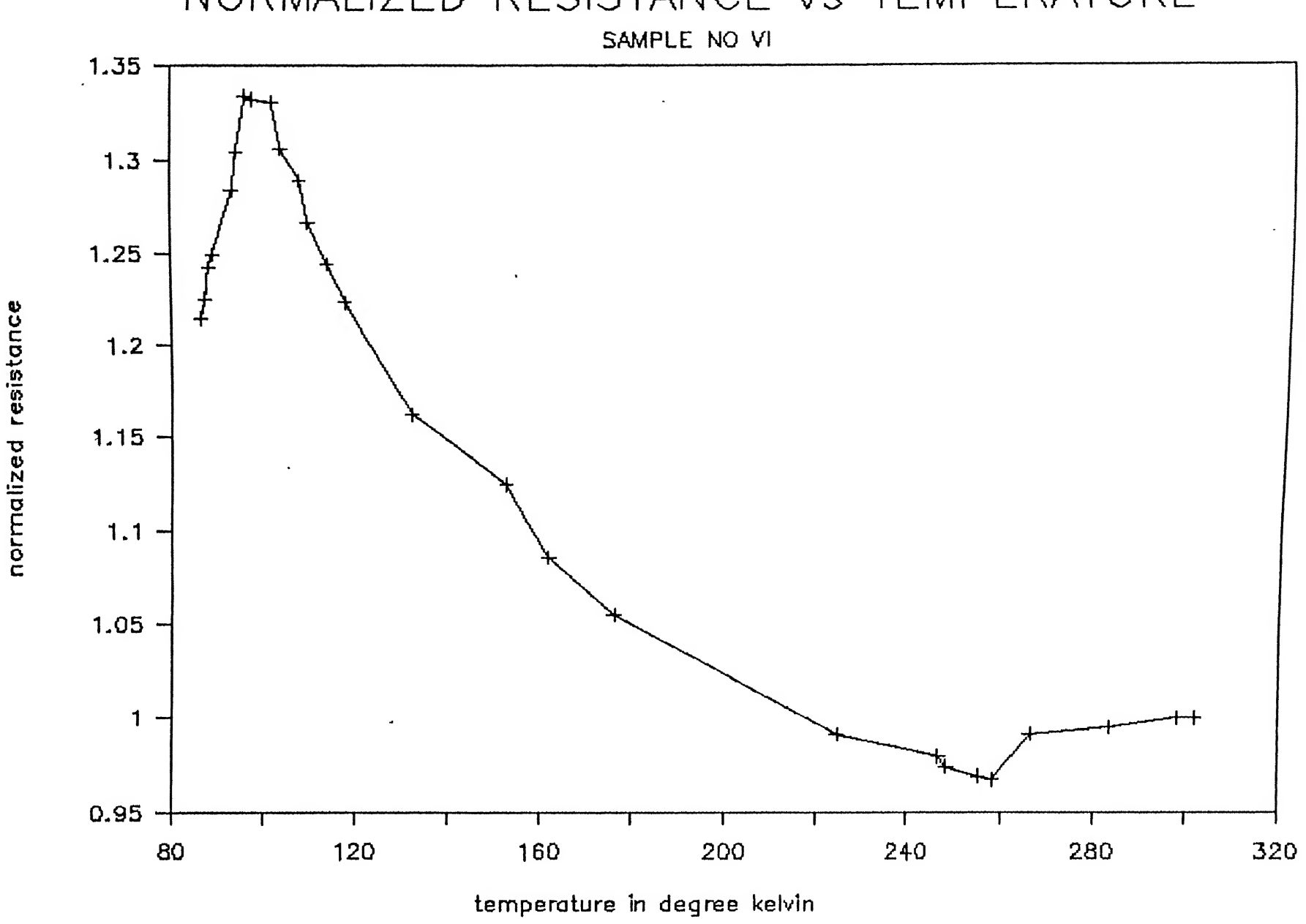
NORMALIZED RESISTANCE VS TEMPERATURE
SAMPLE NO VI
normalized resistance
1.35
1.3
1.25
1.2
1.15
1.1
1.05
1
0.95
80
120
160
200
240
280
320
temperature in degree kelvin

FIGURE 3.14

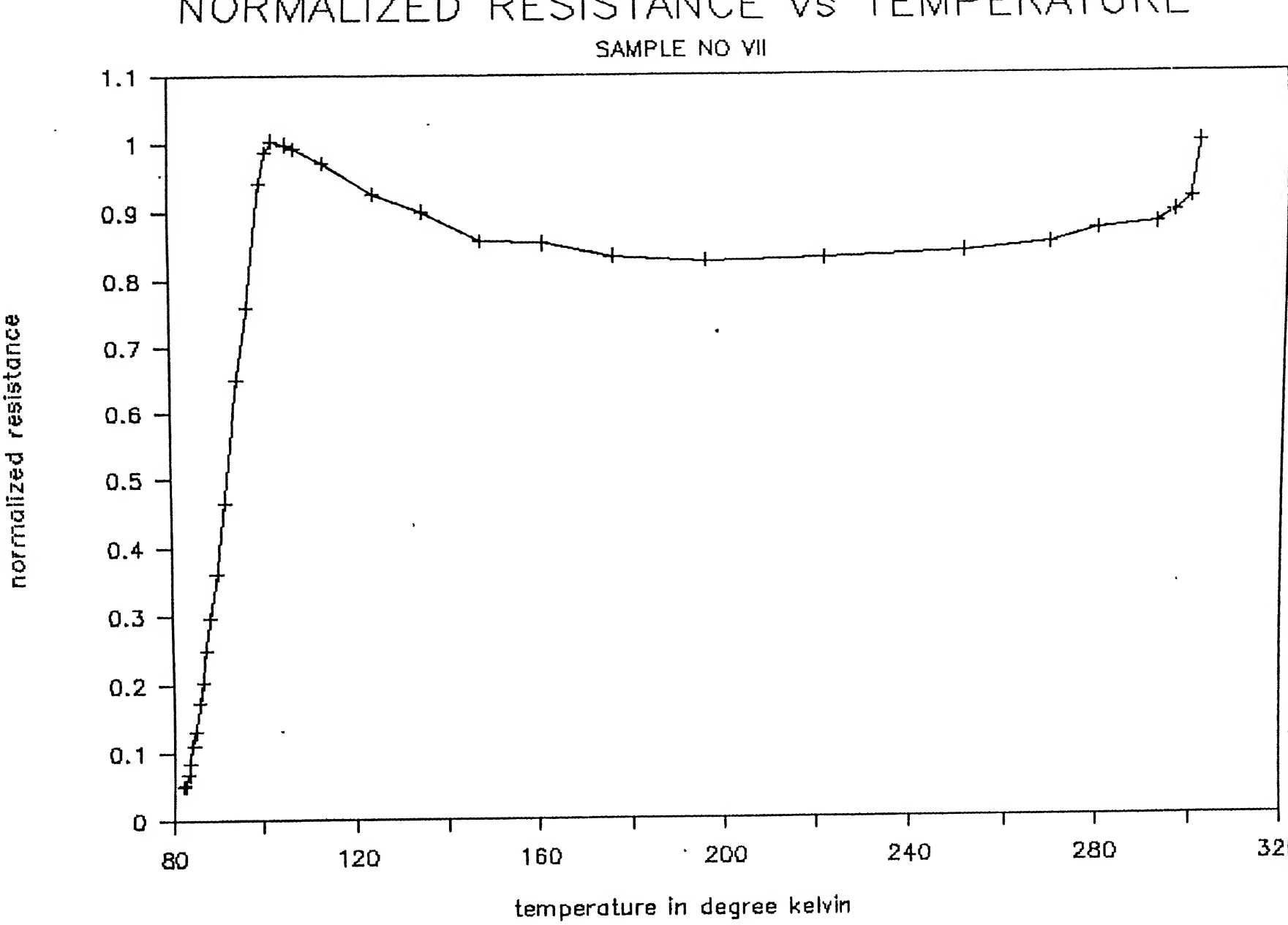
NORMALIZED RESISTANCE VS TEMPERATURE
SAMPLE NO VII
normalized resistance
1.1
1
0.9
0.8
0.7
0.6
0.5
0.4
0.3
0.2
0.1
0
80
120
160
200
240
280
temperature in degree kelvin

FIGURE 3.15

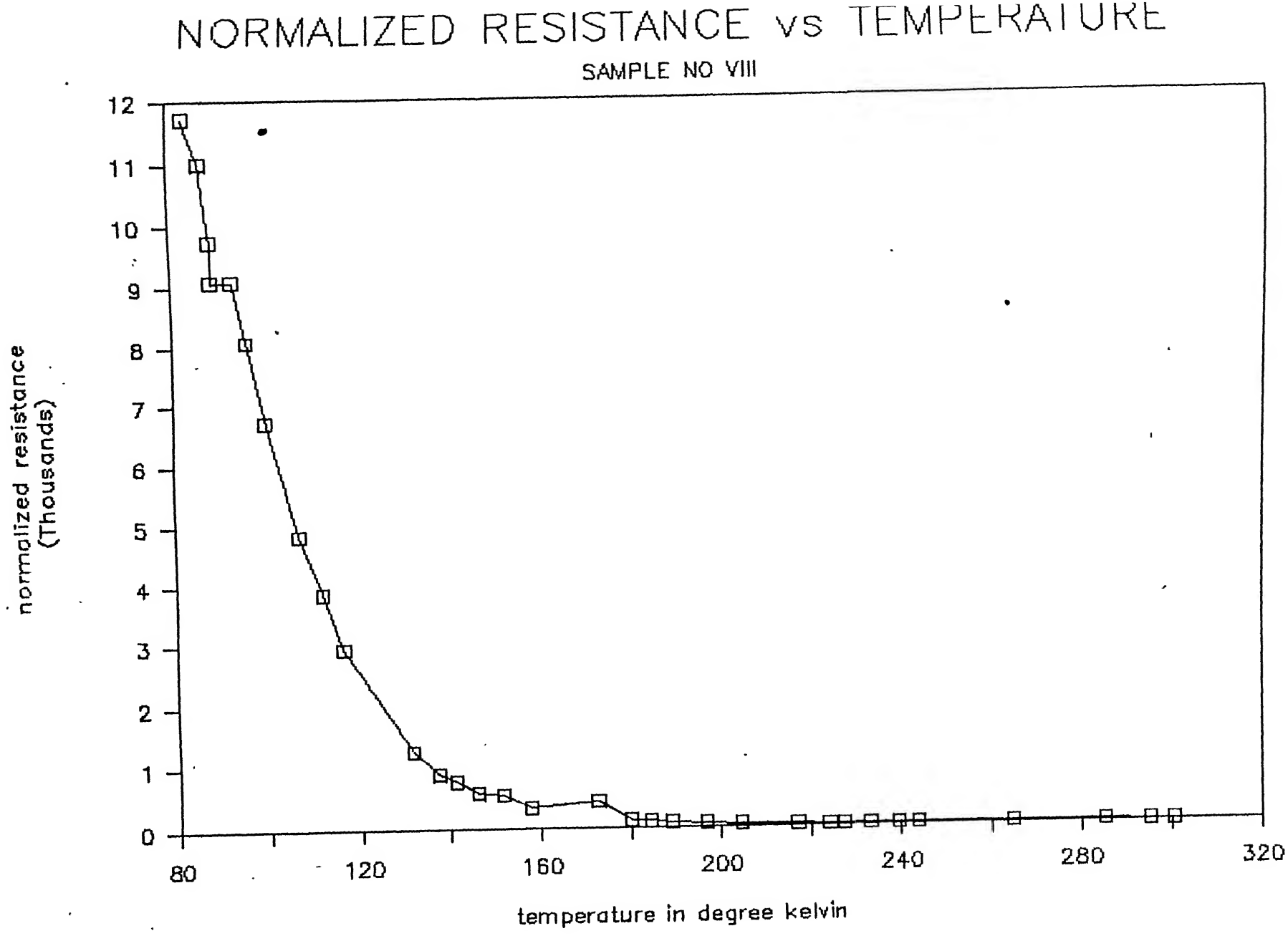
NORMALIZED RESISTANCE vs TEMPERATURE
SAMPLE NO VIII
normalized resistance
(Thousands)
12
11
10
9
8
7
6
5
4
3
2
1
0
80
120
160
200
240
280
320
temperature in degree kelvin

FIGURE 3.16

NORMALIZED RESISTANCE vs TEMPERATURE

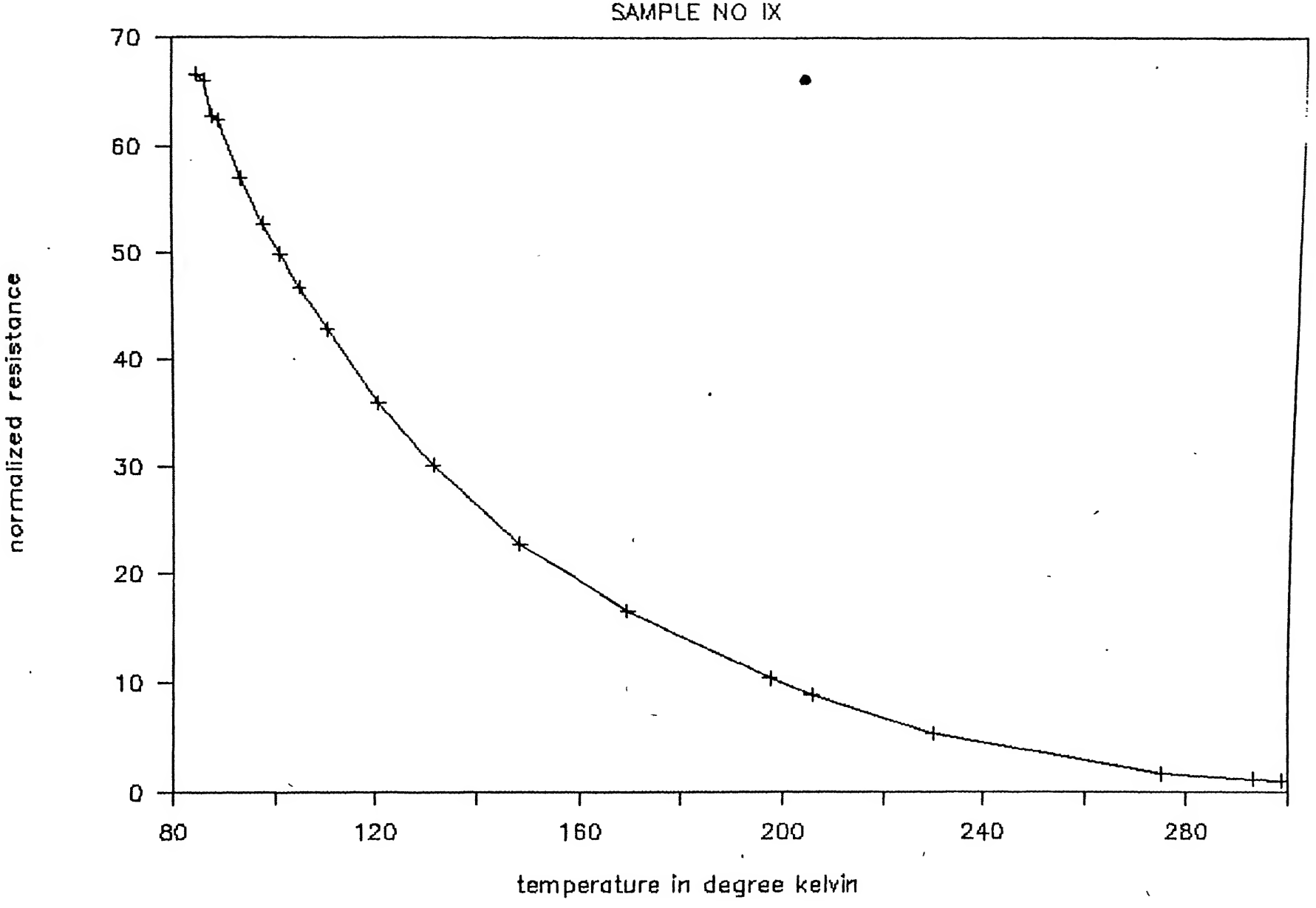

Table 3.17(b) : The Oxygen Content (x) and Critical Temperature (T_c) of Various Superconducting Samples of $YBa_2Cu_3O_x$

Sample No.	Oxygen Content (x)	Critical Temperature T_c (^oK)
1.	6.37	98.86
2.	6.36	94.74
3.	6.34	91.82
4.	6.31	97.40
5.	6.05	87.94
6.	6.03	87.00
7.	5.82	--
8.	5.68	--
9.	5.67	--

Note: The T_c's for Samples No. 6 to 9 were below the temperature that could be achieved inside the cryostate using LN_2 as coolant.

admittance measurements (using four terminal coaxial lead techniques) from 4.3K to 300K. These unusually large values of dielectric constant prompted us to reexamine the dielectric constant of the quenched tetragonal phase of $YBa_2Cu_3O_x$.

The technique used by us is same as described elsewhere(33). The dielectric constant K was obtained from capacitance, using the relation:

$$C = \frac{A \varepsilon_o K}{d}$$

$$= 0.0885 \times \frac{KA}{d}$$

where, C is the capacitance in picofarads (pf), K is the dielectric constant, A is the sample area (in cm^2) and d is the distance (in cm) between the plates assuming that the total plate-to-plate distance is filled by the dielectric material. The dielectric constant K is obtained as

$$K = \frac{d\,C}{A \times 0.0885}$$

$$= 11.2994 \times \left(\frac{d}{A}\right) \times C.$$

It was found that the capacitance and hence the dielectric constant K depends strongly on the contact resistance. Some of the results have been summarized in Table 3.18.

It was observed that the capacitance and hence the dielectric constant is a strong function of contact resistance. The resistance of the sample lies between 0.1 to 1Ω , whereas the two electrode measurement shows a resistance that lies in the range of 10Ω to 30KΩ . This suggests that the contact resistance is much larger than the sample resistance. We have found that lower the contact resistance, the better is the contact and hence higher is the dielectric constant. For higher contact resistance, the contact is bad and hence lower is the dielectric constant.

Dielectric constant also varies strongly with frequency. A typical result is given in Table 3.19.

Table 3.18 (Continued):

Sample No.	Electrodes	Special Treatments, (if any)	Frequency	Capacitance	Resistance (Ohm)	Dielectric constant K
9.	Gold deposited + stainless steel electrodes + platinum foils	Measured after cooling it to room temperature	20 KHz 500 KHz	8.490 nF 4.253 nF	375.3 26.69	16683.81 8357.626
10.	Gold deposited + stainless steel electrodes + platinum foils	Measured after 4 days	20 KHz 500 KHz	158.24 pF 38.70 pF	21.62K 4.025K	310.959 76.0498

Table 3.19 : Variation of Dielectric Constant with Frequency

Temperature = $30^{o}C$

Signal Level = 1V

Electrode used = Gold deposited backed-up by platinum foil electrode sandwitched between stainless steel electrodes

Thickness of sample = 0.18 cm; sample area = 1.035 cm^2

Frequency (KHz)	Capacitance (nF)	Resistance (Ohm)	Dielectric constant K
0.5	15.46	4725	30381
1	13.87	4147	27256
10	9.734	678	19128
20	8.490	375	16684
50	6.968	165	13693
100	5.991	91	11773
800	4.741	38	9316
500	4.253	27	8357
1000	3.659	18	7191
5000	-1.3216	9	-2597
10000	-0.5602	7	-1101

3.6 DISCUSSION

3.6.1 Resistivity and XRD Analysis:

The summary of resistivity at room temperature, oxygen content, lattice parameter, and intensity ratio with their corresponding critical temperatures has been given in Table 3.20.

Figure (3.18) shows the plot of oxygen deficiency (δ) as a function of intensity ratio. In general one observes that intensity ratio decreases with increasing oxygen deficiency. This means that the amount of the orthorhombic phase decreases and that of the tetragonal phase increases with decreasing oxygen content (x) or increasing oxygen deficiency (δ). Only Sample #4 has shown some ambiguity, namely, even though its oxygen content (x) as determined by weight measurement is lower than those of samples #2 and #3, its intensity ratio as determined by XRD is higher than those of samples #2 and #3. The two results thus are self contradictory; the oxygen content determination suggests a lower value of oxygen content and hence smaller concentration of superconducting ortho phase in sample #4 than those in sample #2 and #3, while the intensity ratio suggests otherwise. This issue can be resolved to an extent by the resistivity (ρ) and critical temperature (T_c) data. In general ρ decreases and T_c increases with oxygen content (x), see Figs. 3.9 to Figs.3.17 . It is evident from Fig.3.7 that the sample #4 has a lower ρ than samples #2 and #3 suggesting that former has higher

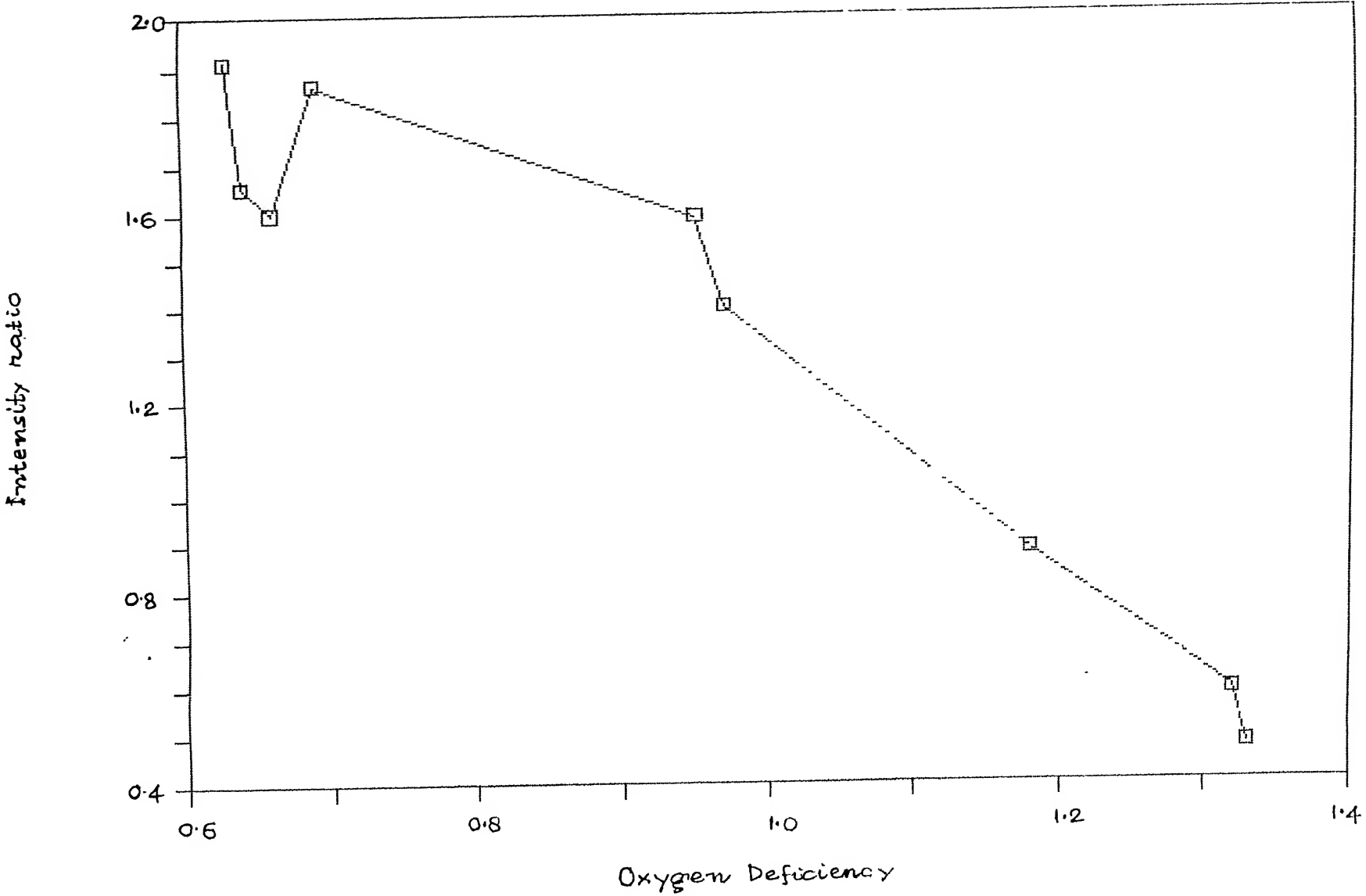
2·0
1·6
1·2
0·8
0·4
Intensity ratio
0·6
0·8
1·0
1·2
1·4
Oxygen Deficiency

FIGURE 3·18

Table 3. 20 : Summary of Resistivity, Oxygen Content, Lattice Parameter and Intensity Ratio with Their Corresponding Critical Temperatures

Sample No.	Oxygen content (x)	Oxygen deficiency (δ)	Lattice Constants (Å) a	b	c	Intensity Ratio (I_1/I_2)	Resistivity at room temperature (Ohm cm)	Critical temperature T_c (^oK)
1.	6.37	0.63	3.823(3)	3.883(7)	11.649(2)	1.91	9.97×10^{-4}	98.9
2.	6.36	0.64	3.824(5)	3.889(2)	11.673(3)	1.65	2.88×10^{-3}	94.8
3.	6.34	0.66	3.834(0)	3.900(7)	11.704(8)	1.60	4.65×10^{-3}	91.8
4.	6.31	0.69	3.824(0)	3.824(9)	11.659(7)	1.86	1.94×10^{-3}	97.4
5.	6.05	0.95	3.846(2)	3.891(5)	11.686(7)	1.59	5.41×10^{-3}	87.94
6.	6.03	0.97	3.830(3)	3.887(0)	11.659(3)	1.40	2.12×10^{-2}	--
7.	5.82	1.18	3.857(8)	3.857(8)	11.690(7)	0.88	5.55×10^{-2}	--
8.	5.68	1.32	3.884(0)	3.884(0)	11.779(2)	0.59	3.17	--
9.	5.67	1.33	3.876(5)	3.876(5)	11.817(5)	0.48	3.47	--

+ Oxygen deficiency $\delta = 7-x$.

orthorhombic phase and hence possibly high oxygen content than samples #2 and #3. These results suggest that the intensity ratio determination is a better way of determining the relative concentrations of ortho and tetra phases even though the weight measurement has yielded consistent results except in one case, i.e. sample #4.

Figures 3.9 to 3.17 show the normalized resistance as a function of temperature for $YBaCu_3O_x$ samples containing different amounts of oxygen. The behaviour is metallic for orthorhombic phase and semiconductor like for tetragonal phase. For samples #1 and #4 (Figs.3.9 and 3.12) which have higher orthorhombic phase, the normalized resistance (hence normalized resistivity) decreases with decreasing temperature. For sample #2 the resistance decreases, but the rate of decrease is slower than that of samples #1 and #4. There is a gradual switch-over towards mixed behaviour as evident from the results for sample #3 (Fig.3.11); there is a decrease in resistivity and just before T_c, there is a slight increase once more just before dropping to zero. For sample #6 and #7, initially the semiconducting behaviour is seen, before showing a possible transition at lower temperatures (below our experimental limits). Sample #8 and #9 show purely semiconducting behaviour (Figs.3.16 and 3.17).

From the plot of lattice constant c vs. oxygen deficiency (Fig.3·20) and intensity ratio (Fig.3.22), one also observes that there is an elongation of c axis with decreasing oxygen content. Figure (3·19) and figure (3·22) show that the lattice constants a,b approach each other and finally coincide as the dominant phase in the sample turns from orthorhombic to tetragonal phase.

3.6.2 Dielectric Measurements:

It has been found that the capacitance and hence the dielectric constant is inversely related with contact resistance. This behaviour can be explained by considering a material of dielectric constant K between two parallel plates as shown in the following figure.

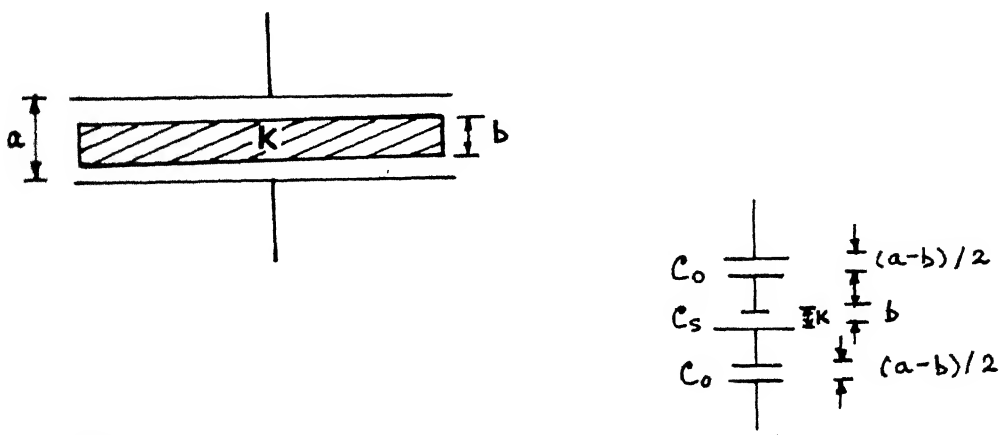

Figure 3.

Let us assume that the resistivity and hence the resistance of the material is low (~ few Ohms) so that the contact resistance is usually orders of magnitude higher than

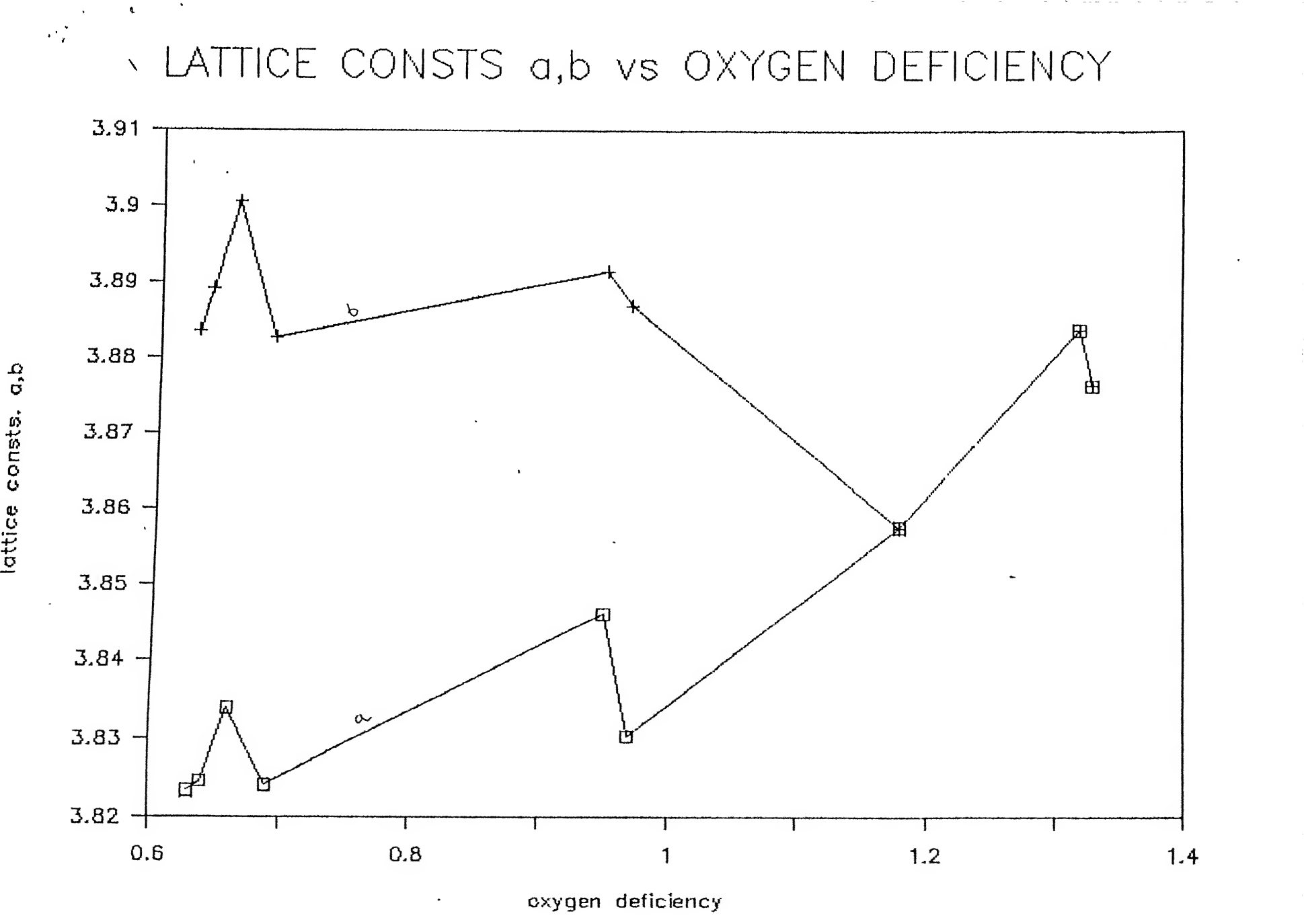
LATTICE CONSTS a,b vs OXYGEN DEFICIENCY
lattice consts. a,b
3.91
3.9
3.89
3.88
3.87
3.86
3.85
3.84
3.83
3.82
b
a
0.6
0.8
1
1.2
1.4
oxygen deficiency

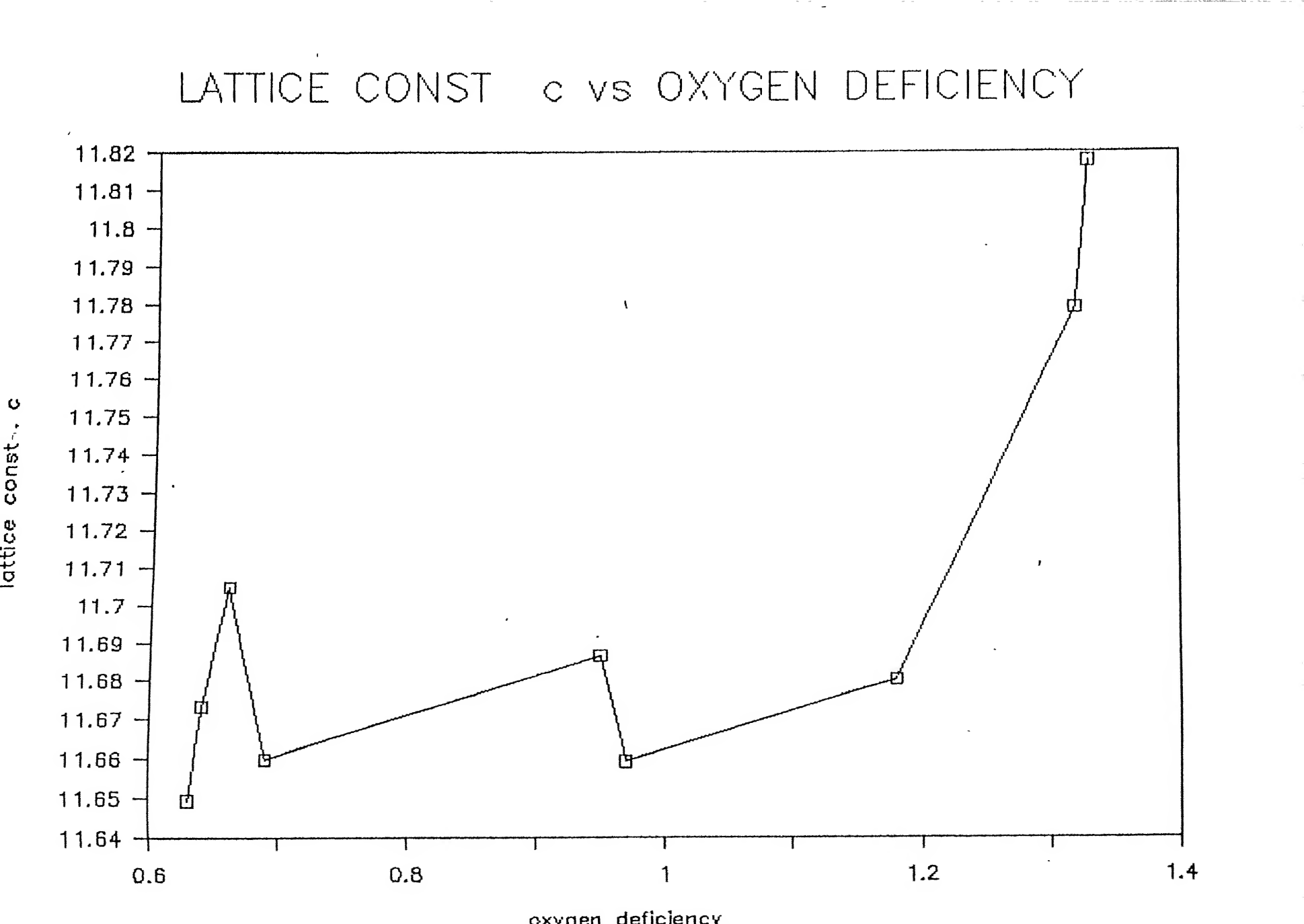
LATTICE CONST c vs OXYGEN DEFICIENCY
lattice const., c
11.82
11.81
11.8
11.79
11.78
11.77
11.76
11.75
11.74
11.73
11.72
11.71
11.7
11.69
11.68
11.67
11.66
11.65
11.64
0.6
0.8
1
1.2
1.4
oxygen deficiency

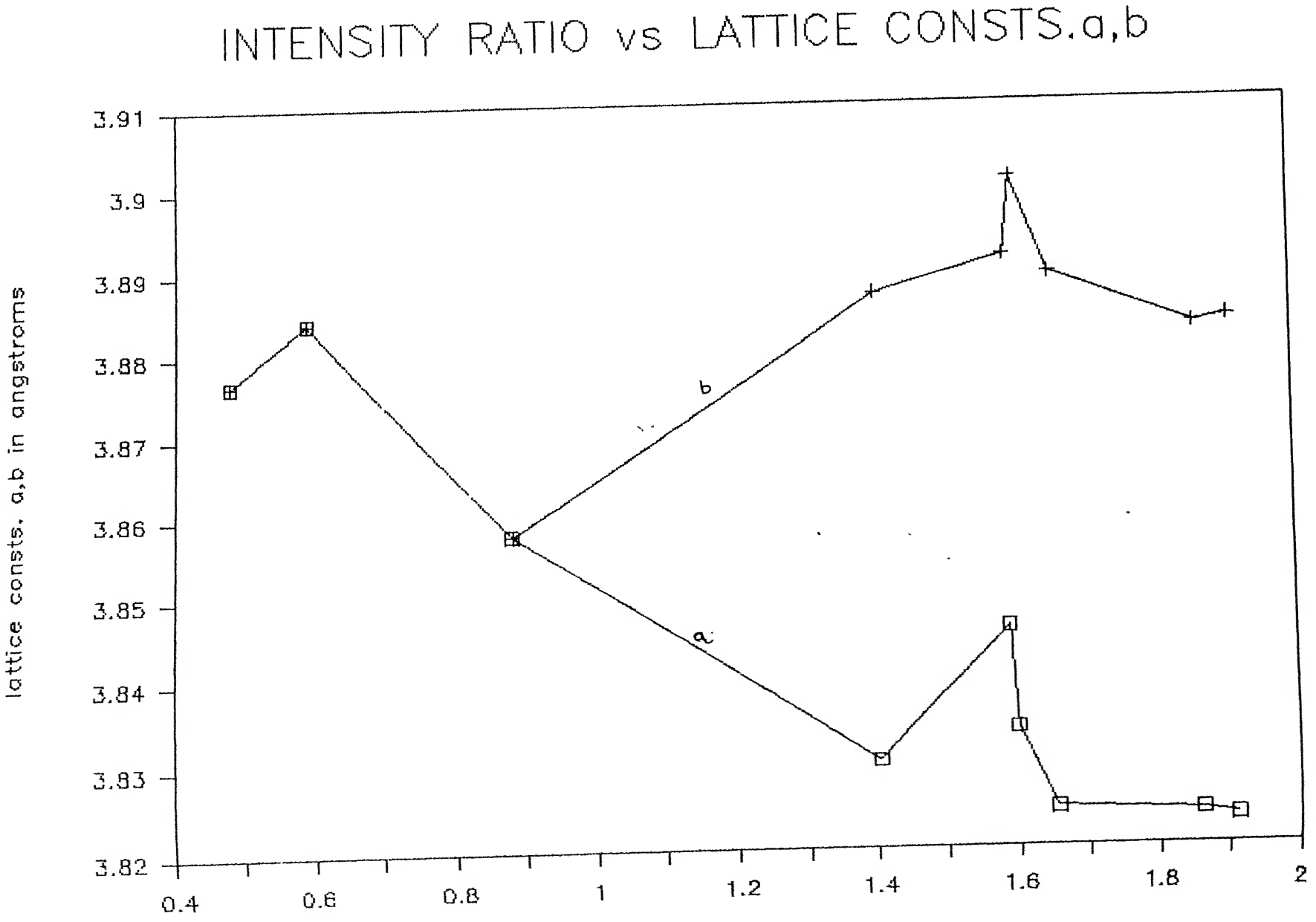
INTENSITY RATIO vs LATTICE CONSTS.a,b
lattice consts. a,b in angstroms
3.91
3.9
3.89
3.88
3.87
3.86
3.85
3.84
3.83
3.82
0.4
0.6
0.8
1
1.2
1.4
1.6
1.8
2
b
a

INTENSITY RATIO vs LATTICE CONSTANT c

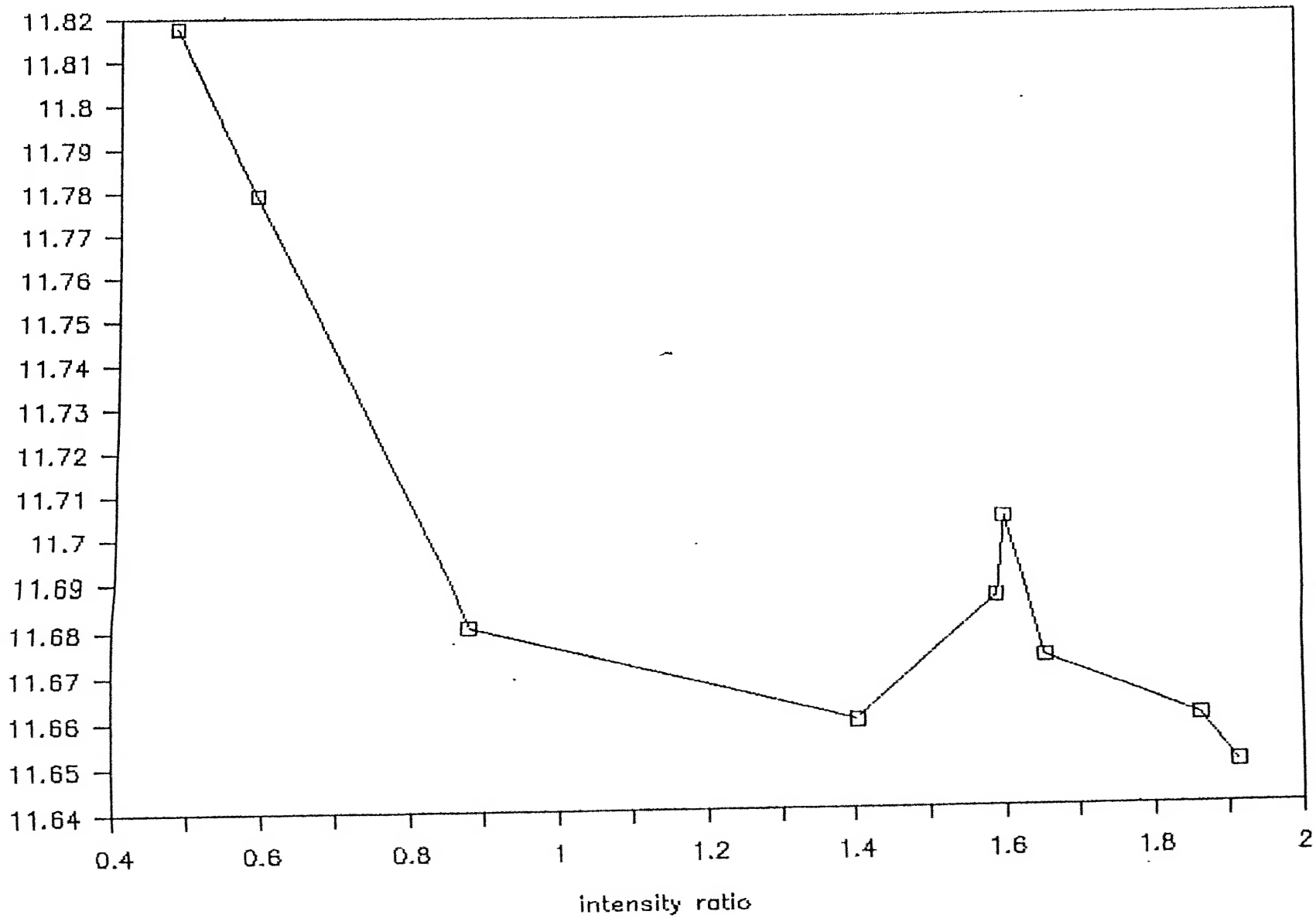

ln RESISTIVITY vs CRITICAL TEMPERATURE

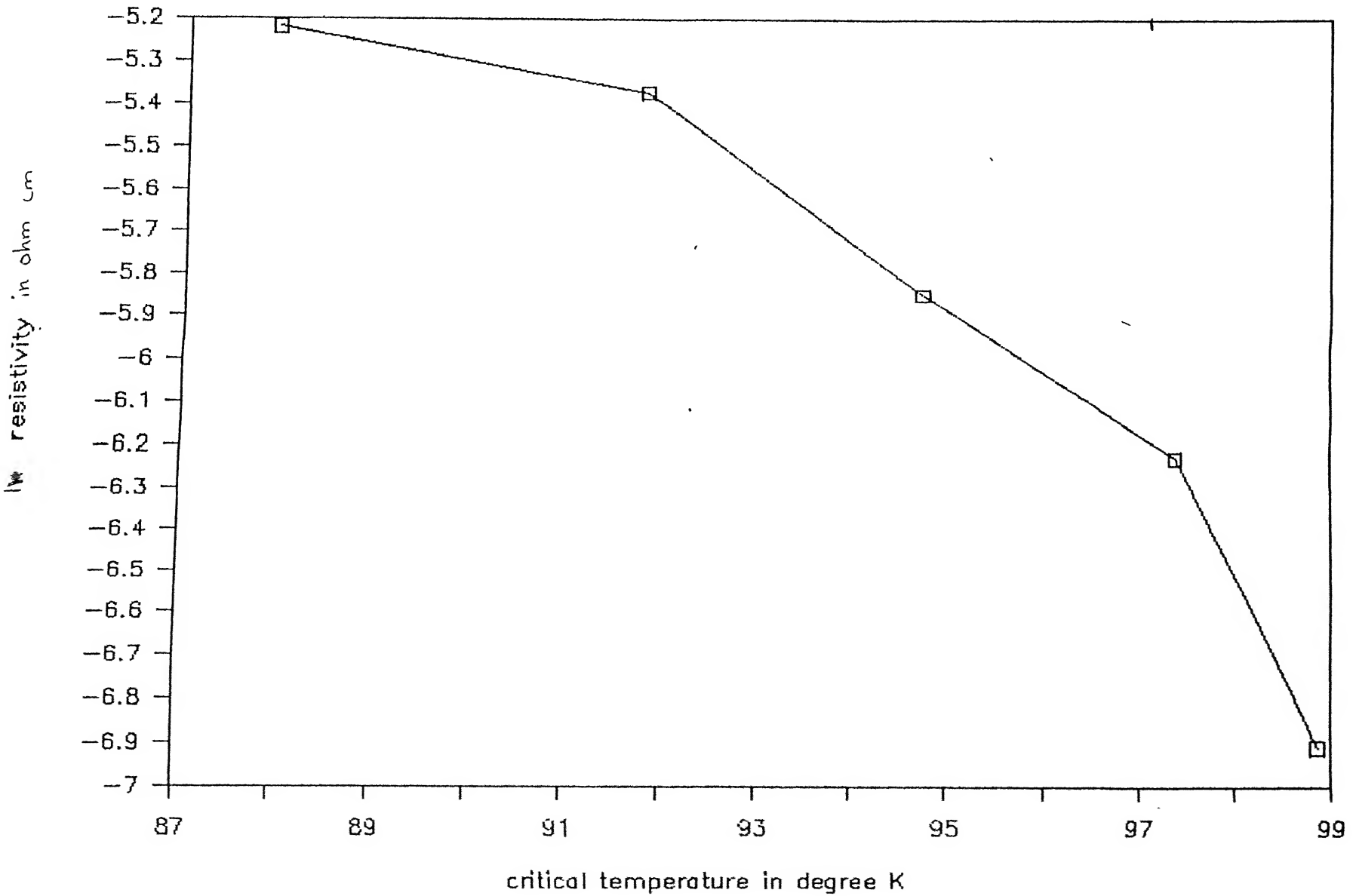

CRITICAL TEMPERATURE vs OXYGEN DEFICIENCY

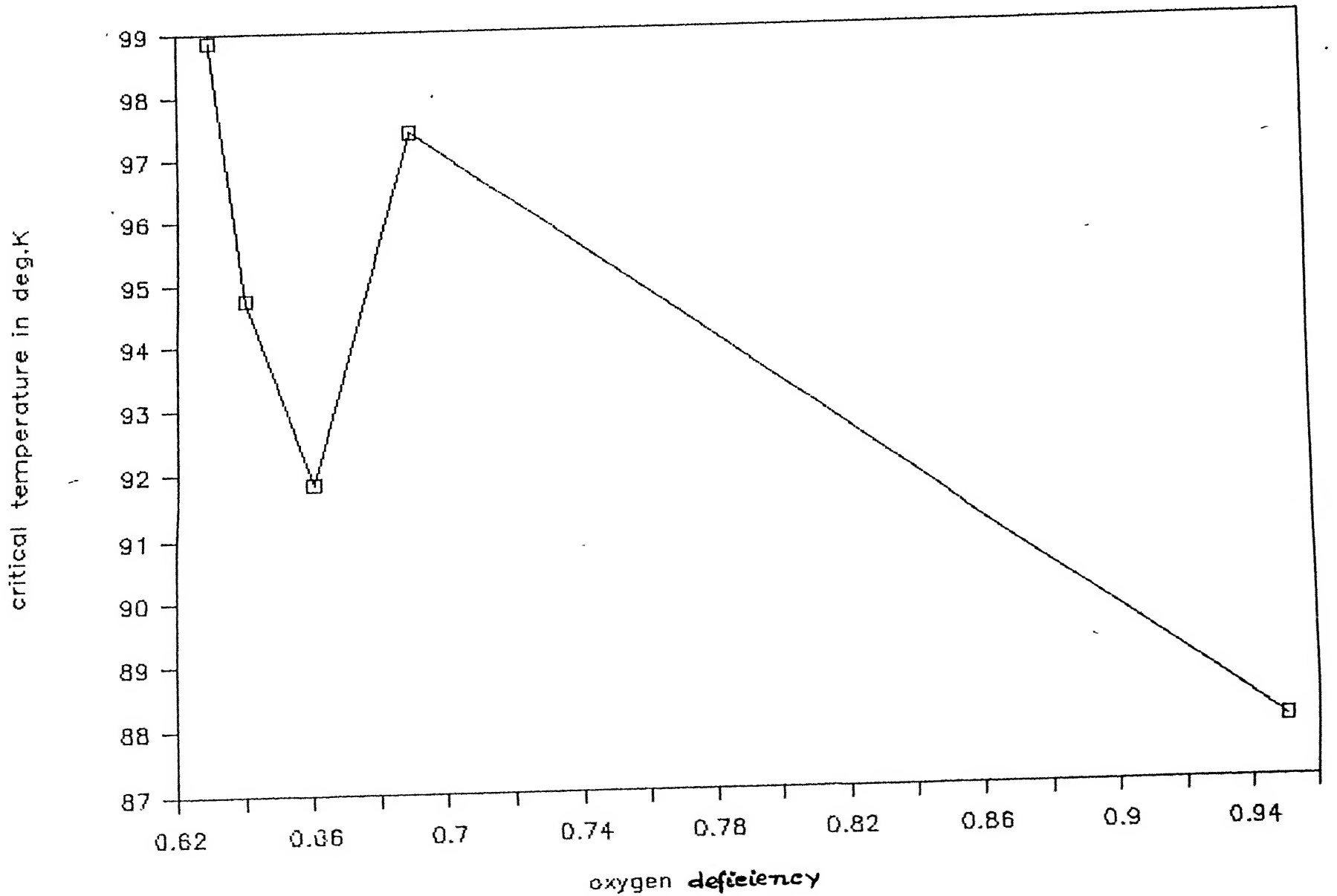

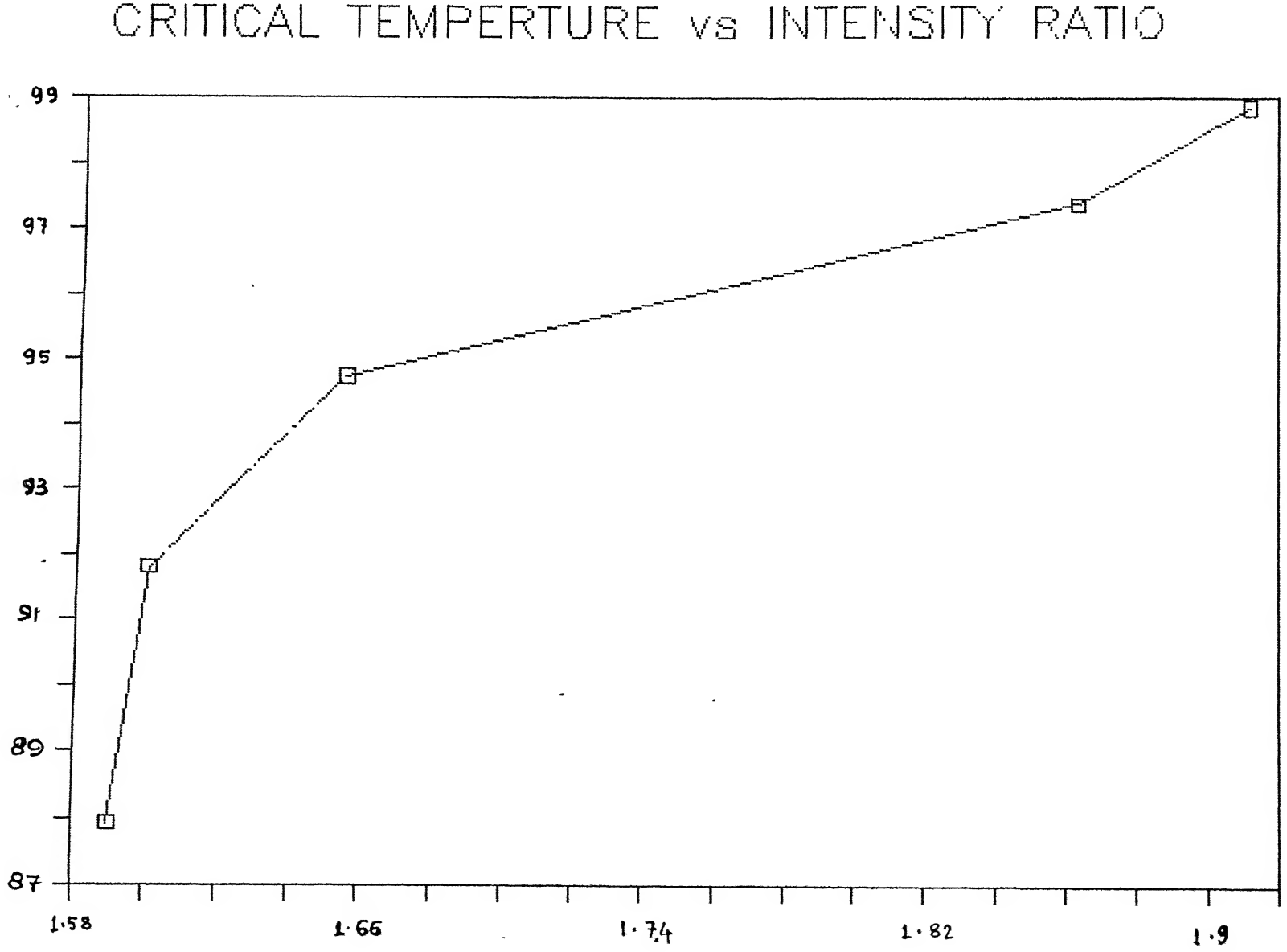
CRITICAL TEMPERTURE vs INTENSITY RATIO
99
97
95
93
91
89
87
1·58
1·66
1·74
1·82
1·9
Intensity ratio

FIGURE 3·25

the bulk sample resistance. In the event of poor contact, there must be some air gap between the sample and the electrode. The upper layer of the sample will act as an electrode. Equivalently, we can think of the sample/electrode assembly to consist of three capacitances in series. The equivalent capacitance being given by

$$\frac{1}{C} = \frac{1}{C_o} + \frac{1}{C_o} + \frac{1}{C_s}$$

or

$$C = \frac{C_s C_o}{2C_s + C_o}$$

where C_o and C_s respectively are capacitances due to air gaps and sample. If K_{tr} is the true dielectric constant of the material and K_{eff} the measured dielectric constant, then

$$\frac{K_{eff} A}{a} = \frac{K_{tr}(A/b) \times A/(a-b)/2}{2 \times A/b\, K_{tr} + A/((a-b)/2)}$$

$$K_{eff}/a = 2K \times \left[\frac{1}{K_{tr}(a-b) + b}\right]$$

$$K_{eff} = \frac{1}{[\,(1 - b/a) + (\frac{1}{K_{tr}})(b/a)\,]}$$

Now, for good contacts the air gap (a-b) is negligible, i.e., $a-b \simeq 0$ or $b/a \simeq 1$ and hence $K_{eff} \simeq K_{tr}$. Whereas, for bad contacts the air gap (a-b) is finite and its magnitude

increases as the contact gets worse, or b/a becomes increasingly smaller than 1 as the contact gets worse and hence K_{eff} becomes increasing lower than the K_{tr}. Take for example a material with $K_{tr} = 100$, and three different situations, (as the contact worsens) characterized by b/a = 0.99, 0.98 and 0.95 (b/a = 1 means perfect contact and $K_{eff} = K_{tr}$). The above equation yields K_{eff} = 50, 33 and 16.8 respectively. Thus we find that even an allowance of 1% air gap is capable of decreasing the dielectric constant by 50% (from 100 to 50).

It is worth pointing out here that this contact problem would not pose a great threat when the material under investigation is a true dielectric, i.e. more like an insulator, say for example, teflon with a dielectric constant, $K_{tr} = 5$. An air gap of 1% corresponding to b/a = 0.99 would yield

$$K_{eff} = \frac{1}{(1 - 0.99) + \frac{0.99}{5}} = \frac{1}{0.01 + 0.198} = 4.8$$

which is only 4% off from the true value of dielectric constant 5.

An all out effort was made to measure the dielectric constant of the tetragonal phase, but the reliability and reproductibility of the data became a suspect. However, these measurements have clearly brought out the reasons for poor

reproductibility and suggest the kind of care that has to be exercised for reliable measurements. Finally, our results put a big question mark over the reliability of the reported dielectric data (30).

Table 3.19 further reveals that at higher frequencies (> 5 MHz) a negative value of capacitance and hence K_{eff} is observed. Furthermore, whenever the contact is better, the capacitance becomes negative even at a lower frequency.

This phenomenon is observed because the HP4192A impedance analyser treats the sample as a 'black box'. It measures impedance Z and phase factor θ at various frequencies From Z and θ the equipment internally determines the real and imaginary parts of the impedance for a particular mode viz., a parallel R and C combination, and gives them as resistance R and reactance X respectively, i.e.,

$$Z\,\mathrm{Cos}\theta + j\,Z\,\mathrm{Sin}\theta = R + jX.$$

From X it calculates the capacitance C and the inductance L, i.e.,

$$C = -1/\omega X \quad \text{or} \quad L = X/\omega .$$

Actually,

$$X = \omega L_o - 1/\omega C_o ,$$

where , C_o is the actual capacitance and L_o is the inductance (lead inductance etc.) in the circuit.

When C_o is high, X becomes positive and hence is displayed as a negative value of capacitance. Similarly for high values of frequency (ω), X becomes positive (since $\omega = 2\pi f$) and once again negative capacitance is observed.

CONCLUSION

Our experimental results on weight loss measurements, XRD, electrical resistivity, critical temperature T_c and dielectric constant, & their subsequent analysis lead us to the following conclusions:

(1) The oxygen content and hence the relative amounts of ortho and tetragonal phases in $YBa_2Cu_3O_x$ could be controlled by the oxygen concentration in the atmosphere and by monitoring the cooling rate.

(2) The relative concentration of superconducting ortho phase decreases and that of the tetragonal phase increases with decreasing oxygen content.

(3) The intensity ratio as determined by the XRD is a better method for determining the relative concentrations of ortho and tetragonal phases though weight loss measurement can also be used.

(4) The behaviour of orthorhombic phase is metal - like whereas that of tetragonal phase is semiconductor-like. The resistivity of the orthorhombic phase is closer to those of poor metallic conductors or even semi metals - ($\sim 10^{-4}$ to $10^{-3}\Omega$ cm), and on the other hand, that of tetragonal phase is more like a conducting semiconductor ($\sim 1\Omega$cm).

(5) The critical temperature T_c, is proportional to the amount of orthorhombic phase present in the sample. Higher the amount of orthorhombic phase, higher is the T_c.

(6) There is an elongation along C-axis of the lattice, as the oxygen content decreases.

(7) Our results suggest a rather new technique for making superconducting samples with higher oxygen content, without passing oxygen. For details see the preparation technique for samples #2 and #4 described in Chapter 3. Sample #4 shows all the features which are similar to sample #1, prepared by normal technique of passing oxygen.

(8) The dielectric constant of tetragonal $YBa_2Cu_3O_x$ reported by Testardi et al. (30) is probably unreliable. Moreover our experiments point out that for conducting samples the dielectric constant measurements could be very difficult owing to large contact resistance compared to actual sample resistance. For reliable data the contacts must be very good. This can be checked by comparing the resistance with the actual (four probe) resistance. Also the lead inductance must be kept to a minimum otherwise the measurements at high frequencies will not be possible.

REFERENCES

1. F. London and H. London; Proc. Roy. Soc. (London); A146; 72; (1935).

2. F. London and H. London; Physica; 2; 341; (1935).

3. H. Kamerling Onnes; Akad. Van Weterschapen (Amsterdam); 14; 113; 818; (1911).

4. H. Kamerling Onnes; Commun. Phys. Lab. Univ. Leide 120b; 3; (1911).

5. J.R. Gavaler; Appl. Phys. Lett.; 23; 480; (1973).

6. J.G. Bendroz and K.A. Muller; Z. Phys. B; 64; 189; (1986).

7. H.P.R. Frederikse; J.F. Schooley; W.R. Thurber; E. Pferffer and W.R. Hosler; Phys. Rev. Letts; 16; 579; (1966).

8. G. Binnig; A. Baratoff; H.E. Hoenig and J.G. Bednorz; Phys. Rev. Letts; 45; 1352 (1980).

9. D.C. Johnston, H. Prakash, W.H. Jachariasen and R. Viswanathan; Mat. Rex. Bull; 8; 777 ; (1973).

10. A.W. Sleight, J.L. Gillson and P.E. Bierstedt; Solid State Comm.; 17; 27; (1975).

11. A. Baratoff et al., Superconductivity in d- and f-Band Metals; W. Buckel and W. Weber (eds.); Kemforschung Zentrum Karlsruhe;(1982).

12. T.D. Thanal; Appl. Phys; 22; 205; (1980).

13. J. Barden, L.N. Cooper, J.R. Schrieffer; Phys. Rev; 108; 1175; (1957).

14. C. Michel and B. Ravean; Rev. Chim. Miner; 21, 407, (1984).

15. C.W. Chu; P.H. Hor, R.L. Meng, L. Gao, Z.J. Huang and Y.Q. Wang; Phys. Rev. Letts.; 508; 4; 58; 405; 1987.

16. M.K. Wu; J.R. Ashburn, C.J. Torng, P.H. Hor, R.L. Meng, L. Gao, Z.J. Huang, Y.Q. Wang and C.W. Chu; Phys. Rev. Letts.; 9; 58; 908, (1987).

17. C. Michel, M. Herivieu, M.M. Borel, A. Grandin, F.Deslandes, J. Provost and B. Raveau; Z. Phys. B, 68, 421 (1987).

18. H. Maeda, Y. Tanaka, M. Fukutomi and T.Asano; Jpn. J. Appl. Phys. 27, L209 (1988).

19. Z.Z. Sheng and A.M. Hermann; Nature; 138; (1988).

20. P.A. Bierstedt, T.A. Bither and F.J. Darnell; 4; 25; (1966).

21. C.W. Chu et al.; Science; 238; 567; (1987).

22. R.J. Cava, R.B. van Dover, B. Baltogg and E.A. Rietman; Phys. Rev. Letts; 54; 4; 408, (1987).

23. Pawer et al; Solid State Commn; 67, 1, 47, (1988).

24. Dalichaouch et al; Solid State Commn; 65, 9, 1001; (1988).

25. P.H. Hor, L. Gao, R.L. Meng, Z.J. Huang, Y.Q. Wang, K. Forster, J. Vassilions and C.W. Chu; Phys. Rev. B, 58, 9, 911 (1987).

26. Paule D. Beale; Solid State Commun; 65, 10, 1145, (1988).

27. B.T. Takatake et al; Solid State Commun; 66, 4, 413, (1988).

28. P. Strobel, C. Paulsen and J.L. Tholes; Solid State Commun, 65, 7 (1988).

29. Eiji Takayama - Muromachi, Yoshishige, Uchida, Ken Yakino Tata Takako Tanaka and Katsuo Kata; Jpn. J. of Appl. Phys., 26; 5; L665; (1987).

30. L.R. Testardi, W.G. Moulton, H. Matias, H.K. Ng and C.M. Rey; Phys. Rev. B; 37 ; 4, 2374; (1988).

31. H.C. Montgomery; J. Appl. Phys; 42; 7; 2971, (1971).

32. B.F. Logan, Rice and R.F. Wick; J. Appl. Phys., 42; 7,2975 (1975).

33. J.M. Van Vleck; Theory of Electrical and Magnetic Susceptibility; Oxford; (1932).